INFORMATION TO USERS

The most advanced technology has been used to photograph and reproduce this manuscript from the microfilm master. UMI films the text directly from the original or copy submitted. Thus, some thesis and dissertation copies are in typewriter face, while others may be from any type of computer printer.

The quality of this reproduction is dependent upon the quality of the copy submitted. Broken or indistinct print, colored or poor quality illustrations and photographs, print bleedthrough, substandard margins, and improper alignment can adversely affect reproduction.

In the unlikely event that the author did not send UMI a complete manuscript and there are missing pages, these will be noted. Also, if unauthorized copyright material had to be removed, a note will indicate the deletion.

Oversize materials (e.g., maps, drawings, charts) are reproduced by sectioning the original, beginning at the upper left-hand corner and continuing from left to right in equal sections with small overlaps. Each original is also photographed in one exposure and is included in reduced form at the back of the book.

Photographs included in the original manuscript have been reproduced xerographically in this copy. Higher quality 6" x 9" black and white photographic prints are available for any photographs or illustrations appearing in this copy for an additional charge. Contact UMI directly to order.

U·M·I

University Microfilms International
A Bell & Howell Information Company
300 North Zeeb Road, Ann Arbor, MI 48106-1346 USA
313/761-4700 800/521-0600

Order Number 9111941

Stability and instability in two laser models

Jakobsen, Per Kristen, Ph.D.

The University of Arizona, 1990

U·M·I
300 N. Zeeb Rd.
Ann Arbor, MI 48106

Stability and Instability In Two Laser Models

by

Per Kristen Jakobsen

A Dissertation Submitted to the Faculty of the

COMMITTEE ON APPLIED MATHEMATICS (GRADUATE)

In Partial Fulfillment of the Requirements
For the Degree of

DOCTOR OF PHILOSOPHY

In the Graduate College

THE UNIVERSITY OF ARIZONA

1 9 9 0

THE UNIVERSITY OF ARIZONA
GRADUATE COLLEGE

As members of the Final Examination Committee, we certify that we have read the dissertation prepared by Per Kristen Jakobsen

entitled Stability and Instability for Two Laser Models

and recommend that it be accepted as fulfilling the dissertation requirement for the Degree of Doctor of Philosophy.

Dr. A.C. Newell	July 2, 1990 Date
Dr. M. Brio	July 2, 1990 Date
Dr. J. Gibbs	July 2, 1990 Date
	Date
	Date

Final approval and acceptance of this dissertation is contingent upon the candidate's submission of the final copy of the dissertation to the Graduate College.

I hereby certify that I have read this dissertation prepared under my direction and recommend that it be accepted as fulfilling the dissertation requirement.

Dissertation Director, A.C. Newell	July 2, 1990 Date

STATEMENT BY AUTHOR

This dissertation has been submitted in partial fulfillment of requirements for an advanced degree at The University of Arizona and is deposited in the University Library to be made available to borrowers under rules of the Library.

Brief quotations from this dissertation are allowable without special permission, provided that accurate acknowledgement of source is made. Requests for permission for extended quotation from or reproduction of this manuscript in whole or in part may be granted by the head of the major department or the Dean of the Graduate College when in his or her judgement the proposed use of the material is in the interests of scholarship. In all other instances, however, permission must be obtained from the author.

SIGNED: Per K. Jakobsen

Acknowledgments

A dissertation is never the work of one person only. My dissertation is not an exception to this rule. First I will thank my advisor Alan Newell for always having time to listen to what I had to say and for inspiring me to go on when things were looking bleak.I will extend my gratitude to Robert Indik for listening to my daily complaints and for giving me so many good ideas. Finally I will thank Jerry Moloney for relentlesly pushing me towards the finishing line and never letting me slow down. These three have each in their way made this dissertation possible.

I will also thank Yves Pomeau and Pierre Coullet for interesting discussions and remarks. Lousie Gorsky deserves my gratitude for keeping an eye on various deadlines and making sure that all practical things were running smoothly.

Finally I will thank my wife Ellen Johansen for beeing such a good fiend and for giving my life a focus.

I will acknowledge The Norwegian Research Counsil For Sciences And Humanities (NAVF) for their very generous support during the last three years. This work has in part been supported by Arizona Center for Mathematical Sciences (ACMS). ACMS is sponsored by AFOSR contract F49620-86-C0130 with the University Research Initiative Program at the University of Arizona. In addition the author wish to thank the Pittsburgh Supercomputing Center for computational support under grants DMS9000005P and DMS880037P.

Table of Contents

List of Figures

ABSTRACT

We study linear stability of travelling wave solutions of a system of equations derived from the Maxwell-Bloch system by adiabatically eliminating the polarization. For the reduced system we find exact conditions for stability and instability. We also find that the adiabatic elimination procedure produces a very badly behaved system in the presence of diffraction. The full Maxwell-Bloch system or the system we get by removing both the polarization and the inversion adiabatically does not have these problems.

Chapter 1

INTRODUCTION

The Maxwell-Bloch (MB) coupled system of field-material equations has been used by many investigators [9], [10], [11] , [12] to study instabilities and coherent pulse propagation in pumped two level media. Recently several investigators [1], [13] have studied the theory of transverse, diffraction mediated instabilities and pattern formation in lasers using the MB system. Due to the size of the linear stability problem for MB, analytic stability results are not easy to find. We have approached this problem by studying a smaller system of equations (RMB) that we get from MB by adiabatically eliminating the polarization from MB. For this system we analytically characterize the linear stability of planewaves. The RMB system has, however, some very undesirable properties that are a result of the adiabatic elimination applied to the MB system. We also study the linear stability of the nonlasing solution for the full MB system and derive amplitude equations describing the nonlinear evolution of the instabilities. Some of these results have already been described by P. Coullet et. al.[13] Finally we compare the linear stability of the lasing solution in (MB), (RMB) and the equation obtained by also eliminating the inversion adiabatically (FRMD).

The work is organized as follows. Most of the work is relegated to appendices.

In section 1 we describe the nonlasing and the lasing travelling wave solutions of the full Maxwell-Bloch system . A derivation of the (MB) equations from first principles can be found in appendix A. In section 2 we do the linear stability analysis of the nonlasing solutions. The derivation of the amplitude equations for the nonlinear evolution of perturbations close to threshold is relegated to appendix G. In section 3 we describe the reduced system and the assumptions that its derivation is based on. The planewave solutions are described in section 3 and in section 4 we do the linear stability analysis for these solutions. In section 5 we describe the result of numerical simulations of (RMB). Section 6 contains a discussion of the relation between the (MB), (RMB) and (FRMD). Finally section 7 gives conclusions.

Chapter 2

TRAVELLING WAVE SOLUTIONS FOR MB

In appendix A we have derived the Maxwell-Bloch equations for a planewave with slowly varying amplitude propagating along the z-axis in a two level diffusive medium with homogenous broadening. The equation for the inversion density N, polarization envelope P and electric field envelope E were found using the slowly varying envelope approximation.From appendix A eqns. (8.26), (8.27) and (8.28) we have

$$\frac{\partial E}{\partial t} + v_z \frac{\partial E}{\partial z} + \mu E - \imath a \nabla_\perp^2 E = \beta_1 P \tag{2.1}$$

$$\frac{\partial P}{\partial t} + \gamma_1(1 + \imath\Delta)P = \beta_2 EN \tag{2.2}$$

$$\frac{\partial N}{\partial t} + \gamma_2(N - N_0) - D\nabla^2 N = -\frac{1}{2}\beta_2(EP^* + E^*P) \tag{2.3}$$

The above equations are a system of nonlinear coupled partial differential equations, and typically nontrivial solutions are not easy to find. The above system has, however, some simple special solutions. It has planewave solutions of the form

$$\begin{pmatrix} E \\ P \end{pmatrix} = \begin{pmatrix} \bar{E} \\ \bar{P} \end{pmatrix} e^{\imath(\vec{k_0}\cdot\vec{x} + \Omega t)}$$
$$N = \bar{N},$$

where $\vec{k}_0$ is a wave vector transverse to the carrier wave propagation direction (z-axis) and $\vec{x} = (x, y, 0)$ denotes transverse coordinates. The amplitudes $\bar{E}$, $\bar{P}$, $\bar{N}$

are

$$\begin{aligned} \bar{E} &= \sqrt{\frac{\gamma_2\beta_1}{\mu\beta_2}(N_0 - \bar{N})} \\ \bar{P} &= \frac{\mu + i(\Delta + a\vec{k}_0^2)}{\beta_1}\bar{E} \\ \bar{N} &= \frac{\mu\gamma_1}{\beta_1\beta_2}(1 + (\frac{\gamma_1\Delta - a\vec{k}_0}{\gamma_1 + \mu})^2) \\ \Omega &= -\gamma_1\frac{\mu\Delta + a\vec{k}_0^2}{\gamma_1 + \mu} \end{aligned} \tag{2.4}$$

Note that we are considering planewaves whose phase only depends on the transverse coordinate $\vec{x}$. This is because E and P are envelopes of a carrier planewave propagating along the z-axis so any z dependence in the phase can be absorbed into the carrier phase. The solutions (2.4) described above are planewaves propagating at right angle to the z-axis, adding the carrier wave we see that they correspond to electric field waves propagating at an angle to the z-axis. Since the Maxwell-Bloch equations were derived on the assumption that the envelope varies slowly compared to the carrier wave, we observe that the angle between the z-axis and the electric field wave corresponding to (2.4) must be very small. All solutions we study are propagating along the z-axis or at a small angle to the z-axis. Calling the wavenumber of the carrier wave k_z' as in appendix A we have that the solutions (2.4) must satisfy $\vec{k}_0/k_z' \ll 1$. The frequency Ω derived above is the frequency that the dispersion relation forces to compensate for the small transverse component $\vec{k}_0$ to the wavenumber of the carrier wave.

In addition to the planewave solutions described above we have solutions of the form

$$E = P = 0,\ N = N_0 \tag{2.5}$$

These solutions correspond to the situation when the laser is off. We define threshold to be the value of N_0 were these solutions loose their stability and the laser turns on. We will call these solutions (2.5) the nonlasing solutions and the planewave solutions (2.4) lasing solutions.

Chapter 3

LINEAR STABILITY OF THE NONLASING SOLUTIONS

In this section we study the linear stability of the nonlasing solutions (2.5). The details of this analysis can be found in appendix B. Here we will summarize the principle ideas and results. We perturb the nonlasing solution slightly writing $E = e$, $P = p$, $N = N_0 + n$ and derive a linear system for the small quantities e, p, n. The linear system is

$$e_t + v_z e_z + \mu e - \imath a \nabla_\perp^2 e = \beta_1 p \tag{3.1}$$

$$p_t + \gamma_1(1 + \imath\triangle)p = \beta_2 e N_0 \tag{3.2}$$

$$n_t + \gamma_2 n - D\nabla^2 n = 0 \tag{3.3}$$

Without loss of generality we may assume that the solution is of the form

$$\begin{pmatrix} e \\ p \\ n \end{pmatrix} = \begin{pmatrix} e_0 \\ p_0 \\ n_0 \end{pmatrix} e^{\lambda t + \imath k \cdot \vec{r}}$$

Where $\vec{k} = (\vec{k}_\perp, k_z)$ is the perturbation wave number and $\vec{r} = (x, y, z)$ is the position vector. The characteristic polynomial for λ is

$$(\lambda + \gamma_2 + D\vec{k}^2)(\lambda + \imath v_z k_z + \mu + \imath a \vec{k}_\perp^2)(\lambda + \gamma_1(1 + \imath\triangle)) - \beta_1\beta_2 N_0 = 0$$

One eigenvalue is $\lambda = -\gamma_2 - D\vec{k}^2$. This eigenvalue does not contribute to instability for any parameter values since γ_2 and D are both positive. The two other roots are found to give instability when the pumping N_0 is above the threshold value N_{th}

$$N_0 > N_{th} = \frac{\mu\gamma_1}{\beta_1\beta_2}(1 + (\frac{\gamma_1\Delta - v_z k_z - ak_\perp^2}{\gamma_1 + \mu})^2) \tag{3.4}$$

We observe from equations (2.4) that N_{th} is equal to the amplitude $\bar{N}$ for the lasing solution. The threshold for instability of the nonlasing solution coincides with the threshold for existence of the travelling wave lasing solutions. Later in this section we derive equations describing the nonlinear evolution close to threshold and find that under certain conditions that evolution will saturate onto a particularone of these solutions. The central idea of this method is that the nonlinear evolution will be determined mainly by the first wavenumber that reaches threshold. This wavenumber is easy to find using the expression for the threshold derived above. We find that there are two cases:

(i) The defocussing case, $\Delta < 0$: If $k_z > -\gamma_1|\Delta|/v_z$ then $\vec{k}_\perp = 0$ will go unstable first when we increase the pumping N_0 above threshold, i.e. if the longitudinal perturbation wave number is large enough, the fastest growing perturbation will be purely longitudinal. If $k_z < -\gamma_1|\Delta|/v_z$, then the wavenumbers $|\vec{k}_\perp| = \sqrt{(|v_z k_z| - \gamma_1|\Delta|)/a}$ will go unstable first,i.e. if the longitudinal perturbation wavenumber is small enough, the fastes growing perturbations will consist of narrow cones centered on the z-axis pointing along positive z.

(ii) The focussing case, $\Delta > 0$: If $k_z > \gamma_1\Delta/v_z$ then $\vec{k}_\perp = 0$ will first go unstable. Above this positive value the fastest growing perturbation will be purely longitudinal. For $k_z < \gamma_1\Delta/v_z$ the wavenumbers $|\vec{k}_\perp| = \sqrt{(\gamma_1\Delta - v_z k_z)/a}$ will go unstable first. These will, as in the defocussing case $\Delta < 0$, correspond to narrow

cones centered on the z-axis.

P. Coullet et. al. [13] found that the nonlinear evolution of the instability in the defocussing case is described by the complex Ginsburg Landau (CGL) equation. We have rederived this result and also found that in the focussing case the nonlinear evolution of the instability in described by two coupled CGL equations. In order to derive these equations we used the weakly nonlinear method as described in [7]. We have studied the linear stability of the space homogenous solutions of these equations hoping that this would give us the approximate location of the threshold where the lasing solutions loose stability. This attempt failed and the derivation of the amplitude equations and the linear stability analysis of their solutions have been relegated to appendix H.

Chapter 4

TRAVELLING WAVE SOLUTIONS FOR REDUCED MB

In order to get some understanding of the stability of the travelling wave solutions of the Maxwell-Bloch equations we will study a reduced system. This system is derived by assuming that the polarization decays much faster than the electric field and inversion density. This is the assumption of adiabatic elimination that often is used to separate dynamics that occur on widely different time scales. The adiabatic elimination is done in appendix A. From appendix A equations (8.29), (8.30) the reduced system can be written

$$\frac{\partial E}{\partial t} + v_z \frac{\partial E}{\partial z} + \mu E - \frac{1}{2}\beta(1 - \imath\Delta)EN - \imath a \nabla_\perp^2 E = 0 \tag{4.1}$$

$$\frac{\partial N}{\partial t} + \gamma_2(N - N_0) - D\nabla^2 N + \beta|E|^2 N = 0, \tag{4.2}$$

where we have changed notation from appendix A using E for the electric field envelope and dropped the prime on the variable N. Note that N has been rescaled as compared to the N in the full Maxwell-Bloch equations. The rescaled N is essentially the inversion energy density. The parameter $\beta > 0$ is defined in appendix A. The travelling wave solutions of this system are

$$E = \bar{E} e^{\imath(\vec{k_0}\cdot\vec{x} + \Omega t)}$$

$$N = \bar{N}$$

where

$$\bar{E} = \sqrt{\frac{\gamma_2}{2\mu}(N_0 - \bar{N})} \tag{4.3}$$

$$\bar{N} = \frac{2\mu}{\beta} \tag{4.4}$$

$$\Omega = -\mu\Delta - a\vec{k_0}^2 \tag{4.5}$$

How do these solutions relate to the travelling wave solutions for the full Maxwell-Bloch equations? Introducing the scaling of N from appendix A into the expressions above for $\bar{E}$,$\bar{N}$ and Ω and comparing with the corresponding expressions from the (MB) we observe that one reduces to the other in the limit

$$\frac{a\vec{k}_0^2}{\mu}, \frac{\mu}{\gamma_1} \ll 1$$

This condition expresses the assumption of adiabatic elimination as applied to the travelling wave solution. The time scale, γ_1^{-1}, for variation in P, must be much larger the the time scale, $a\vec{k}_0^{-2}$, for variation in E. For fixed parameters, the adiabatic elimination will break down if $\vec{k}_0$ becomes large enough. For the same reason we should be suspicious of any solution of the reduced system that contains very high wavenumbers, since these wavenumbers will produce fast time variation through the dispersion relation. High wavenumbers should also be avoided both in the full Maxwell-Bloch and the reduced system considered here for another reason. In the derivation we used the assumption that the envelope varied slowly compared to the carrier wave. This makes solutions with too much energy in high wavenumbers suspect even in the full Maxwell-Bloch system. This constraint on the solutions of the Maxwell-Bloch system is called the paraxial wave approximation. We have

found that the reduced system of equations even if they were derived in a natural way do in fact violate the paraxial wave approximation.

Chapter 5

LINEAR STABILITY FOR REDUCED SYSTEM

Linearize the reduced system by writing

$$\begin{aligned} E &= (\bar{E} + e)e^{\imath(\vec{k_0}\cdot\vec{x}+\Omega t)} \\ N &= \bar{N} + n \end{aligned} \tag{5.1}$$

where as usual e and n are small perturbations. Keeping only linear terms from (4.1), (4.2) we find

$$e_t + v_z e_z = \frac{1}{2}\beta(1 - \imath\Delta)\bar{E}n - 2ak_{0x}e_x - 2ak_{0y}e_y + \imath a\nabla_\perp^2 e \tag{5.2}$$

$$n_t = -(\gamma_2 + \beta\bar{E}^2)n - \beta\bar{E}\bar{N}(e + e^*) + D\nabla^2 n \tag{5.3}$$

Without loss of generality the solution of this system may be written

$$\begin{pmatrix} e^r \\ e^i \\ n \end{pmatrix} = \begin{pmatrix} e_0^r \\ e_0^i \\ n_0 \end{pmatrix} e^{(\lambda t + \imath\vec{k}\cdot\vec{x})}$$

where all symbols with subscripts are constant in space and time. The characteristic polynomial of the resulting linear matrix system for e_0^r, e_0^i and n is

$$(s + p)(s^2 + 1) - q(\Delta - s) = 0 \tag{5.4}$$

where

$$\begin{aligned} p &= \frac{1}{a\vec{k}_\perp^2}(\gamma_2 + \beta\bar{E}^2 + D\vec{k}^2) - 2i\frac{\tilde{k}\cdot\vec{k}}{\vec{k}_\perp^2} \\ q &= \frac{\beta^2\bar{E}^2\bar{N}}{(a\vec{k}_\perp^2)^2} \\ s &= \frac{\lambda}{a\vec{k}_\perp^2} + 2i\frac{\tilde{k}\cdot\vec{k}}{\vec{k}_\perp^2}, \end{aligned} \tag{5.5}$$

and $\vec{k}_\perp$ is the transverse part of the perturbation wave number. Stability of the travelling wave solutions of the reduced Maxwell-Bloch system of equations is determined by the real part of the roots of the polynomial (5.4). Approximate expressions for the roots of this polynomial will be described later. First we will derive exact conditions determining when the polynomial (5.4) has roots with positive real part. This we can do without knowing the roots themselves. These conditions are derived in detail in appendix E. The conditions we find are

$$\frac{q\triangle}{p_r} > 1 \tag{5.6}$$

or

$$p_r + \triangle < 0 \tag{5.7}$$

or

$$|p_i| > \frac{1}{|\triangle|}\sqrt{\frac{p_r - q\triangle}{p_r}}(p_r + \triangle) \tag{5.8}$$

Where p_r, p_i are the real and imaginary parts of the parameter p in (5.4). We will first consider the case when the longitudinal term is removed from the equation by constraining the system longitudinally [1]. Later we will consider the general case.

5.1 Uniform Field Limit

In the uniform field limit we assume $\frac{\partial}{\partial z} = 0$. If there is no inversion diffusion $D = 0$ and purely longitudinal waves $\vec{k}_0 = 0$, then the instability behavior splits into two parts according to whether the system is focussing $\Delta > 0$ or defocussing $\Delta < 0$.

The instability condition for the focussing case is

$$N_0 > \frac{4\mu^2\Delta}{\beta(2\mu\Delta - a\vec{k}_\perp^2)} \tag{5.9}$$

or equivalently

$$\vec{k}_\perp^2 < \frac{2\Delta\mu}{a}(1 - \frac{\bar{N}}{N_0}) \tag{5.10}$$

This is a long wavelength instability. From appendix E we also note that this is a real instability in the sense that the unstable mode has a purely exponential growth.

The instability condition for the defocussing case is

$$\bar{N} < N_0 < \bar{N}\frac{|\Delta|a\vec{k}_\perp^2}{\gamma_2} \tag{5.11}$$

For fixed parameters, condition (5.11) will be satisfied for all sufficiently large $\vec{k}_\perp$

$$\vec{k}_\perp^2 > \frac{\gamma_2}{a|\Delta|} \tag{5.12}$$

In the defocussing case arbitrary high wave numbers will be unstable and so participate in the dynamics. This is a very pathological behavior. It does not mesh well with the paraxial wave approximation and adiabatic ellimination used to derive the reduced model. Figures 5.1 and 5.2 show the growth curves for the focussing and defocussing cases.

The unit on the x-axis is the length of the transverse wavenumber scaled by 2π. The curves are reflection symmetric around the y-axis. Note that the growth

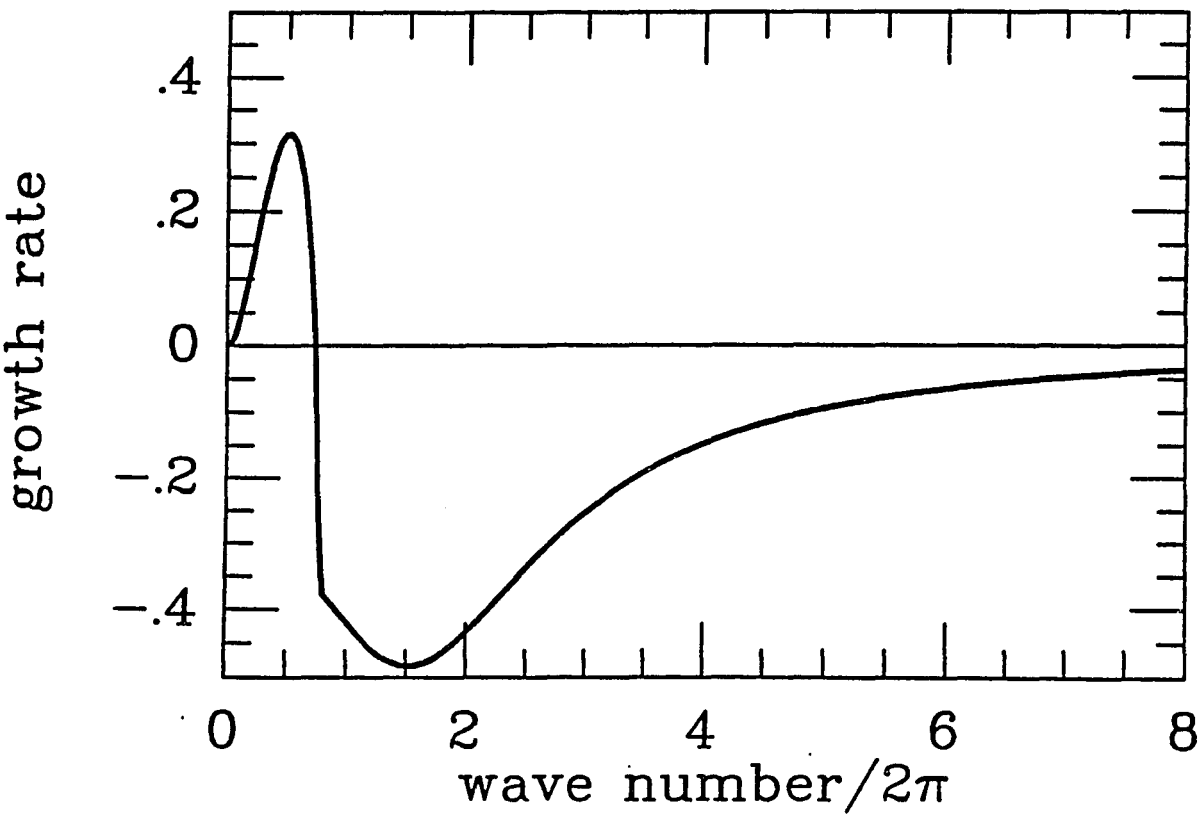

Figure 5.1: Growth rate as a function of wave number,focussing case. The x-axis is scaled by 2π. Parameter values are $D = 0$, $\beta = 0.1$, $\mu = 0.3$, $\gamma = 1.0$, $\delta = 2.0$, $N_0 = 10$, and $a = 0.05$.

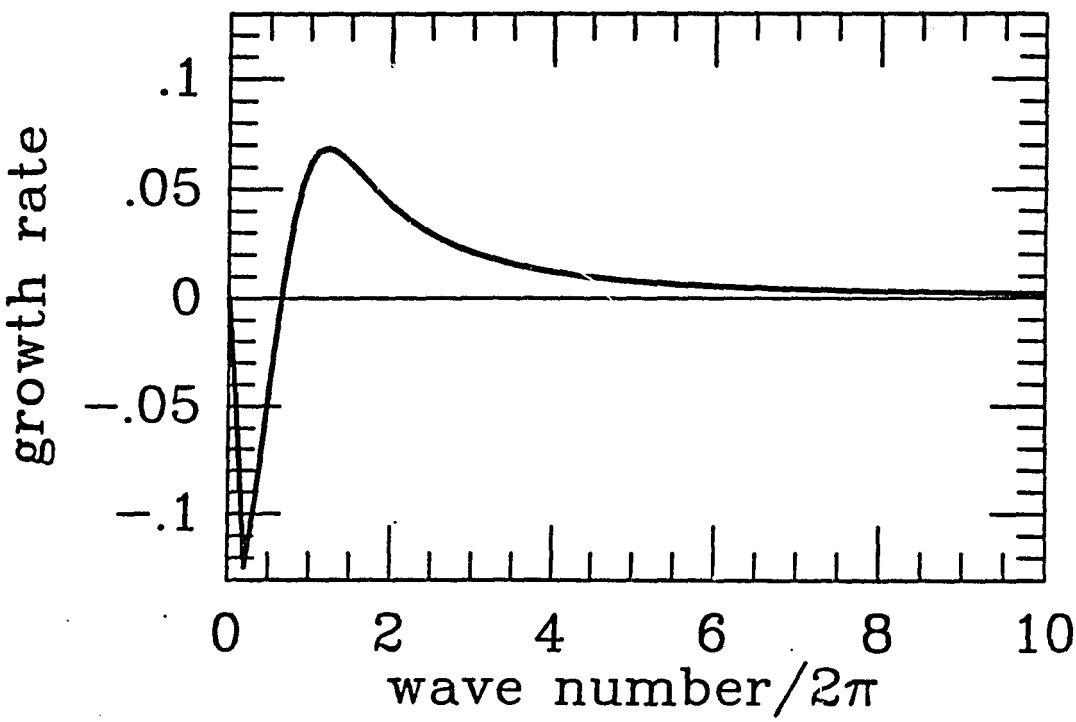

Figure 5.2: Growth rate as a function of wave number,defocussing case. The x-axis is scaled by 2π. Parameter values are $D = 0$, $\beta = 0.1$, $\mu = 0.3$, $\gamma = 1.0$, $\delta = -2.0$, $N_0 = 10$, and $a = 0.05$.

curve in the defocussing case has an infinite tail. This is the result predicted by the analysis above. This infinite tail can be described analytically (c.f. appendix F). We find

$$\lambda \approx -\frac{\beta^2 \bar{E}^2 \bar{N}}{2} \frac{\frac{\gamma_2 N_0}{\bar{N}} + \Delta a \vec{k}_\perp^2}{(\frac{\gamma_2 N_0}{\bar{N}})^2 + (a\vec{k}_\perp^2)^2}, \tag{5.13}$$

when

$$\vec{k}_\perp^4 \gg \frac{\beta\gamma_2}{a^2}(N_0 - \bar{N}).$$

The growth curve is proportional to $\Delta/\vec{k}_\perp^2$ for very large transverse wavenumbers. The system behaves badly both in the focussing and defocussing case. The growth curve goes to zero from below in the foccusing case and there will exist infinitely many wavenumbers with growth rate arbitrarily close to zero. One should expect any initial disturbance to lift the almost neutral wavenumbers above threshold, so that even in the focussing case infinitely high wavenumbers take part in the dynamics. These results have grave consequences not only for the physical interpretation of the equations but also for any attempt to simulate them numerically or to study their nonlinear evolution using the weakly nonlinear method. Since the highest wavenumber that can exist on your computational grid will be closest to being neutral, that wavenumber will be the first to grow. The more grid points you use the closer the highest wavenumber will be to neutral, and the faster its growth will be. The weakly nonlinear method [7] is useless for this problem since you have to include an infinite number of active modes in your expansion. This can hardly be said to represent a simplification over the original equations. The formula for the growth rate will, depending on the values of the various parameters, apply even for rather small values of $\vec{k}_\perp$. This will be true if we for example have weak coupling or are close to threshold. Under these restrictions the asymptotic formula for the

growth rate will give us the wavenumber that is growing fastest

$$|\vec{k}_\perp|_{max} = \sqrt{\frac{\gamma_2 N_0}{a|\Delta|\bar{N}}(1+\sqrt{1+\Delta^2})} \tag{5.14}$$

From numerical solution of the eigenvalue problem and also from formula (5.13) we find that the growth curve in the defocussing case and focussing case connect at zero detuning through a completely flat growth curve.

Let us now turn to the effect of diffusion on the focussing and defocussing instability. Using the expressions (5.5) in the instability conditions (5.6), (5.7) we find that instability occurs if and only if (i) $\Delta > 0$:

$$N_0 > \frac{2\Delta\mu\gamma_2 + aD\vec{k}_\perp^4}{\gamma_2(\Delta\beta - \frac{a\vec{k}_\perp^2}{\bar{N}})} \tag{5.15}$$

(ii) $\Delta < 0$:

$$\bar{N} < N_0 < \bar{N}(\frac{a\vec{k}_\perp}{\gamma_2}(|\Delta| - \frac{D}{a})) \tag{5.16}$$

The effect of diffusion on the focussing instability is to increase the threshold for any given wavenumber, affecting high wavenumbers more strongly than low wavenumbers. This is typical for the effect of diffusion on any wave system. Figure 5.3 show the effect of diffusion on the growth rate of the focussing instability.

The effect of diffusion on the defocussing instability is much more pronounced. In fact for diffusion above the critical value $\bar{D} = a|\Delta|$ the instability vanishes completely. Note that for all values of the diffusion where the instability still exists the infinite tail persists. Figure 5.4 shows the effect of diffusion on the growth rate in the defocussing case. Diffusion will not remove the infinitely many close to neutral modes of the system. With diffusion the growth rate for large $\vec{k}_\perp$ is

$$\lambda \approx -\frac{\beta_2 \bar{E}^2 \bar{N}}{2} \frac{(\frac{\gamma_2 N_0}{\bar{N}} + D\vec{k}^2) + \Delta a\vec{k}_\perp^2}{(\frac{\gamma_2 N_0}{\bar{N}} + D\vec{k}^2)^2 + (a\vec{k}_\perp^2)^2}$$

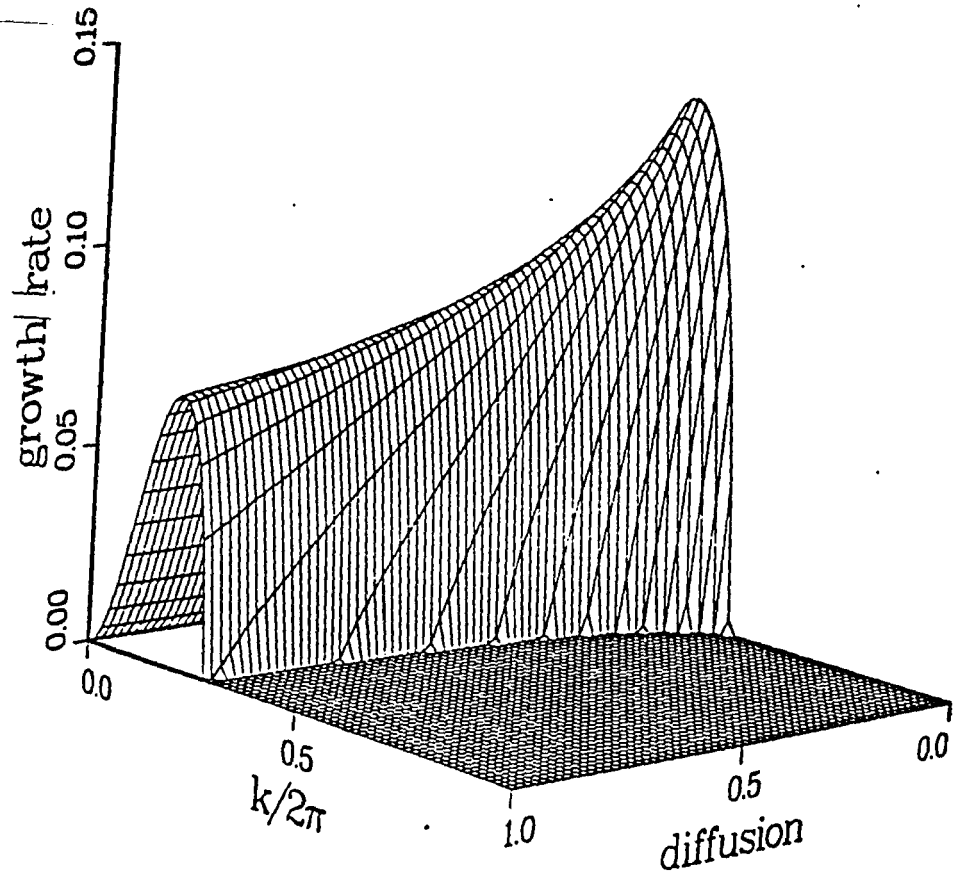

Figure 5.3: Growth rate as a function of wavenumber and diffusion,focussing. The x-axis is scaled by 2π. The parameter values are $\beta = 0.1$, $\mu = 0.3$, $\gamma_2 = 1.0$, $\delta = 2.0$, $N_0 = 10$, and $a = 0.05$.

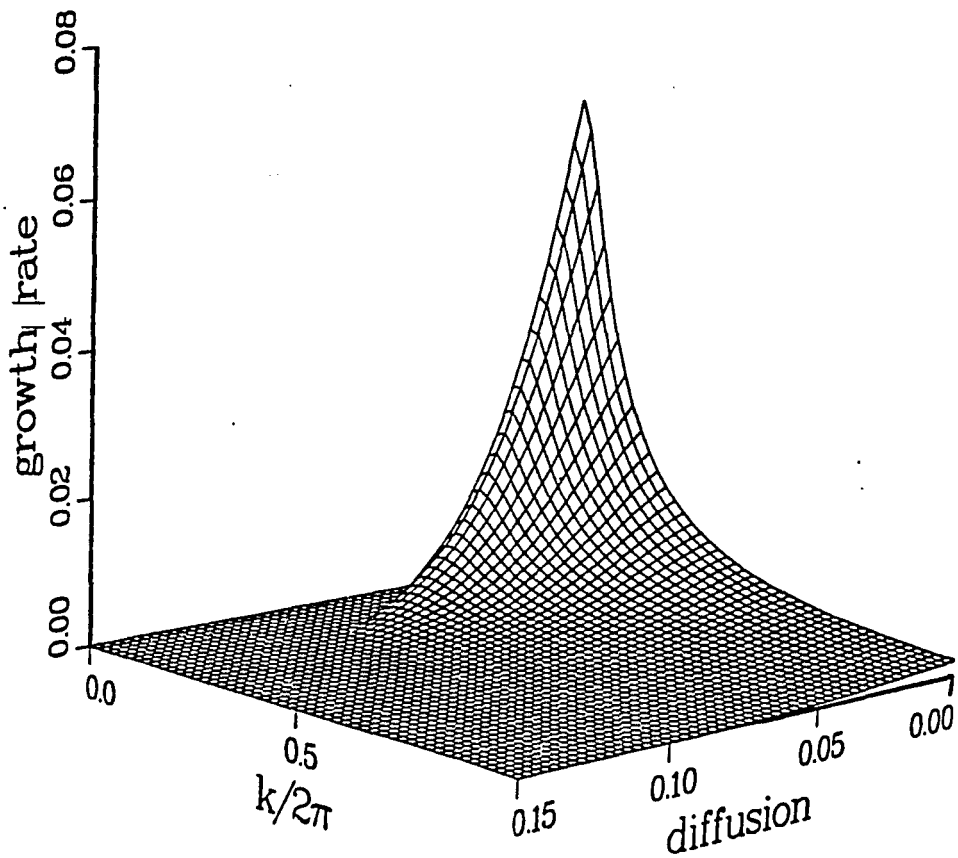

Figure 5.4: Growth rate as a function od wavenumber and diffusion,defocussing. The x-axis is scaled by 2π. The parameter values are $\beta = 0.1$, $\mu = 0.3$, $\gamma_2 = 1.0$, $\delta = -2.0$, $N_0 = 10$, and $a = 0.05$.

The growth curve converges to zero for any value of the diffusion.

We have been considering instability of purely longitudinal waves $\vec{k}_0 = 0$. We will now turn to the more general case $\vec{k}_0 \neq 0$. We continue to assume z independence, $\partial_z = 0$. The only effect of this change on the characteristic polynomial (5.4) is to make the parameter p complex. We have shown in appendix E that we have instability in the same parameter regime as for $\vec{k}_0 = 0$, but that in addition we have instability when condition (5.8) is satisfied. Introducing the parameter expressions from (5.5) we find instability when

$$||\vec{k}_0| \cos\theta| > \frac{1}{2}|\vec{k}_\perp|(\frac{D}{\bar{D}} \pm 1 + \tilde{Q}\vec{k}_\perp^{-2})\sqrt{1 - \hat{Q}\vec{k}_\perp^{-2}} \tag{5.17}$$

where

$$\tilde{Q} = \frac{N_0\gamma_2}{\bar{N}a|\triangle|}, \text{ and } \hat{Q} = \frac{2\mu\gamma_2\triangle(N_0 - \bar{N})}{a(\gamma_2 N_0 + \bar{N}D\vec{k}_\perp^2)}$$

We choose the positive sign in the focussing case and the negative sign in the defocussing case.The angle between the travelling wave $\vec{k}_0$ and the perturbation $\vec{k}_\perp$ is θ.

Increasing $|\vec{k}_0|$ or increasing the angle between $\vec{k}_0$ and the transverse perturbation wave number $\vec{k}_\perp$ in the focussing case moves the instability boundary to higher transverse wavenumbers.

In the defocussing case for $D < \bar{D}$ all travelling wave solutions have a growth curve with a low wavenumber cutoff and an infinite tail. The larger $|\vec{k}_0| \cos\theta$ is the lower the cutoff moves, so that waves moving at a larger angle with the z-axis will be more unstable than waves with the same value of $|\vec{k}_0|$ but moving at a smaller angle. For $D > \bar{D}$ all travelling waves with $|\vec{k}_0| \cos\theta$ below a certain critical value will be stable, whereas waves moving with a larger angle with respect to the z-axis

will have a domain of stability with both a low and a high wavenumber cutoff. For large enough diffusion the infinite tail is removed from the growth curve of waves that are "transverse" enough. Any particular wave $\vec{k}_0$ will become stable for high enough diffusion when the lower and upper boundaries of the domain of growing wavenumbers merge. The growth curve will converge to zero for large wavenumbers, so still we have the problem of the infinitely many almost neutral wavenumbers.

5.2 The General Case

We will now consider the case when the system is not constrained along the z direction. We will in this section only consider the case $D = 0$. Observe that for purely transverse perturbations everything that was said in the last section applies. In addition we find from (5.16) that there will be instability if

$$\frac{|\vec{k}_0 \cdot \vec{k}_\perp + k_z' k_z|}{\vec{k}_\perp^2} > \frac{1}{2}(\frac{D}{\bar{D}} \pm 1 + \tilde{Q}\vec{k}_\perp^{-2})\sqrt{1 - \tilde{Q}\vec{k}_\perp^{-2}}$$

Where k_z' is the longitudinal wave number of the carrier wave and k_z is the longitudinal perturbation wavenumber. Since $k_z' \gg k_z$, $\vec{k}_\perp$ perturbations with a longitudinal component have a much larger domain of instability in wavenumber space than perturbations that are purely transverse. Not all of these wavenumbers $\vec{k} = (k_x, k_y, k_z)$ will be growing at the same rate. For the defocussing case we have under the same restrictions on $\vec{k}_\perp$ as in the previous section that the growth curve is given by

$$\lambda^\pm \approx -\frac{\beta_2 \bar{E}^2 \bar{N}}{2} \frac{\frac{\gamma_2 N_0}{\bar{N}} + \triangle(a\vec{k}_\perp^2 \pm 2a\tilde{k} \cdot \vec{k})}{\frac{\gamma_2 N_0}{\bar{N}})^2 + (a\vec{k}_\perp^2 \pm 2a\tilde{k} \cdot \vec{k})^2}$$

Note that in this general case as the earlier ones the growth curve goes asymptotically to zero for large values of $\vec{k}_\perp^2$. When it goes to zero from above we will have unstable modes with arbitrarily high wavenumbers and when it goes to zero from below we

will have the possibility that any unstable modes with lower wavenumbers will excite high wavenumbers that are stable but close to neutral. The maximum growth in the absense of diffusion occurs when

$$\frac{k_z}{|\vec{k}_\perp|} = \pm\frac{1}{2k_z'}\left(\frac{\gamma_2 N_0}{|\vec{k}_\perp|a|\triangle|\bar{N}}(1+\sqrt{1+\triangle^2}) - |\vec{k}_\perp| \mp 2|\vec{k}_0|\cos\theta\right),$$

where θ is the angle between the travelling wave $\vec{k}_0$ and the transverse part of the peturbation. Increasing the diffraction will reduce the ratio $k_z/|\vec{k}_\perp|$, so increased diffraction favors transverse over longitudinal perturbations.

Chapter 6

NUMERICAL SIMULATIONS

We have done some numerical simulations of the reduced Maxwell-Bloch system in the case of no longitudinal effects and only one transverse space dimension. We used periodic boundary conditions and discretized the Laplacian in the partial differential equations using a 6^{th} order finite difference scheme. The discrete Laplacian is computed using a library routine from MACLIB [15] The time integeration was done using the ode package SDRIV [14]. This gives us a lot of overhead in the computations but since we are working with only one space dimension the overhead is not important. We know from the discussion above that it is actually impossible to simulate the system accurately for very long because of the appearance of oscillations on the scale of the discretization. We stress that these oscillations are not the result of any particular discretization of the partial differential equations but are a property of the reduced Maxwell-Bloch equations themselves. In order to check the accuracy of the numerical scheeme one typically monitors some conserved quantity of the equations. The reduced Maxwell-Bloch equations studied in this work are dissipative and do not have any obvious conserved quantities. For special combinations of the parameters μ and γ, we do however have a quantity that is asymptotically

time invariant. This quantity is simply the total energy of the system H.

$$H = \int_V (|E|^2 + N),$$

where V is the domain where the fields are nonzero. In the numerical simulations this will be our computational interval. Let this have length L. By manipulating the reduced Maxwell-Bloch equations we find quickly that H satisfies the equation

$$\frac{dH}{dt} = -\gamma_2 H + \gamma_2 N_0 L$$

This equation will hold if we have the special relation $\gamma_2 = 2\mu$. This relation intuitively corresponds to assuming that the amount of energy gained through the pumping is the same as the energy lost through linear absorption. The equation for H clearly predicts that the total energy H decay exponentially to the constant value $N_0 L$. When we do our numerical simulations we always monitor the quantity in order to see if it behaves as expected. In addition to this quantitative test of the code we have also done some qualitative tests. These tests amount to considering special parameter values where the behavior of the solutions to the reduced Maxwell-Bloch system is known.

Figure 6.1 is a picture of the time evolution of the power spectrum for parmeter values $a = 0.05$, $\beta = 0.5, \mu = 1.0$, $\gamma_2 = 2$, $N_0 = 5$, and $\Delta = 2$ These values are not choosen for any physical reason, only for computational convenience. The linear stability analysis makes us confident that what we see in Figure 6.1 is in fact representative for the behaviour in the focussing case. The number of gridpoints in this simulations is 30. The space homogenous $k_0 = 0$ solution is perturbed by a single wavenumber in the unstable regime $k = \pi$. Initially we observe that the energy is shifted back and forth between only two wavenumbers. This is because

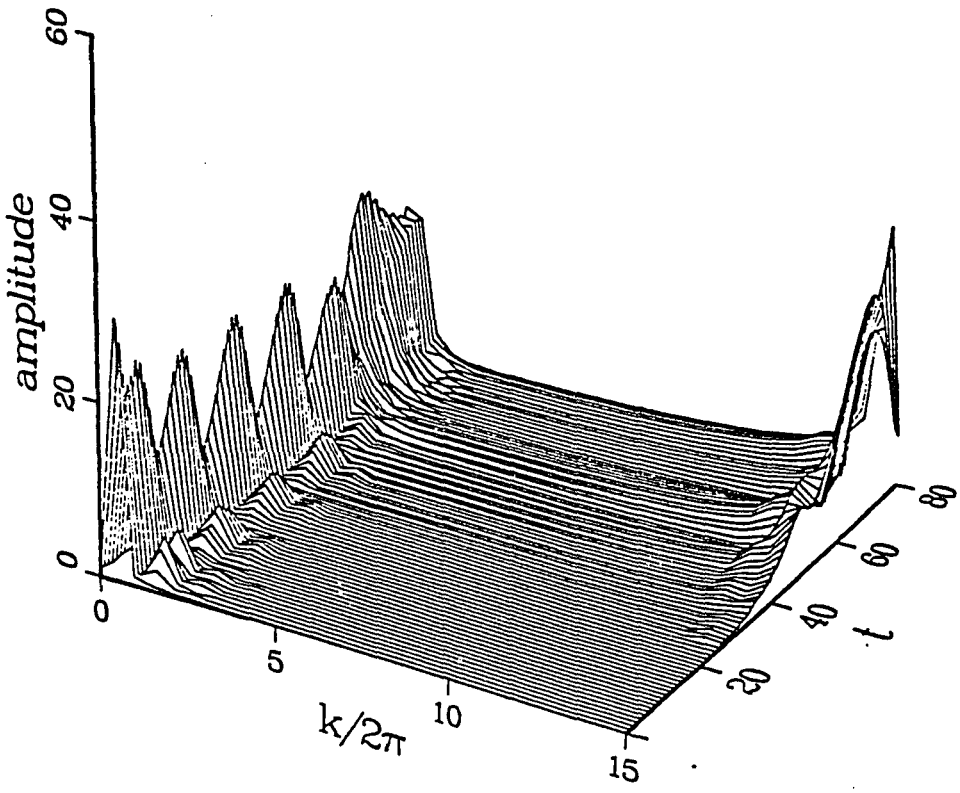

Figure 6.1: Time evolution of fourier transform of electric field. Parameter values are $a = 0.05$, $\beta = 0.5$, $\mu = 1.0$, $\gamma_2 = 2.0$, $N_0 = 5$ and $\Delta = 2$. Number of grid points $N = 60$.

with the parameter values we are using, only two unstable wave numbers actually fit inside the computational interval. As time proceeds we observe, however, that the highest wavenumber supported on the grid starts to grow and after a while start to dominate the dynamics. Of course long before that the whole simulation is highly suspect since we are not resolving the dynamics. At this point one would typically increase the number of grid points in order to resolve the dynamics or start looking for a numerical instability. In this case, because of the results from the last section, we know that this is not a numerical instability and using more grid points is actually going to make the situation worse. This was checked numerically.

Figure 6.2 is a picture of the dynamics of the inversion density as a function of

time for the same parameter values as in Figure 6.2. The number of gridpoints has been reduced to 30 so the high wavenumbers will make their apperance after longer time that in Figure 6.1. Physically one can understand the apperance of oscillations as follows : Where the inversion initially is high the refractive index is high so light is focused into this region. It grows by feeding of the inversion density by stimulated emision until the inversion becomes depleted. This weakens the refractive index and diffraction takes over and disperses the light. At the same time the inversion is growing to saturation in areas of weak electric field. This domain then starts to focus light and the process repeats. Since the condition $\gamma_2 = 2\mu$ is in effect in these simulations, asymptotically the combined energy is constant so the process can repeat indefinitely were it not for the high wave number instability.

Figure 6.3 is a picture of the power spectrum as a function of time for the same parameter values as Figure 6.1 except that Δ has the value -2. The number of grid points has been increased to 60 in this simulation. The evolution in this case is very different from the focussing case discussed above but the final result is clearly the same. All the energy in the simulation is concentrated in the highest available wavenumber. The way the energy gets to the highest wavenumber is different. In the defocussing case it seems to be cascading towards the highest wavenumber supported on the grid. We do not at the present time have a physical understanding of this behavior comparable to the above focussing case.

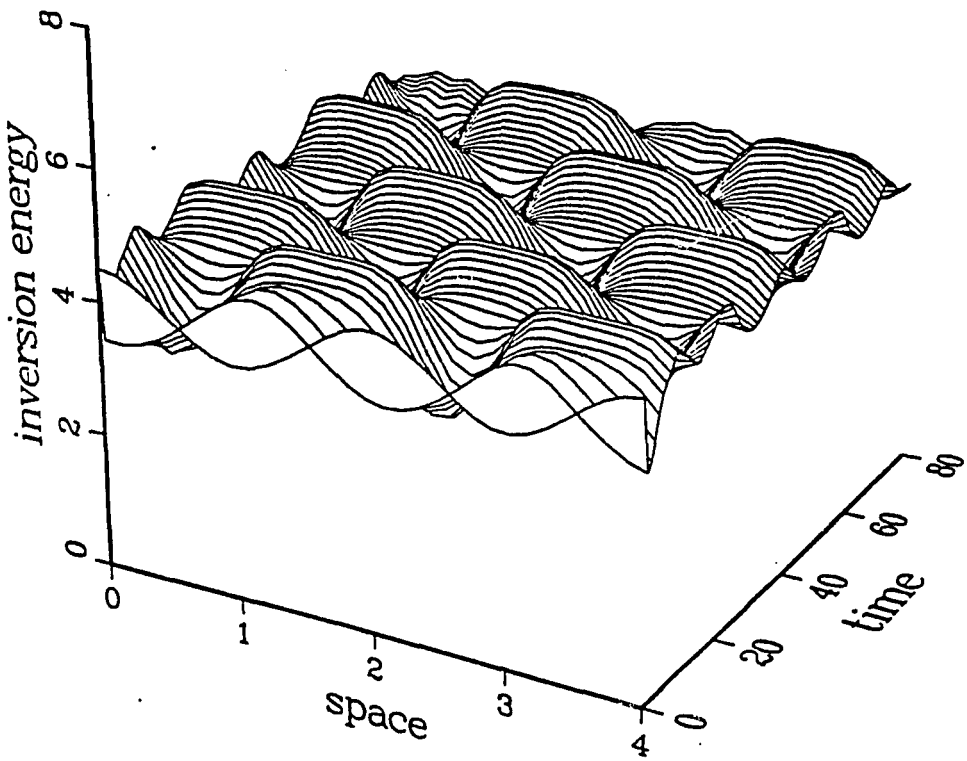

Figure 6.2: Time evolution of the inversion,focussing. Parameter values are $a = 0.05$, $\beta = 0.5$, $\mu = 1.0$, $\gamma_2 = 2.0$, $N_0 = 5$ and $\Delta = 2$. Number of grid points is $N = 30$.

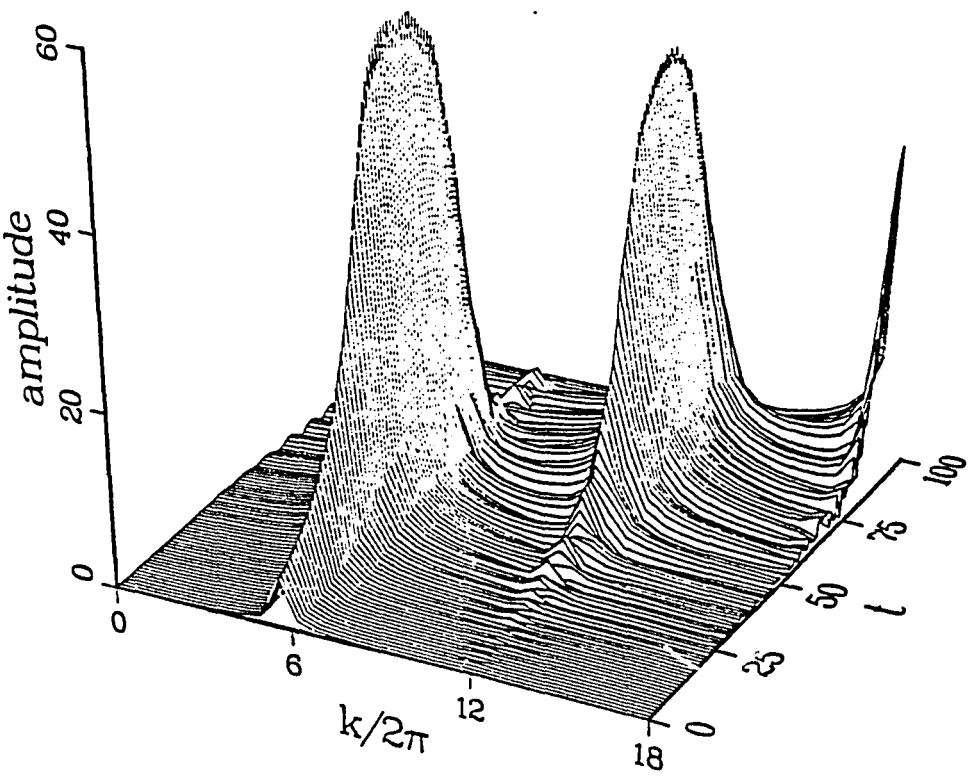

Figure 6.3: Time evolution of the fourier transform of the electric field,defocussing. Parameter values are $a = 0.05$, $\beta = 0.5$, $\mu = 1.0$, $\gamma_2 = 2.0$, $N_0 = 5$ and $\Delta = -2$. Number of grid points is $N = 60$.

Chapter 7

RELATION TO THE FULL MAXWELL-BLOCH SYSTEM

We have seen that even if studying the reduced model gives us a very good understanding of the second instability threshold, the reduced model has some very undesirable properties. The dynamics puts so much energy into the high wavenumbers that the assumptions used to derive the model surely break down. One might ask if the Maxwell-Bloch equations themselves have this bad behavior. Fortunately this is not the case (appendix F). The existence of the infinite tail of the instability in the defocussing case and the infinitely many almost neutral modes in the focussing case are artifacts of the adiabatic elimination procedure used to derive the reduced model. If we also adiabatically eliminate the inversion density we are left with a CGL type equation with a saturable nonlinearity. The only instability this equation has is the well know long wavelength Benjamin Feir instability. In the completely reduced case and in the full Maxwell-Bloch system there is no problem with high wavenumbers. The adiabatic elimination of the inversion amounts to letting γ_2 go to infinity. From condition (5.16) we see that in this limit, the high wavenumber instability moves off to infinity. By solving the linear stability problem for the full Maxwell-Bloch system numerically we have found that when the adiabatic limit is

approached the stability curve will in the focussing case developes a longer and longer tail. The growth curve for the Maxwell-Bloch system in the defocussing case always retains its high wavenumber cutoff so there will never be a problem with resolving the dynamics. Physically the adiabatic ellimination procedure means that the polarization is slaved to variation of the electric field. The polarization will respond to arbitrary fast variations in the electric field, that is high wavenumbers. This means that the interaction term P^*E will always be slowly varying and so can influence the inversion. If we do not slave the polarization to the electric field the polarization oscillatse at its natural frequency and the interaction term will vary quickly for high wavenumbers and give very small interaction. This interpretation is consistent with the results from appendix F where we find that for high wavenumbers, perturbations of the full Maxwell-Bloch equations decay with the uncoupled linear decay rates.

Chapter 8

CONCLUSIONS

In this report we have described our work studying the Maxwell-Bloch system of equations when we include transverse diffraction. We have studied the behavior of the nonlasing solution at its instability threshold using linear and nonlinear techniques. The main part of the work has been concerned with studying a reduced set of equations. For this system we have been able to get a good understanding of the stability behaviour of travelling wave solutions. In the process we have discovered that the reduced system of equations has a pathological behavior for high wavenumbers that essentially makes it impossible to simulate this system numerically to any high degree of presision since you will always end up with oscillations in the highest mode supported on the grid. This was initially rather suprising since the method used to derive the reduced system was the time honored adiabatic ellimination. We have supplemented the analytical work with numerical solutions both of the linear stability problem and the reduced system of equations.

APPENDIX A

We will in this appendix derive the model equations studied in the main text. These are the Maxwell Bloch equations with diffusion and dissipation added fenomenological. They have been derived by several authors, but are rederived here for completness.

We consider a two level atom with atom center at $\vec{r}$. Let the electron position be $\vec{r}+\vec{R}$. Assume there is an electric field $\vec{E}$ present and that the atom is so small the the electric field can be assumed to be constant across the atom. Then classically this electric field will give the electron circling the atom an potential energy of the form

$$V = -e\vec{E}\cdot\vec{R},$$

where e is the electronic charge. The electric field is evaluated at the center of the atom $\vec{r}$. We want to compute the polarization $\vec{P}$ induced by the electric field $\vec{E}(\vec{r},t)$ through a material excitation. The atom is assumed to have only two accessible energy levels denoted by a and b.This is the two-level approximation. Let ψ_a and ψ_b be the wave functions for state a and b. Under the two level approximation the electron wave function can be written as

$$\psi = a(\vec{r},t)\psi_a(\vec{R}) + b(\vec{r},t)\psi_b(\vec{R}) \tag{8.1}$$

a and b depends on the spatial coordinate $\vec{r}$ through the spatial variations of the

electric field $E(\vec{r},t)$. The state functions ψ_a and ψ_b only depend on $\vec{R}$, that is we are looking at a set of identical atomic systems. ψ_a and ψ_b are assumed to be eigenfunctions of the unperturbed hamiltonian for the atom alone with no electric field present. It follows that we are assuming the electric field to be weak compared to the atomic field strenght. This is true for most laser systems. If H_0 is the unperturbed Hamiltonian we have

$$\begin{aligned} H_0\psi_a &= \hbar\omega_a\psi_a \\ H_0\psi_b &= \hbar\omega_b\psi_b \end{aligned}$$

The eigenstates are assumed to have the following normalization

$$\int \psi_a\psi_a^* d\vec{R} = \int \psi_b\psi_b^* d\vec{R} = 1 \tag{8.2}$$

$$\int \psi_a\psi_b^* d\vec{R} = 0 \tag{8.3}$$

$$\int \vec{R}\psi_a\psi_a^* d\vec{R} = \int \vec{R}\psi_b\psi_b^* d\vec{R} = 0 \tag{8.4}$$

$$\int \psi_a e\vec{R}\psi_b^* d\vec{R} = \int \psi_a^* e\vec{R}\psi_b d\vec{R} = \xi \tag{8.5}$$

Equations (8.4) express the assumption that the eigenstates have no fixed polarization, that is they are symmetric states. In the state ψ the system will have a polarization given by

$$\langle e\vec{R}\rangle = \int \psi e\vec{R}\psi^* d\vec{R} = \vec{\xi}(ab^* + a^*b)$$

The next step is to determine how the quantity $ab^* + a^*b$ depends on the perturbing electric field $\vec{E}$ and then sum the effect over all the atoms to get the total polarization induced by $\vec{E}$. The eigenfunction ψ satisfie the schrödinger equation

$$\imath\hbar\frac{\partial\psi}{\partial t} = (H_0 + V)\psi \tag{8.6}$$

Substitute (8.1) into (8.6). We then get

$$\begin{aligned}\imath\hbar a_t\psi_a + \imath\hbar b_t\psi_b &= \hbar\omega_a a\psi_a - e\vec{E}\cdot\vec{R}a\psi_a \\ +\hbar\omega_b b\psi_b - e\vec{E}\cdot\vec{R}b\psi_b\end{aligned}$$

Multiply by ψ_a^*,ψ_b^*, integrate and use the ortogonality properties of the eigenstates in order to find equations for the amplitudes a and b.

$$a_t = -\imath\omega_a a + \imath\frac{\vec{E}\cdot\vec{\xi}}{\hbar}b \tag{8.7}$$

$$b_t = -\imath\omega_b b + \imath\frac{\vec{E}\cdot\vec{\xi}}{\hbar}a \tag{8.8}$$

As a test of these equations observe that

$$\begin{aligned}(aa^* + bb^*)_t &= a_t a^* + aa_t^* + b_t b^* + bb_t^* \\ &= (-\imath\omega_a a + \imath\frac{\vec{E}\cdot\vec{\xi}}{\hbar}b)a^* + a(\imath\omega_a a^* - \imath\frac{\vec{E}\cdot\vec{\xi}}{\hbar}b^*) \\ &\quad +(-\imath\omega_b b + \imath\frac{\vec{E}\cdot\vec{\xi}}{\hbar}b)b^* + b(\imath\omega_b b^* - \imath\frac{\vec{E}\cdot\vec{\xi}}{\hbar}a^*) \\ &= -\imath\omega_a aa^* + \imath\frac{\vec{E}\cdot\vec{\xi}}{\hbar}ba^* + \imath\omega_a aa^* - \imath\frac{\vec{E}\cdot\vec{\xi}}{\hbar}ab^* \\ &\quad -\imath\omega_b bb^* + \imath\frac{\vec{E}\cdot\vec{\xi}}{\hbar}ab^* + \imath\omega_b bb^* - \imath\frac{\vec{E}\cdot\vec{\xi}}{\hbar}a^*b \\ &= 0\end{aligned}$$

So we have conservation of probability density. By assumption only the states a and b are accesible to the system so since both these are included in expansion

of ψ we should certainly have conservation of probability density. Later we will take account of the presence of the other levels by introducing loss in the equations. Observe that the physical quantities are unchanged under the transformation

$$\begin{aligned} a &\rightarrow ae^{-\imath\frac{\omega_a+\omega_b}{2}t} \\ b &\rightarrow be^{-\imath\frac{\omega_a+\omega_b}{2}t} \end{aligned}$$

This transformation removes the ultrafine timescale from the evolution of the quantities a and b. Calling the new quantities by the same names a and b, we get the following evolution equations for the new quantities

$$a_t = -\imath\frac{\omega_{ab}}{2}a + \imath\frac{\vec{E}\cdot\vec{\xi}}{\hbar}b \tag{8.9}$$

$$b_t = \imath\frac{\omega_{ab}}{2}b + \imath\frac{\vec{E}\cdot\vec{\xi}}{\hbar}a \tag{8.10}$$

The electric field will now be assumed to be almost harmonic of the form

$$\vec{E} = \vec{F}e^{-\imath\omega' t} + \vec{F}^* e^{\imath\omega' t} \tag{8.11}$$

Where $\vec{F}$ vary slowly on the timescale $\frac{2\pi}{\omega'}$. Typically in laser applications ω_{ab} and ω' are on the order of $10^{15<}s^{-1}$. The quantity $\vec{E}\cdot\vec{\xi}/\hbar$ has dimension of frequency and is called the Rabi frequency. It is typically of the order of $10^8 - 10^{11}s^{-1}$. So if ω' is not close to ω_{ab} the off diagonal terms are only $10^{-4} - 10^{-7}$ of the diagonal terms and in this case (nonresonant interaction) the equations (8.9),(8.10) could be solved iteratively. But in the case $\omega' \approx \omega_{ab}$ we must be more careful. Assume the following multiple timescale perturbative expansion for a and b.

$$a = a_0(t)e^{-\imath\frac{\omega'}{2}t} + a_1(t)e^{-\imath\frac{\omega'}{2}t} \tag{8.12}$$

$$b = b_0(t)e^{\imath\frac{\omega'}{2}t} + b_1(t)e^{\imath\frac{\omega'}{2}t} \tag{8.13}$$

In this equation a_0,b_0 vary slowly on the timescale $2\pi/\omega'$ and a_1,b_1 vary on the fast timescale but are much smaller than a_0 ,b_0. The equations for the quantities a_1,b_1 are

$$a_{1t} = -a_{0t} - \imath\zeta a_0 + \imath\frac{\vec{F}\cdot\vec{\xi}}{\hbar}b_0 + \imath\frac{\vec{F}^*\cdot\vec{\xi}}{\hbar}b_0 e^{2\imath\omega' t} \tag{8.14}$$

$$b_{1t} = -b_{0t} - \imath\zeta b_0 + \imath\frac{\vec{F}^*\cdot\vec{\xi}}{\hbar}a_0 + \imath\frac{\vec{F}\cdot\vec{\xi}}{\hbar}a_0 e^{-2\imath\omega' t} \tag{8.15}$$

Where $\zeta = \frac{1}{2}(\omega_{ab} - \omega'_a)$ and where we have dropped second order terms like ζa_1 and ζb_1. Observe that if we integrate (8.14),(8.15) the three first terms will give secular growt of a_1 and b_1 that will violate the perturbation assumption after a finite time. The last term will not give secular growt and is ok. So in order to be consistent a_0 and b_0 must satisfy the following equations.

$$a_{0t} = -\imath\zeta a_0 + \imath\frac{\vec{F}\cdot\vec{\xi}}{\hbar}b_0 \tag{8.16}$$

$$a_{0t} = \imath\zeta b_0 + \imath\frac{\vec{F}^*\cdot\vec{\xi}}{\hbar}a_0 \tag{8.17}$$

we will now write the equations in terms of more physical variables. Define

$$\Lambda = 2a_0 b_0^*$$

$$N = aa^* - bb^*$$

N is the inversion density and the polarization is the real part of Λ.

$$\vec{p} = real\Lambda\vec{\xi}$$

The equation for Λ can be found by differentiation and substitution of the expressions for a_{0t},b_{0t} from (8.16),(8.17). We find

$$\Lambda_t + 2\imath\zeta\Lambda = -2\imath\frac{\vec{F}\cdot\vec{\xi}}{\hbar}N$$

The system is closed by computing the timevariation of N. We find

$$N_t = \frac{\imath\vec{\xi}}{\hbar}\cdot(\vec{F}\Lambda^* - \vec{F}^*\Lambda) \tag{8.18}$$

So the equations describing the microscopic material response are

$$\Lambda_t + 2\imath\zeta\Lambda = -2\imath\frac{\vec{F}\cdot\vec{\xi}}{\hbar}N \tag{8.19}$$

$$N_t = \frac{\imath\vec{\xi}}{\hbar}\cdot(\vec{F}\Lambda^* - \vec{F}^*\Lambda) \tag{8.20}$$

$$\vec{p} = real\Lambda\vec{\xi}e^{\imath\omega' t} \tag{8.21}$$

These are the Bloch equations. They allow us to express the polarization as a function of the electric field in a resonant situation. The Bloch equations for the two level atom are without any loss. Losses due to other atomic levels etc. will now be taken into account by introducing linear loss terms into the equations. Add terms Λ/T_2 and $(N+1)/T_1$ to the lefthand side of equations (8.19),(8.20). T_1 and T_2 will then be characteristic times for decay of inversion density and polarization. We will also introduce a certain amount of pumping $(N_0+1)/T_2$ to the righthand side of equation (8.20). Finally we will allow for the fact that the excitations can

be local and add a diffusive term to the lefthand side of equation (8.20). The Bloch equations with loss and diffusion added are then

$$\Lambda_t + (\frac{1}{T_2} + 2i\zeta)\Lambda = -2i\frac{\vec{F}\cdot\vec{\xi}}{\hbar}N \tag{8.22}$$

$$N_t + \frac{1}{T_1}(N - N_0) - D\nabla^2 N = \frac{i\vec{\xi}}{\hbar}\cdot(\vec{F}\Lambda^* - \vec{F}^*\Lambda) \tag{8.23}$$

$$\vec{p} = real\Lambda\vec{\xi}e^{i\omega' t} \tag{8.24}$$

Where $D > 0$ is the diffusion coeficient. The extra terms introduced into the Bloch equations above take care of effects that are the same for all atoms, the so called homogenous broadning effects. We will now for completenes consider effects that vary from atom to atom. These are local effects like the doppler effect or variable crystal environment. We will consider the case of doppler shifted frequencies. Because the atoms are moving the various atoms will experience different values of the detuning due to the doppler effect. Let $g(2\zeta)$ be the distribution of the random variable $2\zeta = \omega_{ab} - \omega'_a$. The macroscopic polarization is then given by

$$\vec{P} = \frac{1}{2}n\vec{\xi}(\langle\Lambda\rangle e^{-i\omega' t} + \langle\Lambda^*\rangle e^{i\omega' t})$$

Where n is the number density of atoms in the medium and where

$$\langle\Lambda\rangle = \int g(2\zeta)\Lambda(\vec{r}, t, \zeta)d(2\zeta)$$

The number density n is assumed to be constant. The model for the interaction between field and matter in now closed by adding the Maxwell equations in the slowly varying envelope approximation. That is we assume that the electric field is planepolarized and almost monocromatic, propagating along the z direction with a

slowly varying envelope. If F is the field envelope as in (8.11) the assumption on the electric field E translates into $F = Ge^{\imath k'z}$ and G is assumed to vary slowly in space on the scale $2\pi/k_z$. Earlier we have assumed that F vary slowly in time on the scale $2\pi/\omega'$ so thie also applies to G. Geometrically these asumptions amounts to considering plane polarized waves that are travelling along an axis z or are travelling with a small angle to this axis. The above assumptions applied to Maxwell's equations give

$$\nabla_T^2 G + 2\imath k' \frac{\partial G}{\partial z} + 2\imath \frac{\omega'}{c^2}\left(\frac{\partial G}{\partial t} + 2\pi\sigma G\right) = \frac{2\pi n_0 \varrho \omega'}{c^2}\imath\langle\lambda\rangle \tag{8.25}$$

Where a linear loss factor has been added in order to simulate various linear loss mechanisms,n_0 is the number density of atoms and where we have defined λ by $\lambda = \Lambda e^{-\imath k'z}$. The diffraction term $\nabla_\perp^2$ includes only derivatives in the transverse x and y directions. The Maxwell-Bloch system of equations can be written as

$$\frac{\partial G}{\partial t} + v_z \frac{\partial G}{\partial z} + \mu G - \imath a \nabla_\perp^2 G = \beta_1 P \tag{8.26}$$

$$\frac{\partial P}{\partial t} + \gamma_1(1 + \imath\Delta)P = \beta_2 GN \tag{8.27}$$

$$\frac{\partial N}{\partial t} + \gamma_2(N - N_0) - D\nabla^2 N = -\frac{1}{2}(GP^* + G^*P) \tag{8.28}$$

Where we have defined

$$\gamma_1 = \frac{1}{T_1},\ \beta_1 = \pi n_0 \varrho \omega'$$

$$\gamma_2 = \frac{1}{T_2},\ \beta_2 = \frac{2\varrho}{\hbar},\ \triangle = 2T_2\zeta$$
$$\mu = 2\pi\sigma,\ a = \frac{c^2}{2\omega'},\ v_z = \frac{c^2 k_z'}{\omega'}, P = \imath\lambda$$

In the main text we also study the reduced model we get by elliminating P adiabatically. The reduced system can be written in the form

$$\frac{\partial G}{\partial t} + v_z\frac{\partial G}{\partial z} + \mu G - \frac{1}{2}\beta(1-\imath\triangle)GN' - \imath a\nabla_\perp^2 G = 0 \qquad (8.29)$$
$$\frac{\partial N'}{\partial t} + \gamma_2(N'-N_0') - D\nabla^2 N' + \beta|G|^2 N' \qquad (8.30)$$

Where we have $\beta = \beta_2^2/(\gamma_1(1+\triangle^2))$ and where N' now essentially is the inversion energy density $N' = \pi n_0\hbar\omega' N$. We have assumed that there are no inhomogenous broadning effects so the averaging has been dropped from the field equation.

This completes the derivation of the Maxwell-Bloch system of equations for the interaction between a electrix field and a two level atom including dissipative,diffusive and Doppler effects. In the main text we always consider the case when there are no doppler effects. That is $g(x)$ is a delta distribution centred at a certain resonance frequency.

APPENDIX B

We will in this appendix do the linear stability analysis at the lasing threshold for the full Maxwell-Bloch system. The model is

$$E_t + v_z E_z + \mu E - \imath a \nabla_\perp^2 E = \beta_1 P \tag{8.31}$$

$$P_t + \gamma_1(1 + \imath\triangle)P = \beta_2 EN \tag{8.32}$$

$$N_t + \gamma_2(N - N_0) - D\nabla^2 N = -\beta_2 \frac{1}{2}(P^* E + P E^*) \tag{8.33}$$

Where we have changed notation from appendix A, writing E for the electric field envelope and removed the $'$ from the inversion energy density. The system has as we have seen in the main text a nonlasing solution of the form $E = P = 0, N = N_0$. We will now linearize the above system around this solutions. For the linearization write $E = e, P = p, N = N_0 + n$, where p,e,n are small perturbations. The linearized system for p,e and n is

$$e_t + v_z e_z + \mu e - \imath a \nabla_\perp^2 e = \beta_1 p \tag{8.34}$$

$$p_t + \gamma_1(1 + \imath\triangle)p = \beta_2 e N_0 \tag{8.35}$$

$$n_t + \gamma_2 n - D\nabla^2 n = 0 \tag{8.36}$$

With no loss of generality we can assume that the solution is of the form

$$\begin{pmatrix} e \\ p \\ n \end{pmatrix} = \begin{pmatrix} e_0 \\ p_0 \\ n_0 \end{pmatrix} e^{\lambda t + \imath \vec{k} \cdot \vec{r}}$$

where $\vec{k} = (\vec{k}_\perp, k_z)$ is the perturbation wavenumber and $\vec{r} = (x, y, z)$ is the position vector. We then get the following matrix eigenvalue problem

$$\begin{pmatrix} \lambda + \mu + \imath v_z k_z + \imath a k_\perp^2 & -\beta_1 & 0 \\ -\beta_2 N_0 & \lambda + \gamma_1(1 + \imath\Delta) & 0 \\ 0 & 0 & \lambda + \gamma_2 + D\vec{k}^2 \end{pmatrix} \begin{pmatrix} e_0 \\ p_0 \\ n_0 \end{pmatrix} \tag{8.37}$$

So the eigenvalue equation becomes

$$(\lambda + \gamma_2 + D\vec{k}^2)(\lambda + \imath v_z k_z + \mu + \imath a \vec{k}_\perp^2)(\lambda + \gamma_1(1 + \imath\Delta)) - \beta_1\beta_2 N_0 = 0 \tag{8.38}$$

One eigenvalue is clearly $\lambda = -\gamma_2 - D\vec{k}^2$. This eigenvalue does not give any growth. The rest of the eigenvalues are determined from

$$(\lambda + \mu + \imath v_z k_z + \imath a k_\perp^2)(\lambda + \gamma_1(1 + \imath\Delta)) = \beta_1\beta_2 N_0 \tag{8.39}$$

Physically N_0 is the pumping of the system. On physical grounds we expect the system to be nonlasing as N_0 start increasing from 0 until the threshold for lasing is reached. At this value of the pumping the laser turns on. So in terms of the eigenvalue problem (8.39) all the eigenvalues will start in the left halfplane when N_0 is zero and when N_0 increases at least one of the eigenvalues will cross over into the right halfplane when the lasing threshold is reached. So the lasing threshold is determined as the value of N_0 that gives purely imaginary roots of (8.39). Inserting $\lambda = \imath s$ with s real into the eigenvalue equation (8.39) we find by separating real and imaginary parts that

$$\mu\gamma_1 - (s + v_z k_z + a k_\perp^2)(s + \gamma_1 \triangle) = \beta_1 \beta_2 N_0 \tag{8.40}$$

$$\gamma_1(s + v_z k_z + a k_\perp^2) + \mu(s + \gamma_1 \triangle) = 0 \tag{8.41}$$

From equation (8.40) we find

$$s = -\frac{\gamma_1(\mu\triangle + v_z k_z + a k_\perp^2)}{\gamma_1 + \mu} \tag{8.42}$$

Substitute (8.42) into (8.40). We then get an expression for the lasing threshold

$$N_{th} = \frac{\mu\gamma_1}{\beta_1\beta_2}(1 + (\frac{\gamma_1\triangle - v_z k_z - a k_\perp^2}{\gamma_1 + \mu})^2) \tag{8.43}$$

This formula display exactly at which value N_{th} a choosen wavenumber k will go unstable.

APPENDIX C

In this appendix we will derive the linear system describing the stability of the lasing solutions of the full Maxwell-Bloch system described in the main text. We have seen in the main text that above the first lasing threshold there exist exact travelling wave solutions to the full Maxwell-Bloch system of equations. They were of the form

$$E = \bar{E}e^{i(\vec{k}_0\cdot\vec{x}+\delta t)} \tag{8.44}$$

$$P = \bar{P}e^{i(\vec{k}_0\cdot\vec{x}+\delta t)} \tag{8.45}$$

$$N = \bar{N} \tag{8.46}$$

The quantities $\bar{E}, \bar{P}, \delta$ and $\bar{N}$ are defined in the main text.Where $\vec{k}_0 = (k_{0x}, k_{0y})$ and $\vec{x} = (x, y)$. For the linearization assume that the fields are of the form

$$E = (\bar{E} + e)e^{i(\vec{k}_0\cdot\vec{x}+\delta t)} \tag{8.47}$$

$$P = (\bar{P} + p)e^{i(\vec{k}_0\cdot\vec{x}+\delta t)} \tag{8.48}$$

$$N = \bar{N} + n \tag{8.49}$$

Where as usual e, p and n are small perturbations. Inserting (8.47), (8.48) and (8.49) into the Maxwell-Bloch equations we find the following linearized system for

the quantites e,p and n.

$$
\begin{aligned}
e_t + v_z e_z + (\mu + \imath(\delta + a\vec{k}_0^2))e &= -2ak_{0x}e_x - 2ak_{0y}e_y + \imath a\nabla_\perp^2 e + \beta_1 p \quad (8.50)\\
p_t + (\gamma_1 + \imath(\delta + \gamma_1\triangle))p &= \beta_2(\bar{N}e + \bar{E}n) \quad (8.51)\\
n_t + \gamma_2 n - D\nabla^2 n &= -\beta_2\bar{E}(p^* + \alpha^* e) \quad (8.52)
\end{aligned}
$$

Where we have used the fact that $\bar{P} = \alpha\bar{E}$ with $\alpha = (\mu + \imath(\delta + a\vec{k}_0^2))/\beta_1$. Both in numerical and asymptotic calculations we will use the linear system written in real form. This is achived by writing the fields as sums of real and imaginary quantities

$$
\begin{aligned}
e &= e^r + \imath e^i\\
p &= p^r + \imath p^i
\end{aligned}
$$

A simple calculation now give the linear system in real form

$$
\begin{aligned}
e_t^r + v_z e_z^r + \eta_1^r e^r - \eta_1^i e^i &= -2ak_{0x}e_x^r - 2ak_{0y}e_y^r - a\nabla_\perp^2 e^i + \beta_1 p^r\\
e_t^i + v_z e_z^i + \eta_1^r e^i + \eta_1^i e^r &= -2ak_{0x}e_x^i - 2ak_{0y}e_y^i + a\nabla_\perp^2 e^r + \beta_1 p^i\\
p_t^r + \eta_2^r p^r - \eta_2^i p^i &= \beta_2\bar{N}e^r + \beta_2\bar{E}n\\
p_t^i + \eta_2^r p^i + \eta_2^i p^r &= \beta_2\bar{N}e^i\\
n_t + \gamma_2 n - D\nabla^2 n &= -\beta_2\bar{E}(p^r + \alpha^r e^r + \alpha^i e^i)
\end{aligned}
$$

Where we have defined the constants $\eta_1 = \mu + \imath(a\vec{k}_0^2 + \delta)$ and $\eta_2 = \gamma_1 + \imath(\delta + \gamma_1\triangle)$. We can without loss of generality assume that the solution of the linear system is of the form

$$\begin{pmatrix} er \\ e^i \\ p^r \\ p^i \\ n \end{pmatrix} = \begin{pmatrix} e_0^r \\ e_0^i \\ p_0^r \\ p_0^i \\ n_0 \end{pmatrix} e^{(\lambda t + \imath \vec{k} \cdot \vec{r})}$$

Where now $\vec{k} = (k_x, k_y, k_z)$ is the perturbation wavenumber and $\vec{r} = (x, y, z)$ is the position vector. Inserting this form of the solution into the real form of the linearized equations we find that the matrix of the resulting eigenvalue problem is

$$\begin{pmatrix} \eta_1^r - 2a\tilde{k} \cdot \vec{k} & -\eta_1^i - a\vec{k}_\perp^2 & -\beta_1 & 0 & 0 \\ \eta_1^i + a\vec{k}_\perp^2 & \eta_1^r - 2a\tilde{k} \cdot \vec{k} & 0 & -\beta_1 & 0 \\ -\beta_2 \bar{N} & 0 & \eta_2^r & -\eta_2^i & -\beta_2 \bar{E} \\ 0 & -\beta_2 \bar{N} & \eta_2^i & \eta_2^r & 0 \\ \beta_2 \alpha^r \bar{E} & \beta_2 \alpha^i \bar{E} & \beta_2 \bar{E} & 0 & \gamma_2 + D\vec{k}^2 \end{pmatrix} \tag{8.53}$$

Where $\tilde{k} = (\vec{k}_0, k_z')$. So $\tilde{k}$ is the wavevector of the real electric field, not only the envelope. The slowly varying envelope approximation used in deriving the field equation implies that $k_z' \gg |\vec{k}_0|$ so the waves are all travelling at very small angles to the z axis.

APPENDIX D

In this appendix we will derive the linearization of the reduced Maxwell- Bloch system around the travelling wave solutions. The reduced system of equations is

$$E_t + v_z E_z + \mu E - \frac{1}{2}\beta(1 - \imath\triangle)EN - \imath a\nabla_\perp^2 E = 0 \tag{8.54}$$

$$N_t + \gamma_2(N - N_0) + \beta|E|^2 N - D\nabla^2 N = 0 \tag{8.55}$$

In the main text we have found that that the system (8.54),(8.55) has travelling wave solutions of the form

$$E = \bar{E}e^{\imath(\vec{k}_0\cdot\vec{x}-\Omega t)}$$

$$N = \bar{N}$$

Where $\bar{E}$ and $\bar{N}$ are defined in the main text and as in appendix C $\vec{k}_0 = (k_x, k_y)$ and $\vec{x} = (x, y)$. For the linearization we will as usual assume solutions of the form

$$E = (\bar{E} + e)e^{\imath(\vec{k}_0\cdot\vec{x}-\Omega t)} \tag{8.56}$$

$$N = \bar{N} + n \tag{8.57}$$

Where e and n are small perturbations. Inserting the assumptions (8.56),(8.57) into (8.54),(8.55) we find after dropping nonlinear terms that

$$e_t + v_z e_z = \frac{1}{2}\beta(1 - \imath\Delta)\bar{E}n - 2ak_{0x}e_x - 2ak_{0y}e_y + \imath a\nabla_\perp^2 e \tag{8.58}$$

$$n_t = -(\gamma_2 + \beta\bar{E}^2)n - \beta\bar{E}\bar{N}(e + e^*) + D\nabla^2 n \tag{8.59}$$

Writing $e = e^r + \imath e^i$ we find that the linear system for real and imaginary variables is

$$\begin{aligned} e_t^r &= \frac{1}{2}\beta\bar{E}n - v_z e_z^r - 2ak_{0x}e_x^r - 2ak_{0y}e_y^r - a\nabla_\perp^2 e^i \\ e_t^r &= -\frac{1}{2}\beta\bar{E}\Delta n - v_z e_z^i - 2ak_{0x}e_x^i - 2ak_{0y}e_y^i + a\nabla_\perp^2 e^r \\ n_t &= -(\gamma_2 + \beta\bar{E}^2)n - 2\beta\bar{E}\bar{N}e^r + D\nabla^2 n \end{aligned}$$

As usual because of linearity and constant coefficients we can without loss of generality assume that the solutions of this system are of the form

$$\begin{pmatrix} e^r \\ e^i \\ n \end{pmatrix} = \begin{pmatrix} e_0^r \\ e_0^i \\ n_0 \end{pmatrix} e^{(\lambda t + \imath\vec{k}\cdot\vec{x})}$$

We then find that the matrix of the resulting linear eigenvalue problem is

$$\begin{pmatrix} -2a\imath\tilde{k}\cdot\vec{k} & a\vec{k}_\perp^2 & \frac{1}{2}\beta\bar{E} \\ -a\vec{k}_\perp^2 & -2a\imath\tilde{k}\cdot\vec{k} & -\frac{1}{2}\beta\Delta\bar{E} \\ -2\beta\bar{E}\bar{N} & 0 & -(\gamma_2 + \beta\bar{E}^2 + D\vec{k}^2) \end{pmatrix} \tag{8.60}$$

Where $\tilde{k} = (\vec{k}_0, k_z')$ and the assumption is that $k_z' \gg |\vec{k}_0|$. So the characteristic polynomial corresponding to this matrix is

$$(s + p)(s^2 + 1) - q(\Delta - s) = 0 \tag{8.61}$$

Where we have defined the following quantities

$$p = \frac{1}{a\vec{k}_\perp^2}(\gamma_2 + \beta\bar{E}^2 + D\vec{k}^2) - 2i\frac{\tilde{k}\cdot\vec{k}}{\vec{k}_\perp^2} \tag{8.62}$$

$$q = \frac{\beta^2\bar{E}^2\bar{N}}{(a\vec{k}_\perp^2)^2} \tag{8.63}$$

$$s = \frac{\lambda}{a\vec{k}_\perp^2} + 2i\frac{\tilde{k}\cdot\vec{k}}{\vec{k}_\perp^2} \tag{8.64}$$

And λ is the eigenvalue of the matrix (8.60). Observe that the relation between s and λ is such that there are eigenvalues with positive real part if and only if equation (8.61) has roots with positive realpart. Also note that p_r,q both are positive quantities.

APPENDIX E

We will in this appendix investigate the roots of the characteristic polynomial from appendix D. Conditions for existence of roots with positive real part will be derived. Recall from appendix D equation (8.61) that the characteristic polynomial can be reduced to

$$(s+p)(s^2+1) - q(\Delta - s) = 0 \tag{8.65}$$

We will first consider the case $p_i = 0$ so p is real. Later we will use the results for this case to study the case of p complex.

Case p real

We will first find a necessary and sufficient condition for when (8.65) has positive real roots.This condition can be decided by a simple graphical analysis of (8.65). Write (8.65) in the following form

$$s^2 + 1 = q\frac{\Delta - s}{p_r + s} \tag{8.66}$$

Graphing the left hand side and right hand side of (8.66), it is clear from this picture that the two curves will cross for positive s,and as a consequence there will exist positive roots of (8.65), only if

$$\frac{q\Delta}{p_r} > 1 \tag{8.67}$$

Next let us find the conditions for (8.65) having complex roots with positive realpart. This problem will also be solved using graphical analysis but first we must write the problem as a single real equation. Write $s = s_r + \imath s_i$.Separation of (8.65) into real and imaginary form gives

$$(s_r^2 - s_i^2 + 1)(s_r + p_r) - 2s_r s_i^2 - q(\Delta - s_r) = 0 \tag{8.68}$$

$$(s_r^2 - s_i^2 + 1) + 2s_r(p_r + s_r) + q = 0 \tag{8.69}$$

Solve (8.69) with respect to s_i^2 and substitute into (8.68). We then get the following real equation for the realpart s_r of the root.

$$-(s_r^2 + 1) = (s_r + p_r)(3s_r + p_r) + q + q\frac{p_r + \Delta}{2s_r} \tag{8.70}$$

Graphing the left hand side and right hand side of (8.70), it is clear that the condition for existence of complex roots with positive real part is

$$p_r + \Delta < 0 \tag{8.71}$$

So in summary we have that if p is real then we will have roots with positive realpart if and only if

$$\frac{q\Delta}{p_r} > 1 \tag{8.72}$$

$$p_r + \Delta < 0 \tag{8.73}$$

Case p complex

We will now investigate the general case when p is complex. We will do this by considering how the roots move as a function of p_i. First we will prove that if there are roots with positive realpart for $p_i = 0$, then there will exist roots with positive realpart for all $p_i \neq 0$. Observe that when p is complex equation (8.65) will only have real roots if $p_i(s^2 + 1) = 0$. So there are real roots only when $p_i = 0$. So when p_i vary roots will be confined to the upper or lower halfplane. They can not cross from upper to lower or opposite for nonzero p_i. Let us next ask when and for which values of p_i the roots can cross from left to right halfplane or opposite. When they cross there will be a purely imaginary root $s = \imath t$ of the characteristic polynomial (8.65). So we must have

$$\begin{aligned} (1-t^2)p_r - q\triangle &= 0 \\ (1-t^2)(p_i + t) + qt &= 0 \end{aligned}$$

Solving this system we find

$$t = \pm\sqrt{\frac{p_r - q\triangle}{p_r}} \tag{8.74}$$

$$p_i = \mp\frac{1}{\triangle}\sqrt{\frac{p_r - q\triangle}{p_r}}(p_r + \triangle) \tag{8.75}$$

Let us first consider the case when (8.72) is satisfied. Equation (8.65) then has one real root in the right halfplane when $p_i = 0$. When (8.72) is satisfied t in (8.74) is imaginary. Since by assumption t must be real, there are no purely imaginary

solutions for this case. So the root in the right halfplane can not cross over to the left halfplane for any p_i. So there will exist a root with positive realpart for all p_i for this case. Next consider the case when (8.73) is satisfied. When $p_i = 0$ there are one root in the first quadrant and one root in the fourth quadrant. When we let p_i increase through positive values the root in the lower halfplane will because of (8.75) cross over into the left halfplane when

$$p_i = \frac{1}{\Delta}\sqrt{\frac{p_r - q\Delta}{p_r}}(p_r + \Delta)$$

It will cross at the point

$$(0, -\sqrt{\frac{p_r - q\Delta}{p_r}})$$

The root in the first quadrant will for all positive values of p_i be constrained to stay in the first quadrant, and so there will for all positive values of p_i exist a root with positive realpart. A similar argument for negative p_i proves that there will always exist a root in the fourth quadrant for any negative p_i.

So we can conclude that if (8.72) or (8.73) is satisfied there will exist roots with positive realpart for all values of p_i.

Finally assume that neither condition (8.72) nor (8.73) is satisfied. Then all roots are in the left halfplane for $p_i = 0$. From equations (8.74) and (8.75) we observe that for

$$|p_i| > p_0 = \frac{1}{|\Delta|}\sqrt{\frac{p_r - q\Delta}{p_r}}(p_r + \Delta) \tag{8.76}$$

At least one root will have crossed over into the right halfplane.So there will exist at least one root with positive realpart if $p_i > p_0$. Inequalities (8.72),(8.73)

and (8.76) give the exact conditions for when equation (8.65) has roots with positive realpart.

APPENDIX F

We will in this appendix investigate the asymptotic behaviour of the growtrate for large wavenumbers in the reduced and full model.

Reduced model

We have seen in appendix D that the characteristic polynomial for the reduced case can be written as

$$(s+p)(s^2+1) - q(\Delta - s) = 0 \tag{8.77}$$

Where we have defined the following quantities

$$p = \frac{1}{a\vec{k}_\perp^2}(\gamma_2 + \beta\bar{E}^2 + D\vec{k}^2) - 2\imath\frac{\tilde{k}\cdot\vec{k}}{\vec{k}_\perp^2} \tag{8.78}$$

$$q = \frac{\beta^2\bar{E}^2\bar{N}}{(a\vec{k}_\perp^2)^2} \tag{8.79}$$

$$s = \frac{\lambda}{a\vec{k}_\perp^2} + 2\imath\frac{\tilde{k}\cdot\vec{k}}{\vec{k}_\perp^2} \tag{8.80}$$

We are interested in computing an approximation to the real parts of the roots of (8.77) in the limit where the first term in (8.77) dominates the second. This will happend if $q \ll 1$. In fact requiring that $q \ll 1$ we find that a rough condition determining the current case is

$$\vec{k}_\perp^4 \gg \frac{\beta\gamma_2}{a^2}(N_0 - \bar{N})$$

Note that depending on the size of various parameters the above condition does not restrict the wavenumbers to any large degree. With the condition $q \ll 1$ satisfied we find that the roots of the equation (8.77) are to the lowest approximation determined by

$$(s^2 + 1)(s + p_r) \approx 0$$

So the first order approximations to the roots are

$$s = -p_r \tag{8.81}$$

$$s = \pm\imath \tag{8.82}$$

Equation (8.81) give the desired approximation for the real root of (8.77). For (8.82) we must compute the correction to the root in order to find what the realpart is. Write $s = \pm\imath + h_\pm$ where $h_\pm$ is a small correction. Substitute this into (8.77) and expand, keeping only first order terms. We find

$$h_\pm = -\frac{q}{2}\frac{1 \pm \imath\triangle}{p^r + \imath(\pm 1 + p_i)}$$

So the realpart of the second root is approximately

$$r = -\frac{q}{2}\frac{p_r + \triangle(1 \pm p_i)}{p_r^2 + (1 \pm p_i)^2}$$

Using the definitions (8.78),(8.79) and (8.80) we find that asymptotic expressions for the realpart of the eigenvalues are

$$\lambda_1 = -(\gamma_2 + \beta\bar{E}^2 + D\vec{k}^2) \tag{8.83}$$

$$\lambda_2^{\pm} = -\frac{\beta^2\bar{E}^2\bar{N}}{2}\frac{(\frac{\gamma_2 N_0}{\bar{N}} + D\vec{k}^2) + \triangle(a\vec{k}_\perp^2 \pm 2a\tilde{k}\cdot\vec{k})}{(\frac{\gamma_2 N_0}{\bar{N}} + D\vec{k}^2)^2 + (a\vec{k}_\perp^2 \pm 2a\tilde{k}\cdot\vec{k})^2} \tag{8.84}$$

The last eigenvalue is positive for large $\vec{k}_\perp$ if $\triangle$ negative. This is the case discussed as defocussing in the main text. Note that the formula for λ_2 has a maximum in the defocussing case. In fact λ_2 has maximum positive value when (D=0)

$$a\vec{k}_\perp^2 \pm 2a\tilde{k}\cdot\vec{k} = \frac{\gamma_2 N_0}{|\triangle|\bar{N}}(1+\sqrt{1+\triangle^2}) \tag{8.85}$$

Full model

We will now turn to the eigenvalues of the full system. The matrix for the linearized full Maxwell-Bloch system was derived in appendix C.

$$\begin{pmatrix} \eta_1^r - 2a\tilde{k}\cdot\vec{k} & -\eta_1^i - a\vec{k}_\perp^2 & -\beta_1 & 0 & 0 \\ \eta_1^i + a\vec{k}_\perp^2 & \eta_1^r - 2a\tilde{k}\cdot\vec{k} & 0 & -\beta_1 & 0 \\ -\beta_2\bar{N} & 0 & \eta_2^r & -\eta_2^i & -\beta_2\bar{E} \\ 0 & -\beta_2\bar{N} & \eta_2^i & \eta_2^r & 0 \\ \beta_2\alpha^r\bar{E} & \beta_2\alpha^i\bar{E} & \beta_2\bar{E} & 0 & \gamma_2 + D\vec{k}^2 \end{pmatrix} \tag{8.86}$$

The entries in this matrix are defined in appendix C. For us it is only important to notice that there is no implicit $\vec{k}$ dependence in the entries. So for large $\vec{k}$ we can write (8.86) as

$$A = A_0 + A_1 \tag{8.87}$$

Where we have defined A_0 and A_1 as

$$\begin{pmatrix} 2\imath\tilde{k}\cdot\vec{k} & a\vec{k}_\perp^2 & 0 & 0 & 0 \\ -a\vec{k}^2 & 2\imath\tilde{k}\cdot\vec{k} & 0 & 0 & 0 \\ 0 & 0 & 0 & 0 & 0 \\ 0 & 0 & 0 & 0 & 0 \\ 0 & 0 & 0 & 0 & 0 \end{pmatrix} \tag{8.88}$$

and

$$\begin{pmatrix} -\eta_1^r & \eta_1^i & \beta_1 & 0 & 0 \\ -\eta_1^i & -\eta_1^r & 0 & \beta_1 & 0 \\ \beta_2\bar{N} & 0 & -\eta_2^r & \eta_2^i & \beta_2\bar{E} \\ 0 & \beta_2\bar{N} & -\eta_2^i & -\eta_2^r & 0 \\ -\beta_2\alpha^r\bar{E} & -\beta_2\alpha^i\bar{E} & -\beta_2\bar{E} & 0 & -\gamma_2 - D\vec{k}^2 \end{pmatrix} \tag{8.89}$$

The eigenvalues of A_0 are $\lambda = 0$, three-fold degenerate and $\lambda = \pm\imath ak^2 + 2\imath\tilde{k}\cdot\vec{k}$ nondegenerate. We can now compute the corrections to these eigenvalues using perturbation methods. Let us first do the calculation for the eigenvalue $\lambda = \imath ak^2 + 2\imath\tilde{k}\cdot\vec{k}$. Since it is nondegenerate we have the following classical formula for the correction λ

$$\Lambda = \frac{\langle \vec{U}_0, A_1\vec{V}_0\rangle^*}{\langle \vec{U}_0, \vec{V}_0\rangle} \tag{8.90}$$

Where $\langle\ ,\ \rangle$ is the standard hermitean inner product and V_0 is eigenvector of $(A_0 - (\imath\vec{k}_\perp^2 + 2\imath\tilde{k}\cdot\vec{k})I)$ and U_0 is eigenvector of the hermitean conjugate of $(A_0 - \imath a\vec{k}_\perp^2 2\imath\tilde{k}\cdot\vec{k})I)$. A little calculation gives

$$\vec{V}_0 = \begin{pmatrix} 1 \\ \imath \\ 0 \\ 0 \\ 0 \end{pmatrix}$$

And $\vec{U}_0 = \vec{V}_0$. Inserting the values for $\vec{V}_0$ and $\vec{U}_0$ into (8.90) we find that the real correction to both $\pm\imath ak^2 + 2\imath\tilde{k}\cdot\vec{k}$ is

$$\Lambda_r = -\mu \tag{8.91}$$

Let us next consider the three-fold degenerate zero eigenvalue. Again the computation of the correction to the eigenvalue is given by a classical calculation. We find that the correction the eigenvectors is

$$\vec{V} = \sum_{i=3}^{5} a_i e_i$$

where the a_i solves a new smaller linear system with matrix

$$\begin{pmatrix} -\eta_2^r & \eta_2^i & \beta_2 \bar{E} \\ -\eta_2^i & -\eta_2^r & 0 \\ -\beta_2 \bar{E} & 0 & -\gamma_2 - D\vec{k}^2 \end{pmatrix} \tag{8.92}$$

We will only consider the case when we are close to threshold $\bar{E} \approx 0$. We then have from (8.92) that the real corrections to the three-fold zero eigenvalue are

$$\lambda = -\gamma_2 - D\vec{k}^2 \tag{8.93}$$

$$\lambda = -\gamma_1 \tag{8.94}$$

APPENDIX G

We will in this section derive the amplitude equations close to the lasing threshold in the full Maxwell-Bloch system in the case of one space dimension. We will write the solution of the Maxwell-Bloch system close to threshold as a sum of a number of active modes derived from the linear stability analysis in appendix B and passive modes. Evolution equations will then be imposed on the amplitudes of the active modes by requiring that the linear equations for the passive modes does have a solution at each order. Our main reference for this metod is [7]. The calculation of the amplitude equations have several distinct steps to it. In order not to loose ourselves in algebra we will present each step in the calculation in separate sections.

Step 1

The method is applied to problems of the form

$$L(\frac{\partial}{\partial t}, \frac{\partial}{\partial x})v = N(v)$$

Where L is linear in its arguments and N is some nonlinear operator that is a small perturbation on L. Let us identify L and N for the case of the Maxwell-Bloch equations. From Appendix B we have

$$E_t + \mu E - \imath a \partial_{xx} E = \beta_1 P \tag{8.95}$$

$$P_t + \gamma_1(1 + \imath\Delta)P = \beta_2 E(n + N_0) \tag{8.96}$$

$$n_t + \gamma_2 n - D\partial_{xx} n = -\beta_2 \frac{1}{2}(P^* E + P E^*) \tag{8.97}$$

Where we in preparation for the following calculations have defined $n = N - N_0$. Define

$$v = \begin{pmatrix} E \\ P \\ N \end{pmatrix}$$

Then we select L and N to be

$$L(\partial_t, \partial_{xx}, N_0)v = \begin{pmatrix} \partial_t + \mu - \imath a\partial_{xx} & -\beta_1 & 0 \\ -\beta_2 N_0 & \partial_t + \gamma_1(1 + \imath\Delta) & 0 \\ 0 & 0 & \partial_t + \gamma_2 - D\partial_{xx} \end{pmatrix} \tag{8.98}$$

$$Nv = \begin{pmatrix} 0 \\ \beta_2 E n \\ -\frac{1}{2}\beta_2(P^* E + P E^*) \end{pmatrix} \tag{8.99}$$

This completes step 1.

Step 2

Let

$$A = L(\imath\delta^c, \pm\imath k^c, N_0^c)$$

Where N_0^c is the threshold value of the pumping discussed in the main text ,k^c is the critical wavenumber and $\imath\delta^c$ is the critical frequency.We will at a later step need to know the kernel of A and A^* where the $*$ means hermitean conjugate. The kernel of A will give us the eigenvectors of the linearized Maxwell-Bloch system. The kernel of A is determined from

$$\begin{pmatrix} \mu + \imath a k^{c2} + \imath \delta^c & -\beta_1 & 0 \\ -\beta_2 N_0^c & \gamma_1(1 + \imath\triangle) + \imath\delta^c & 0 \\ 0 & 0 & \gamma_2 + D k^{c2} + \imath \delta^c \end{pmatrix} V_0 = 0$$

So we find that

$$V_0 = \begin{pmatrix} 1 \\ x_0 \\ 0 \end{pmatrix} \tag{8.100}$$

Where $x_0 = (\mu + \imath(\delta^c + a k^{c2}))/\beta_1$. So V_0 is basis for the kernel of A. The kernel of the adjoint is determined by

$$\begin{pmatrix} \mu - \imath a k^{c2} - \imath \delta^c & -\beta_2 N_0^c & 0 \\ -\beta_1 & \gamma_1(1 - \imath\triangle) - \imath\delta^c & 0 \\ 0 & 0 & \gamma_2 + D k^{c2} - \imath \delta^c \end{pmatrix} U_0 = 0$$

So we find

$$U_0 = \begin{pmatrix} 1 \\ y_0 \\ 0 \end{pmatrix} \tag{8.101}$$

Where $y_0 = (\mu - \imath(\delta^c + a k^{c2}))/\beta_2 N_0^c$. So U_0 is a basis for the kernel of the adjoint of A. This conclude step 2.

Step 3

The key assumption of the method we are using here is to expand the solution of the nonlinear equation in terms of the unstable modes of the linearized problem and then add small corrections to this expansion.Solvability conditions on the equations of the corrections give evolution equations fo the expansion amplitudes. From the linear stability analysis in Appendix B and from Step 2 we know the unstable modes of the linearized system. It will be useful for later work to distinguise between the

case when $\Delta > 0$ (focussing) and $\Delta < 0$ (defocussing). We will now write down the expansion in active modes for both cases.

(i) $\Delta > 0$

$$v = (A_1 e^{\imath k^c x} + A_2 e^{-\imath k^c x}) e^{\imath \delta^c t} V_0$$

Or in component form

$$\begin{aligned} E &= (A_1 e^{\imath k^c x} + A_2 e^{-\imath k^c x}) e^{\imath \delta^c t} \\ P &= x_0 (A_1 e^{\imath k^c x} + A_2 e^{-\imath k^c x}) e^{\imath \delta^c t} \qquad (8.102) \\ n &= 0 \end{aligned}$$

(ii) $\Delta < 0$

$$v = A e^{\imath \delta^c t} V_0$$

Or in component form

$$\begin{aligned} E &= A e^{\imath \delta^c t} \\ P &= x_0 A e^{\imath \delta^c t} \qquad (8.103) \\ n &= 0 \qquad (8.104) \end{aligned}$$

This completes step 3.

Step 4

The largest amount of work in these calculation is spent evaluating the nonlinear operator N on the expansion of the solution in active and passive modes. In this

section we will do this evaluation in the defocussing case. As mentioned in the beginning of this appendix and also in the last subsection the solution of the full nonlinear problem is expanded in active and passive modes, where the passive modes are only small corrections to the active mode part. Using step 3 we write in the defocussing case.

$$v = Ae^{i\delta^c t}V_0 + v_1 + v_2 + \cdots$$

Where v_i's are that passive modes added as a small correction. Define

$$v_i = \begin{pmatrix} E_i \\ P_i \\ n_i \end{pmatrix}$$

Then in component form the expansion in active and passive modes is

$$\begin{aligned} E &= Ae^{i\delta^c t} + E_1 + E_2 + \cdots \\ P &= x_0 Ae^{i\delta^c t} + P_1 + P_2 + \cdots \\ n &= n_1 + n_2 + \cdots \end{aligned} \tag{8.105}$$

The nonlinear operator is from step 1

$$N\begin{pmatrix} E \\ P \\ n \end{pmatrix} = \begin{pmatrix} 0 \\ \beta_2 En \\ -\frac{1}{2}\beta_2(P^*E + PE^*) \end{pmatrix} \tag{8.106}$$

We will now evaluate the operator N on the expansion (8.105). We find

$$\begin{aligned} En &= (Ae^{i\delta^c t} + E_1 + E_2 + \cdots)(n_1 + n_2 + \cdots) \\ &= An_1 e^{i\delta^c t} + \cdots \end{aligned} \tag{8.107}$$

$$\begin{aligned} P^*E &= (x_0^*A^*e^{-\imath\delta^c t} + P_1^* + P_2^*A)(Ae^{\imath\delta^c t} + E_1 + E_2 + \cdots) \\ &= x_0^*|A|^2 + P_1^*Ae^{\imath\delta^c t} + E_1x_0^*A^*e^{-\imath\delta^c t} + P_1^*E_1 \\ &\quad + x_0^*E_2Ae^{-\imath\delta^c t} + P_2^*Ae^{\imath\delta^c t} + \cdots \end{aligned}$$

$$\begin{aligned} PE^* &= x_0|A|^2 + P_1A^*e^{-\imath\delta^c t} + E_1^*x_0Ae^{\imath\delta^c t} + P_1E_1^* \\ &\quad x_0E_2^*e^{\imath\delta^c t} + P_2A^*e^{-\imath\delta^c t} \end{aligned}$$

So we find

$$\begin{aligned} (P^*E + PE^*) &= (x_0 + x_0^*)|A|^2 + (P_1^*A + x_0E_1^*A)e^{\imath\delta^c t} \\ &\quad (x_0^*E_1A^* + P_1A^*)e^{-\imath\delta^c t} + P_1^*E_1 + P_1E_1^* + \\ &\quad (P_2^*A + x_0E_2^*A)e^{\imath\delta^c t} + (x_0^*E_2A^* + P_2A^*)e^{-\imath\delta^c t} \end{aligned}$$

Write $N = N_1 + N_2 + \cdots$ as a asymptotic series. We then find from the above formula

$$N_1 = -\frac{1}{2}\beta_2(x_0 + x_0^*)|A|^2e_3 \tag{8.108}$$

$$\begin{aligned} N_2 &= \{\beta_2An_1e_2 - \frac{1}{2}\beta_2(P_1^*A + x_0E_1^*A)e_3\}e^{\imath\delta^c t} \\ &\quad -\frac{1}{2}\beta_2(x_0^*E_1A^* + P_1A^*)e_3e^{-\imath\delta^c t} \end{aligned} \tag{8.109}$$

Where e_i is the i'th standard basis vector in 3-space.We will use this notation in the rest of this appendix This conclude step 4.

Step 5

In this section we will evaluate the nonlinear operator on the expansion in active and passive modes in the focussing case. Using the notation from step 4 we find that the expansion for this case is

$$\begin{aligned} E &= (A_1 e^{\imath k^c x} + A_2 e^{-\imath k^c x}) e^{\imath \delta^c t} + E_1 + E_2 + \cdots \\ P &= x_0 (A_1 e^{\imath k^c x} + A_2 e^{-\imath k^c x}) e^{\imath \delta^c t} + P_1 + P_2 + \cdots \\ n &= n_1 + n_2 + \cdots \end{aligned}$$

The expression for the nonlinear operator can be found under step 1 or step 4. Using the expansion above and the expression for the nonlinear operator we find

$$\begin{aligned} En &= \{(A_1 e^{\imath k^c x} + A_2 e^{-\imath k^c x}) e^{\imath \delta^c t} + E_1 + E_2 + \cdots\}\{n_1 + n_2 + \cdots\} \\ &= (n_1 A_1 e^{\imath k^c x} + n_1 A_2 e^{-\imath k^c x}) e^{\imath \delta^c t} + n_1 E_1 + \\ &\quad (n_2 A_1 e^{\imath k^c x} + n_2 A_2 e^{-\imath k^c x}) e^{\imath \delta^c t} + \cdots \end{aligned}$$

$$\begin{aligned} P^* E &= \{x_0^* (A_1^* e^{-\imath k^c x} + A_2^* e^{\imath k^c x}) e^{-\imath \delta^c t} + P_1^* + P_2^* + \cdots\} \\ &\quad \{(A_1 e^{\imath k^c x} + A_2 e^{-\imath k^c x}) e^{\imath \delta^c t} + E_1 + E_2 + \cdots\} \\ &= x_0^* (A_1 A_2^* e^{2\imath k^c x} + |A_1|^2 + |A_2|^2 + A_1^* A_2 e^{-2\imath k^c x}) \\ &\quad + (A_1 P_1^* e^{\imath k^c x} + A_2 P_1^* e^{-\imath k^c x}) e^{\imath \delta^c t} \\ &\quad + x_0^* (A_1^* E_1 e^{-\imath k^c x} + A_2^* E_1 e^{\imath k^c x}) e^{-\imath \delta^c t} + \cdots \end{aligned}$$

SO

$$
\begin{aligned}
PE^* &= \{x_0(A_1e^{\imath k^c x}+A_2e^{-\imath k^c x})e^{\imath\delta^c t}+P_1+P_2+\cdots\} \\
&\quad \{(A_1^*e^{-\imath k^c x}+A_2^*e^{\imath k^c x})e^{-\imath\delta^c t}+E_1^*+E_2^*+\cdots\} \\
&= x_0(A_1^*A_2e^{-2\imath k^c x}+|A_1|^2+|A_2|^2+A_1A_2^*e^{2\imath k^c x}) \\
&\quad +(A_1^*P_1e^{-\imath k^c x}+A_2^*P_1e^{\imath k^c x})e^{-\imath\delta^c t} \\
&\quad +x_0(A_1E_1^*e^{\imath k^c x}+A_2E_1^*e^{-\imath k^c x})e^{\imath\delta^c t}+\cdots
\end{aligned}
$$

Adding the last two expressions we find

$$
\begin{aligned}
P^*E+PE^* &= (x_0+x_0^*)(A_1A_2^*e^{2\imath k^c x}+|A_1|^2+|A_2|^2+A_1^*A_2e^{-2\imath k^c x}) \\
&\quad +\{(A_1P_1^*+x_0E_1^*A_1)e^{\imath k^c x}+(A_2P_1^*+x_0E_1^*A_2)e^{-\imath k^c x}\}e^{\imath\delta^c t} \\
&\quad +\{(x_0^*E_1A_2^*+A_2^*P_1)e^{\imath k^c x}+(x_0^*E_1A_1^*+A_1^*P_1)e^{-\imath k^c x})e^{-\imath\delta^c t}\}+\cdots
\end{aligned}
$$

Writing $N=N_1+N_2+\cdots$ we find that N_1 and N_2 are given by

$$
N_1 = -\frac{1}{2}\beta_2(x_0+x_0^*)(A_1A_2^*e^{2\imath k^c x}+|A_1|^2+|A_2|^2+A_1^*A_2e^{-2\imath k^c x})e_3 \quad (8.110)
$$

$$
\begin{aligned}
N_2 &= -\frac{1}{2}\beta_2[\{(A_1P_1^*+x_0E_1^*A_1)e^{\imath k^c x}+(A_2P_1^*+x_0E_1^*A_2)e^{-\imath k^c x}\}e^{\imath\delta^c t} \\
&\quad +\{(A_2^*P_1+x_0^*E_1A_2^*)e^{\imath k^c x}+(x_0^*E_1A_1^*+A_1^*P_1)e^{-\imath k^c x}\}e^{-\imath\delta^c t}]e_3 \\
&\quad \beta_2(n_1A_1e^{\imath k^c x}+n_1A_2e^{-\imath k^c x})e^{\imath\delta^c t}e_2 \qquad (8.111)
\end{aligned}
$$

This conclude step 5.

Step 6

We will in this step find the perturbation equations to 0^{th},1^{th} and 2^{th} order. Following [7] we write our problem as

$$L(\imath\delta^c + \partial_t, \imath k^c + \partial_x, N_0^c + N')(v_0 + v_1 + v_2 + \cdots) = N_1 + N_2 + \cdots$$

We then expand L in a Taylor series around N_0^c,k^c,δ^c and collect terms of equal order assuming that all derivatives involved are slow. We find

$$\{L^{(0)} + L^{(1)} + L^{(2)}\}\{v_0 + v_1 + v_2 + \cdots\} = N_1 + N_2 + \cdots$$

Where we have defined

$$\begin{aligned} L^{(0)} &= L \\ L^{(1)} &= L_1\partial_t + L_2\partial_x \\ L^{(2)} &= L_{11}\partial_{tt}^2 + L_{12}\partial_{tx}^2 + L_{22}\partial_{xx}^2 + L_3N' \end{aligned} \tag{8.112}$$

All operators are evaluated at $N_0 = N_0^c$,$\delta = \delta^c$ and $k = k^c$. Collecting terms we find

At 0^{th} order:

$$L^{(0)}v_0 = 0 \tag{8.113}$$

This is just the linearized problem and will always be automatically satisfied since v_0 will be a linear combination of solutions of the linear problem

At 1^{th} order:

$$L^{(0)}v_1 = -L^{(1)}v_0 + N_1 \tag{8.114}$$

At 2^{th} order:

$$L^{(0)}v_2 = -L^{(1)}v_1 - L^{(2)}v_0 + N_2 \tag{8.115}$$

We will in the following calculations use these perturbation equations to find the evolution equations for the active mode amplitudes. This conclude step 6.

Step 7

We will in this step solve the first order perturbation equation in the defocussing case. From step 6 and step 4 we find that the equation for the first correction v_1 is

$$L^{(0)}v_1 = -\{L_1\partial_t + L_2\partial_x\}v_0 - \frac{1}{2}\beta_2(x_0 + x_0^*)|A|^2 e_3$$

From step 1 and appendix B we find that in the defocussing case

$$\begin{aligned} L_2 &= 0 \\ L_1 &= I \end{aligned}$$

Where I is the identity operator. Using the expression for v_0 in the defocussing case from step 3 we find that the perturbation equation for v_1 is

$$L^{(0)}v_1 = -A_t e^{i\delta c t}\ V_0 - \frac{1}{2}\beta_2(x_0 + x_0^*)|A|^2 e_3$$

At this point we apply the Fredholm Alternative theorem to make this equation consistent or equivalently we must remove secular terms from the righthand side of the equation above. It is clear that the last term is not secular whereas the first term is secular. In order to remove the secular term we must require

$$\partial_t A = 0$$

This means that the time derivative of the active amplitude must be zero to this order. We can now solve the equation for v_1. As usual in computations like these we only need a special solution. Using the form of $L^{(0)}$ from step 1 evaluated at $N_0 = N_0^c, \delta = \delta^c$ and $k_c = 0$ we find that a special solution is

$$v_1 = -\frac{\beta_2}{2\gamma_2}(x_0 + x_0^*)|A|^2 e_3$$

Or writing

$$v_1 = \begin{pmatrix} E_1 \\ P_1 \\ n_1 \end{pmatrix}$$

we find in component form

$$\begin{aligned} E_1 &= 0 \\ P_1 &= 0 \\ n_1 &= -\frac{\beta_2}{2\gamma_2}(x_0 + x_0^*)|A|^2 \end{aligned} \tag{8.116}$$

This conclude step 7.

Step 8

We will in this section solve the first order perturbation equation for v_1 in the focussing case. From step 5 and step 6 we find that the equation for v_1 now is

$$\begin{aligned} L^{(0)}v_1 &= -\{\mathrm{L}_1\partial_t + L_2\partial_x\}v_0 \\ &\quad -\frac{1}{2}\beta_2(x_0 + x_0^*)\{A_1A_2^* e^{2\imath k^c x} + |A_1|^2 + |A_2|^2 + A_1^* A_2 e^{-2\imath k^c x}\}e_3 \end{aligned}$$

Evaluating L_1 ,L_2 at critical and using the expansion in active modes from step 3 we find that the equation for v_1 is in this case

$$\begin{aligned} L^{(0)}v_1 &= -[(V_0\partial_t A_1 + S_0\partial_x A_1)e^{\imath k^c x} + (V_0\partial_t A_2 - S_0\partial_x A_2)e^{-\imath k^c x}]e^{\imath\delta^c t} \\ &\quad -\frac{1}{2}\beta_2(x_0+x_0^*)\{A_1A_2^*e^{2\imath k^c x} + |A_1|^2 \\ &\quad +|A_2|^2 + A_1^*A_2e^{-2\imath k^c x}\}e_3 \end{aligned} \tag{8.117}$$

Where the vector S_0 is the result of applying L_2 to V_0.

$$S_0 = \begin{pmatrix} 2ak^c \\ 0 \\ 0 \end{pmatrix}$$

We will look for a special solution to (8.117) of the form

$$v_1 = a_1 + (a_2e^{\imath k^c x} + a_3e^{-\imath k^c x})e^{\imath\delta^c t} + a_4e^{2\imath k^c x} + a_5e^{-2\imath k^c x} \tag{8.118}$$

By comparing terms we find the following linear matrix problems for the a_i's.

$$\begin{aligned} B_1a_1 &= -\frac{1}{2}\beta_2(x_0+x_0^*)(|A_1|^2+|A_2|^2)e_3 \\ B_2a_2 &= -(V_0\partial_t A_1 + S_0\partial_x A_1) \\ B_2a_3 &= -(V_0\partial_t A_1 - S_0\partial_x A_1) \\ B_3a_4 &= -\frac{1}{2}\beta_2(x_0+x_0^*)A_1A_2^*e_3 \\ B_3a_5 &= -\frac{1}{2}\beta_2(x_0+x_0^*)A_1^*A_2e_3 \end{aligned}$$

Where we have defined

$$
\begin{aligned}
B_1 &= \begin{pmatrix} \mu & -\beta_1 & 0 \\ -\beta_2 N_0^c & \gamma_1(1+\imath\Delta) & 0 \\ 0 & 0 & \gamma_2 \end{pmatrix} \\
B_2 &= \begin{pmatrix} \imath\delta^c + \imath a k^{c2} + \mu & -\beta_1 & 0 \\ -\beta_2 N_0^c & \imath\delta^c + \gamma_1(1+\imath\Delta) & 0 \\ 0 & 0 & \gamma_2 + \imath\delta^c + D k^{c2} \end{pmatrix} \\
B_3 &= \begin{pmatrix} 4\imath a k^{c2} + \mu & -\beta_1 & 0 \\ -\beta_2 N_0^c & \gamma_1(1+\imath\Delta) & 0 \\ 0 & 0 & \gamma_2 + 4D k^{c2} \end{pmatrix}
\end{aligned}
$$

Using the Fredholm Alternative Theorem on the linear systems for the a_i's we find that a solution v_1 will exist only if

$$
\begin{aligned}
\langle V_0 \partial_t A_1 + S_0 \partial_x A_1, U_0 \rangle &= 0 \\
\langle V_0 \partial_t A_2 - S_0 \partial_x A_2, U_0 \rangle &= 0
\end{aligned}
$$

Where the vector U_0 span the kernel of the adjoint of B_2. It was derived in step 2. From the last two equations we find that a solution for v_1 exist only if

$$
\partial_t A_1 = -\frac{2\gamma_1 a k^c}{\mu + \gamma_1} \partial_x A_1 \tag{8.119}
$$

$$
\partial_t A_2 = \frac{2\gamma_1 a k^c}{\mu + \gamma_1} \partial_x A_2 \tag{8.120}
$$

So to lowest order A_1 and A_2 will be two waves travelling in opposite directions. Corrections to this behaviour will be derived later in this calculation. We can now solve the linear equations for the a_i's and from that find v_1 using (8.118).

$$
a_1 = -s_1(|A_1|^2 + |A_2|^2)e_3 \tag{8.121}
$$

$$a_2 = -\frac{1}{\mu}(\partial_t A_1 + 2ak^c \partial_x A_1)e_1 \quad (8.122)$$

$$a_3 = -\frac{1}{\mu}(\partial_t A_2 - 2ak^c \partial_x A_2)e_1 \quad (8.123)$$

$$a_4 = -s_2 A_1 A_2^* e_3 \quad (8.124)$$

$$a_5 = a_4^* \quad (8.125)$$

Where we have defined

$$s_1 = \frac{\beta_2(x_0 + x_0^*)}{2\gamma_2} \quad (8.126)$$

$$s_2 = \frac{\beta_2(x_0 + x_0^*)}{2\gamma_2 + 4Dk^{c2}} \quad (8.127)$$

We will now write the solution v_1 in component form. Observe that by using equations (8.119) and (8.120) we can write

$$\partial_t A_1 + 2ak^c \partial_x A_1 = s\partial_x A_1$$

$$\partial_t A_2 - 2ak^c \partial_x A_2 = -s\partial_x A_2$$

Where we have defined $s = (2\mu ak^c)/(\mu + \gamma_1)$.So v_1 in component form is

$$E_1 = -\frac{s}{\mu}(\partial_x A_1 e^{\imath k^c x} - \partial_x A_2 e^{-\imath k^c x})e^{\imath \delta^c t} \quad (8.128)$$

$$P_1 = 0 \quad (8.129)$$

$$n_1 = -s_2 A_1 A_2^* e^{2\imath k^c x} - s_1(|A_1|^2 + |A_2|^2) - s_2 A_1^* A_2 e^{-2\imath k^c x} \quad (8.130)$$

This conclude step 8

Step 9

In this section we will use the results from step 5,7,8 to evaluate explicitely the second order nonlinear operator N_2 in the defocussing and focussing case. From step 4 we have N_2 in the defocussing case

$$\begin{aligned} N_2 &= \{\beta_2 A n_1 e_2 - \frac{1}{2}\beta_2(P_1^* A + x_0 E_1^* A)e_3\}e^{\imath\delta^c t} \\ &\quad -\frac{1}{2}\beta_2(x_0^* E_1 A^* + P_1 A^*)e_3 e^{-\imath\delta^c t} \end{aligned}$$

Substituting the expressions we have found for E_1,P_1 and n_1 under step 7 we find immidiately.

$$N_2 = -\frac{\beta_2^2}{2\gamma_2}(x_0 + x_0^*)A|A|^2 e^{\imath\delta^c t}e_2 \tag{8.131}$$

For the focussing case we have found under step 5 the following expression for N_2.

$$\begin{aligned} N_2 &= -\frac{1}{2}\beta_2[\{(A_1 P_1^* + x_0 E_1^* A_1)e^{\imath k^c x} + (A_2 P_1^* + x_0 E_1^* A_2)e^{-\imath k^c x}\}e^{\imath\delta^c t} \\ &\quad +\{(A_2^* P_1 + x_0 E_1 A_2^*)e^{\imath k^c x} + (x_0^* E_1 A_1^* + A_1 P_1)e^{-\imath k^c x}\}e^{-\imath\delta^c t}]e_3 \\ &\quad +\beta_2(n_1 A_1 e^{\imath k^c x} + n_1 A_2 e^{-\imath k^c x})e^{\imath\delta^c t}e_2 \end{aligned}$$

For the focussing case we have the expressions for E_1,P_1 and n_1 from step 8. Inserting them into the expression for N_2 from we find after a some algebra that N_2 for this case is

$$N_2 = -\frac{2}{2\mu}\beta_2[\{x_0 A_1 \partial_x A_2^* e^{2\imath\delta^c t} + x_0 A_2 \partial_x A_2^*$$

$$
\begin{aligned}
&-x_0 A_1 \partial_x A_1^* - x_0 A_2 \partial_x A_1^* e^{-2\imath k^c x}\} e^{\imath \delta^c t} \\
&\{-x_0^* A_2^* \partial_x A_1 e^{2\imath k^c x} + x_0^* A_2^* \partial_x A_2 \\
&-x_0^* A_1^* \partial_x A_1 + x_0^* A_1^* \partial_x A_2 e^{-2\imath k^c x}\} e^{-\imath \delta^c t} \\
&+\beta_2 \{-s_2 A_1^2 A_2^* e^{3\imath k^c x} - ((s_1+s_2) A_1 |A_2|^2 + s_1 A_1 |A_1|^2) e^{\imath k^c x} \\
&-((s_1+s_2) A_2 |A_1|^2 + s_1 A_2 |A_2|^2) e^{-\imath k^c x} \\
&-s_2 A_1^* A_2^2 e^{-3\imath k^c x}\} e^{\imath \delta^c t} e_2
\end{aligned} \tag{8.132}
$$

This conclude step 9.

Step 10

We will in this section derive the second order evolution equation for the active mode amplitude in the defocussing case using Fredholm on the perturbation equation for v_2. From step 6 we have that the equation for v_2 is

$$L^{(0)} v_2 = -L^{(1)} v_1 - L^{(2)} v_0 + N_2$$

Using the expressions for $L^{(1)}$ and $L^{(2)}$ from step 6 and the expression for N_2 from step 8 we find that the equation for v_2 is

$$
\begin{aligned}
L^{(0)} v_2 \;=\; & -\partial_t A V_0 e^{\imath \delta^c t} - L_{22} V_0 \partial_{xx} A e^{\imath \delta^c t} - L_3 V_0 N' A e^{\imath \delta^c t} \\
& \frac{\beta_2}{2\gamma_2}(x_0 + x_0^*) \partial_t |A|^2 e_3 - \frac{\beta_2^2}{2\gamma_2}(x_0 + x_0^*) A |A|^2 e^{\imath \delta^c t} e_2
\end{aligned}
$$

In order to assure that this equation is consistent we apply the Fredholm Alternative and find that the above equation can be solved for v_2 only if

$$-\partial_t A \langle V_0, U_0 \rangle - \langle L_{22} V_0, U_0 \rangle \partial_{xx}$$

$$-\langle L_3 V_0 N', U_0\rangle A - \frac{\beta_2^2}{2\gamma_2}(x_0 + x_0^*)A|A|^2\langle e_2, U_0\rangle = 0$$

But we have

$$\begin{aligned}
\langle L_{22} V_0, U_0\rangle &= \imath a \\
\langle L_3 V_0 N', U_0\rangle &= -y_0^* \beta_2 N' \\
\langle e_2, U_0\rangle &= y_0^* \\
\langle V_0, U_0\rangle &= 1 + x_0 y_0^*
\end{aligned}$$

So the second order evolution equation for the active mode amplitude A is

$$\begin{aligned}
\partial_t A &= \frac{y_0^* \beta_2 N'}{1 + x_0 y_0^*} A - \frac{\imath a}{1 + x_0 y_0^*}\partial_{xx} A \\
&\quad - \frac{\beta_2^2 (x_0 + x_0^*) y_0^*}{2\gamma_2 (1 + x_0 y_0^*)} A|A|^2
\end{aligned} \tag{8.133}$$

This conclude step 10.

Step 11

In this section we derive the second order evolution equation for the active mode amplitudes in the case of focussing. From step 6 we have that the perturbation equation for v_2 in the focussing case is

$$L^{(0)} v_2 = -L^{(1)} v_1 - L^{(2)} v_0 + N_2 \tag{8.134}$$

And we have using, results derived earlier

$$
\begin{aligned}
L^{(2)}V_0 &= \{L_{22}\partial_{xx} + L_3N'\}(A_1e^{\imath k^c x} + A_2e^{-\imath k^c x})V_0e^{\imath\delta^c t} \\
&= \imath a(\partial_{xx}A_1e^{\imath k^c x} + \partial_{xx}A_2e^{-\imath k^c x})e^{\imath\delta^c t}e_1 \\
&\quad + L_3V_0N'(A_1e^{\imath k^c x} + A_2e^{-\imath k^c x})e^{\imath\delta^c t}
\end{aligned}
$$

and

$$
L^{(1)}v_1 = \{\partial_t + L_2\partial_x\}\{(a_2e^{\imath k^c x} + a_3e^{-\imath k^c x}) + NST\}
$$

Where NST denote terms that are surely nonsecular.From (8.122), (8.123) we find

$$
\begin{aligned}
a_2 &= -\frac{1}{\mu}(\partial_t A_1 + 2ak^c\partial_x A_1)e_1 = \frac{s}{\mu}e_1\partial_x A_1 \\
a_3 &= -\frac{1}{\mu}(\partial_t A_2 - 2ak^c\partial_x A_2)e_1 = -\frac{s}{\mu}e_1\partial_x A_2
\end{aligned}
$$

Where we have defined s in step 8. We use these expressions and find that

$$
\begin{aligned}
\{\partial_t + L_2\partial_x\}a_2 &= -r\partial_{xx}A_1 \\
\{\partial_t + L_2\partial_x\}a_3 &= -r\partial_{xx}A_2
\end{aligned}
$$

Where we have defined the vector r by

$$
r = \frac{s}{\mu}\{-\frac{2\gamma_1 ak^c}{\mu+\gamma_1} + \begin{pmatrix} 2ak^c \\ 0 \\ 0 \end{pmatrix}\}
$$

so we have

$$L^{(1)}v_1 = -r(\partial_{xx}A_1 e^{\imath k^c x} + \partial_{xx}A_2 e^{-\imath k^c x})e^{\imath\delta^c t} + NST$$

It is evident that only the term of N_2 that is paralell to e_2 can possibly be secular since $\langle e_3, U_0\rangle = 0$. So applying The Fredholm Alternative on the lefthand side of (8.134) we find thatthe second order evolution equation for A_1 and A_2 are

$$\begin{aligned}
&-\langle V_0, U_0\rangle\partial_t A_1 - \langle L_3 V_0 N', U_0\rangle A_1 - \langle S_0, U_0\rangle\partial_x A_1 \\
&-\imath a\langle e_1, U_0\rangle\partial_{xx}A_1 + \langle r, U_0\rangle\partial_{xx}A_1 \\
&-\beta_2\rangle e_2, U_0\langle((s_1+s_2)A_1|A_2|^2 + s_1 A_1|A_1|^2) = 0
\end{aligned}$$

and

$$\begin{aligned}
&-\langle V_0, U_0\rangle\partial_t A_2 - \langle L_3 V_0 N', U_0\rangle A_2 + \langle S_0, U_0\rangle\partial_x A_2 \\
&-\imath a\langle e_1, U_0\rangle\partial_{xx}A_2 + \langle r, U_0\rangle\partial_{xx}A_2 \\
&-\beta_2\rangle e_2, U_0\langle((s_1+s_2)A_2|A_1|^2 + s_1 A_2|A_2|^2) = 0
\end{aligned}$$

Or introducing the original physical parameters we find

$$\begin{aligned}
\partial_t A_1 = &\frac{\beta_1\beta_2 N'}{\mu+\gamma_1}A_1 - \frac{2a\gamma_1 k^c}{\mu+\gamma_1}\partial_x A_1 \\
&+\frac{4\mu\gamma_1 a^2 k^{c2}}{(\mu+\gamma_1)^3}\partial_{xx}A_1 - \imath\frac{a\gamma_1}{\mu+\gamma_1}\partial_{xx}A_1 \\
&-\frac{\beta_1\beta_2}{\mu+\gamma_1}((s_1+s_2)A_1|A_2|^2 + s_1 A_1|A_1|^2)
\end{aligned} \tag{8.135}$$

$$\begin{aligned}\partial_t A_2 &= \frac{\beta_1\beta_2 N'}{\mu+\gamma_1}A_2 + \frac{2a\gamma_1 k^c}{\mu+\gamma_1}\partial_x A_2 \\ &+\frac{4\mu\gamma_1 a^2 k^{c2}}{(\mu+\gamma_1)^3}\partial_{xx}A_2 - \imath\frac{a\gamma_1}{\mu+\gamma_1}\partial_{xx}A_2 \\ &-\frac{\beta_1\beta_2}{\mu+\gamma_1}((s_1+s_2)A_2|A_1|^2 + s_1 A_2|A_2|^2) \qquad (8.136)\end{aligned}$$

These are the second order evolution equations for the active mode amplitudes in the focussing case.

APPENDIX H

In the following we assume that the system is constrained longitudinally as in Lugiato et. al.[1] so that the situation is described by the Maxwell-Bloch system with the $\frac{\partial}{\partial_z}$ term removed. We also assume that there is one transverse space dimension. For the rest of this appendix we will assume one transverse space dimension and we use k for the transverse perturbation wavenumber earlier denoted by $\vec{k}_\perp$.

The curve describing the lowest instability threshold,N^c, as a function of the detuning Δ is in Figure 8.1. For defocussing $\Delta < 0$ the transversally homogenous $k = 0$ state go unstable first whereas for the focussing two waves with wavenumbers $k^c = \pm\sqrt{(\gamma_1\Delta)/a}$ will start growing first. The growth as a function of k for defocussing and focussing is displayed in Figure 8.2 and 8.3I.10.

I the next section we derive amplitude equations that describe the nonlinear evolution of the perturbation of the nonlasing solution when we are pumping the system slightly above the threshold N^c. Our main reference for the weakly nonlinear method used to derive the amplitude equation is [7]. The main idea of the method is to expand the solution in active and passive modes. The active modes consists of all unstable modes in the linearized problem. In some cases the active mode expansion has to be supplemented with modes that are stable in the linearized problem but that are close enough to being unstable so that the will play a role in the dynamics.This typically happends when the eigenvalues The passive modes are assumed to give

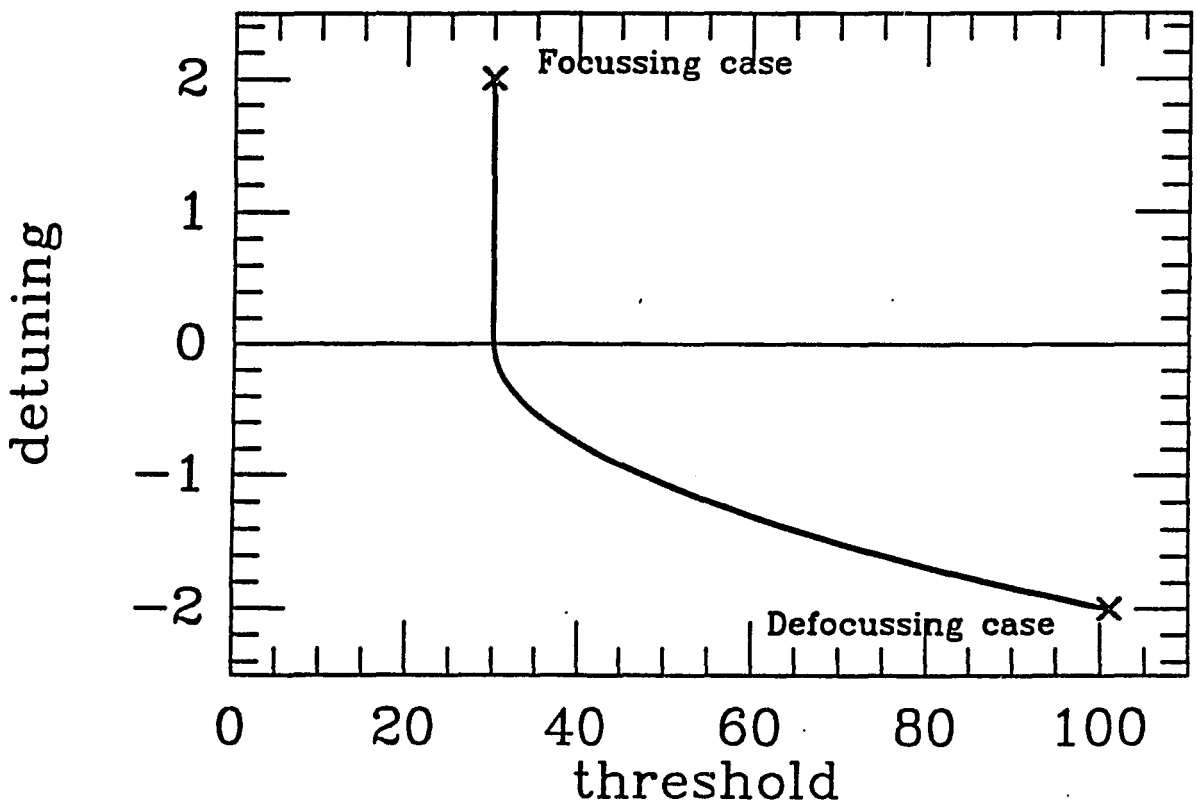

Figure 8.1: Stability treshold as a function of detuning for MB. Parameter values are $\beta_1 = 0.1$, $\beta_2 = 0.1$, $a = 0.2$, $\mu = 0.3$, $\gamma_1 = 1.0$.

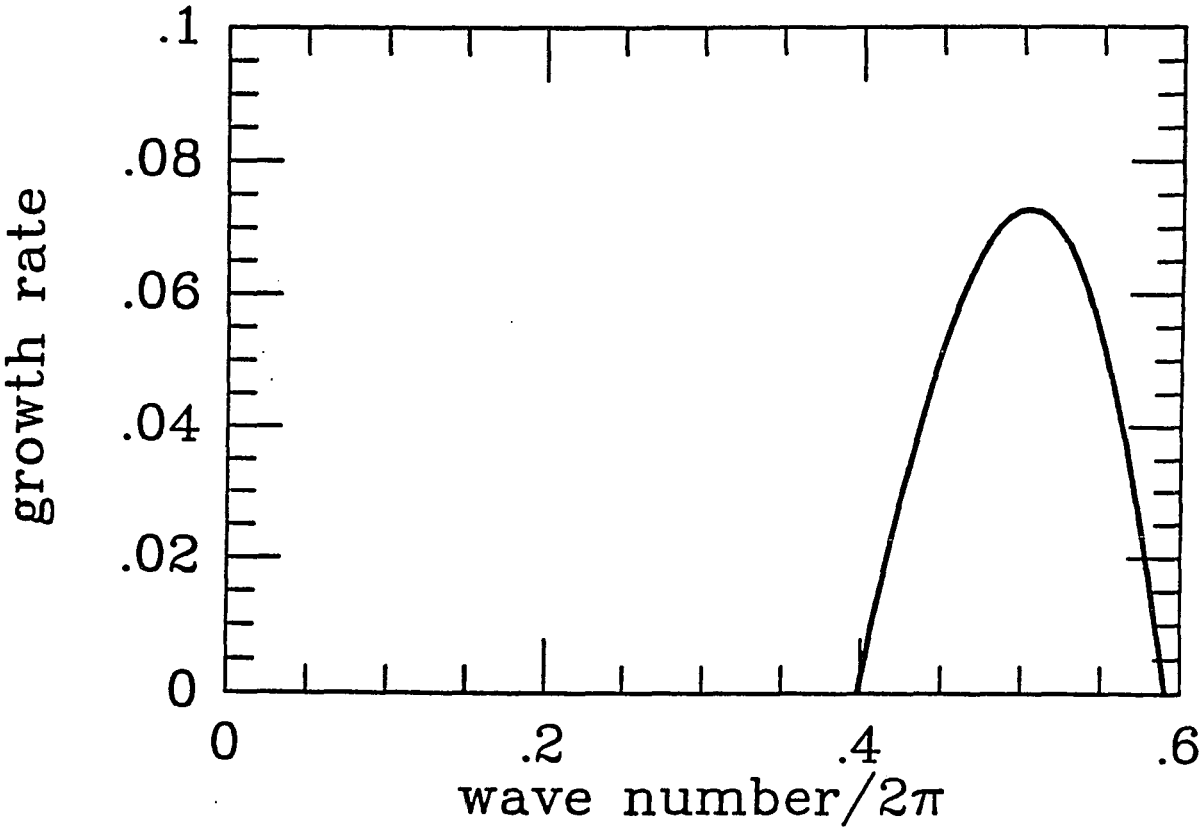

Figure 8.2: Growth rate as a function of wavenumber for MB,defocussing. Parameter values are $\beta_1 = 0.1$, $\beta_2 = 0.1$, $a = 0.2$, $\mu = 0.3$, $\gamma_1 = 1.0$, $\delta = -2$ and $N_0 = 120$.

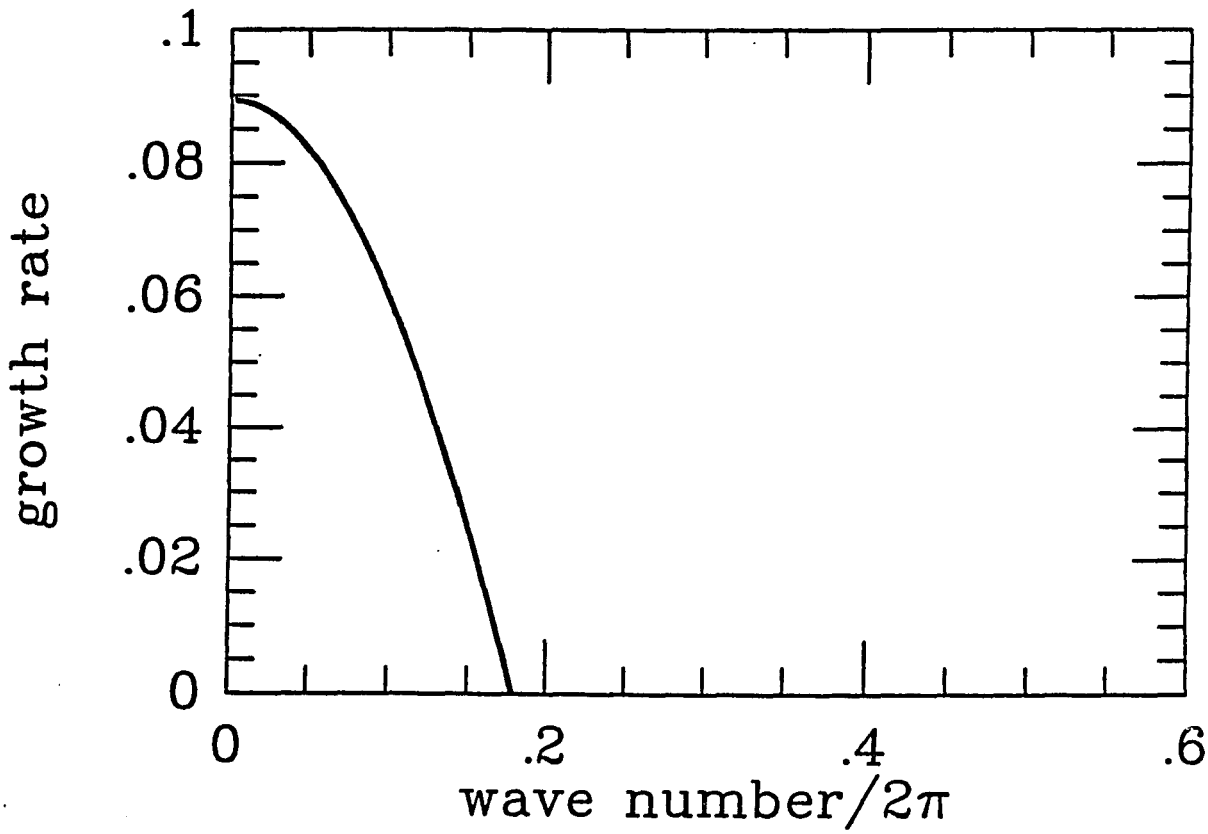

Figure 8.3: Growth rate as a function of wavenumber for MB,focussing. Parameter values are $\beta_1 = 0.1$, $\beta_2 = 0.1$, $a = 0.2$, $\mu = 0.3$, $\gamma_1 = 1.0$, $\delta = 2$ and $N_0 = 120$.

only small corrections. The dynamics in the weakly nonlinear regime will then be determined by the complex amplitudes in the active mode expansion. The evolution equations for the amplitudes are found by requiring that the perturbation equations for the passive modes have a solution. The evolution equations arise as solvability conditions for the passive mode equations, and the passive modes themselves will be slaved to these active modes by solving the perturbation equations. For a discussion of the method see [7]. In Appendix F we apply this method and find the evolution equations for the active mode amplitudes in the defocussing and focussing case.

Amplitude equations for the defocussing case

In the defocussing case we have seen earlier that the homogenous state $k = 0$ first go unstable when N_0 is increased. The active mode expansion will consist of a single term and there will be only one amplitude.

$$v = Ae^{\imath\delta^c t}V_0 + \{Small\ Terms\}, \tag{8.137}$$

where v is the vector (E, P, N),V_0 is the eigenvector of the linearized system and $\delta^c = -\gamma_1\mu\triangle/(\gamma_1 + \mu)$ is the frequency of the unstable homogenous state. We find that the evolution equation for the amplitude A is

$$\begin{aligned}\partial_t A &= \frac{y_0^*\beta_2 N'}{1 + x_0 y_0^*}A - \frac{\imath a}{1 + x_0 y_0^*}\partial_{xx}A \\ &\quad -\frac{\beta_2^2(x_0 + x_0^*)y_0^*}{2\gamma_2(1 + x_0 y_0^*)}A|A|^2\end{aligned} \tag{8.138}$$

This is the universal Complex Ginsburg Landau (CGL) equation. The complex parameters x_0 and y_0 are defined in appendix G. $N' = N_0 - N^c$ is the pumping above threshold. Note that while the linear part of this equation can be had from

the first few terms in the expansion of the dispersion relation for the linearized Maxwell-Bloch equations. The nonlinear term can only be found using the weakly nonlinear theory Let us now investigate what solution this equation will give for A. Let us consider a solution of the form

$$A = A_0 e^{i\omega t},$$

We find that

$$i\omega = \frac{\beta_2 y_0^*}{1 + x_0 y_0^*}(\beta_2 N' A - \frac{x_0^r}{\gamma_2})$$

This implies that $\omega = 0$ and

$$|A|^2 = \frac{\gamma_2 \beta_1}{\mu \beta_2} N'.$$

Since $\omega = 0$ this corresponds to a solution E that oscillates at the frequency δ^c of the linear mode. From equation(8.137) that solution is

$$\begin{pmatrix} E \\ P \\ N \end{pmatrix} = \begin{pmatrix} \frac{\gamma_2 \beta_1}{\mu \beta_2} N' \\ \frac{\mu + i\delta^c}{\beta_1} \frac{\gamma_2 \beta_1}{\mu \beta_2} N' \\ N_0 \end{pmatrix} e^{i\delta^c t} \tag{8.139}$$

Since $N' = N_0 - N^c$ and $N_0 \approx N^c$ to first order (8.139) is the travelling wave solution (2.4). In order to test its stability we use the Lange and Newell criterion [8].That condition says that for a CGL equation

$$A_t = \mu A + \beta A_{xx} - \gamma |A|^2 A, \tag{8.140}$$

the space independent solution is stable only if $real(\beta\gamma^*) > 0$. we find that the condition for our CGL is $-\delta^c > 0$. From (2.4) we observe that δ^c is always negative in the defocussing case, so the space independent solution is stable at least in a small region close to threshold. This leads one to expect that this solution is the asymptotic state for the dynamical evolution of the system for most initial conditions. In

some sense it is a pity that the Lange and Newell criterion predicts stability for the homogenous state for all parameter values. If it did predict instability somewhere beyond the threshold this would give us an analytic expression that approximated the boundary where the laser solutions loose their stability. We will call this the second instability threshold. Finding analytic tractable expressions for this instability boundary by direct linear stability analysis of the full Maxwell-Bloch system has proved unfruitful. We will later investigate this problem in a reduced form.

Amplitude equations for the focussing case

Earlier we saw that in the focussing case there are two modes of the linearized Maxwell-Bloch system that go unstable at the same time when we cross threshold. The active mode expansion consists of two terms representing waves travelling in opposite directions transversally. The expansion of the solution of the Maxwell-Bloch takes the form

$$v = (A_1 e^{\imath k^c x} + A_2 e^{-\imath k^c x}) e^{\imath \delta^c t} V_0 + \{Small\ Terms\} \tag{8.141}$$

The eigenvector of the linearized system V_0 and frequency $\delta^c = -\gamma_1 \Delta$ of the unstable linear modes are different from these in the defocussing case discussed above. Using the weakly nonlinear method we find that the evolution of the two amplitudes is given by two coupled CGL equations.

$$\begin{aligned} \partial_t A_1 &= \frac{\beta_1 \beta_2 N'}{\mu + \gamma_1} A_1 - \frac{2a\gamma_1 k^c}{\mu + \gamma_1} \partial_x A_1 \\ &+ \frac{4\mu\gamma_1 a^2 k^{c2}}{(\mu + \gamma_1)^3} \partial_{xx} A_1 - \imath \frac{a\gamma_1}{\mu + \gamma_1} \partial_{xx} A_1 \\ &- \frac{\beta_1 \beta_2}{\mu + \gamma_1} ((s_1 + s_2) A_1 |A_2|^2 + s_1 A_1 |A_1|^2) \end{aligned} \tag{8.142}$$

$$\begin{aligned}\partial_t A_2 &= \frac{\beta_1\beta_2 N'}{\mu+\gamma_1}A_2 + \frac{2a\gamma_1 k^c}{\mu+\gamma_1}\partial_x A_2 \\ &+\frac{4\mu\gamma_1 a^2 k^{c2}}{(\mu+\gamma_1)^3}\partial_{xx}A_2 - \imath\frac{a\gamma_1}{\mu+\gamma_1}\partial_{xx}A_2 \\ &-\frac{\beta_1\beta_2}{\mu+\gamma_1}((s_1+s_2)A_2|A_1|^2 + s_1 A_2|A_2|^2) \qquad (8.143)\end{aligned}$$

Where $s_1 = \frac{\beta_2\mu}{\beta_1\gamma_2}$ and $s_2 = \beta_2\mu/\beta_1(\gamma_2 + 2Dk^{c2})$. The linear part of these equations could have been found from the dispersion relation of the linearized equations. Consider spatially homogenous solutions. If one of the amplitudes is zero, the active mode expansion would produce a single travelling wave. The nonzero amplitude A must then satisfy

$$A = \frac{1}{s_1}N'$$

This solution is one of the travelling wave laser solutions described in the previous section. Let us try to get a handle on the second instability threshold by using the Lange and Newell condition $real(\beta\gamma^*) > 0$ for stability of the space independent solution. The condition for stability is

$$\frac{2\mu\gamma_1 a^2 k^{c2}}{(\mu+\gamma_1)^3}\frac{\beta_1\beta_2 s_1}{\mu+\gamma_1} > 0$$

Using the expression for s_1 given above we observe that this condition is always satisfied. So the second instability threshold can not be reached using the amplitude equations in the focussing case. The system of coupled CGL equations also has a solution where both amplitudes are nonzero, with

$$A_i = \frac{N'}{2s_1+s_2} \text{ for } i = 1,2$$

This solution represents a standing transverse electric field wave. It is always unstable to long wavelength perturbations. So we would expect the solution with one amplitude equal to zero to dominate the dynamics, at least close to threshold.

References

[1] L.A.Lugiato, C. Oldeano, L.M Narducci, "Cooperative frequency locking and stationary spatial structures in lasers",J.Opt.Soc.Am. B, Vol.5,No.5 May 1988,p 879-888

[2] M.Sargent III, M.O.Scully,and W.E.Lamb Jr., "laser physics", Reading,MA:Addison-Wesley 1974

[3] W.E.Lamb Jr., "Theory of an optical maser",Phys.Rew.,Vol 134 ,pp A1429-A1450, June 1964

[4] Sami T. Hendow and Murray Sargent III, "Theory of single mode laser instabilities", j. opt. soc. am B/Vol.2, Jan 1985,pp 84-101

[5] Amnon Yariv,"Quantum electronics, third edition" Wiley, 1987

[6] A. P. Bogatov, P. G. E, and B. N. Sverdlov, "anomalous interaction of spectral modes in a semiconductor Laser", IEEE Journal of quantum electronics, vol. qe-11,No.7,July 1975

[7] A.C.Newell "The Dynamics and Analysis of Patterns" Complex Systems, Ed. D. Stein, Addison-Wesley Longman Publishing Group Ltd.,1989

[8] Lange C. & Newell A. C. ;Siam J.Appl. Math. 27,441-56,1974.

[9] "Analytical description of ultrashort optical pulse propagation in a resonant medium" G. L. Lamb, Jr. Reviews of modern physics, Vol 43, No. 2, april 1971

[10] "Self induced transparancy" S. L. McCall, E. L. Hahn, Physical review, Vol.183, no.2, july 1969

[11] "Propagation of ultrashort optical pulses" G. L. Lamb Jr, Physics letter, August 1967

[12] "Pulse-area-pulse-energy description of a travelling-wave laser amplifier" S. L. McCall, E. L. Hahn, Physical Review A, Vol.2, No.3 september 1970.

[13] "Optical vorticies."P.Coullet, L. Gil, F. Rocca., Optics comm, Nov. 1989

[14] This is a very robust package of ode solvers written for stiff or non stiff odes. Authors: D. K. Kahaner, National bureau of standards, C. D. Sutherlands, Los Alamos National Laboratory

[15] MACLIB is a set of high level routines for discretization, grid generation etc. Authors: James M. Hyman, Bernard Larrouturou, group T-7, LASL.

The Laser Array Model

Table of Contents

List of Figures

ABSTRACT

We study the stability of index guided laser arrays using an ODE model derived by a coupled mode approach. Stationary solutions to the model equations are found under free running and injection locking conditions and their stability are investigated numerically and analytically for large arrays.

Chapter 1

INTRODUCTION

Evanescently coupled diode laser arrays are being used as high power light sources for many applications. Experiments on two- and ten-element linear arrays as well as broad-stripe structures, have indicated that these lasers are intrinsically unstable in free-running operation [17],[23],[24]. A recent theory by Wang et. al. [18] has shown that the essential nonlinear dynamical features of evanescently coupled laser diode arrays may be adequately captured by coupled mode analysis, in contrast to broad-stripe structures. Experimental and theoretical results to date suggest that these laser systems are ideal candidates for the exploration of space-time complexity in nonlinear extended systems. An understanding of their nonlinear dynamical behavior is essential to their control and successful implementation in wide-ranging application areas. Injection-locking with an external diode laser has proved successful in stabilizing the outputs of both types of laser.

Particular interest lies in stabilizing the laser diode outputs so as to produce a single-lobed far-field profile. This requires a uniform phase front in the near-field across the array. It would be highly desirable to stabilize the output in a free-running mode of operation by say, adjusting the physical parameters such as evanescent coupling or pump current profile prior to fabrication. The theory in

[18] and its extension in appendix B, has established that the output power must be extremely weak in order to maintain stable operation of the phase-locked state and, moreover, that the laser tends to oscillate preferentially in an anti-phase-locked supermode. This produces an undesirable far-field profile. In fact streak camera outputs show that the laser output tends to oscillate in a complicated fashion showing transient evidence of higher order supermode shapes, spiking with most of the energy confined to the edge lasers and symmetry breaking dynamical oscillations. Rather interestingly, effective decoupling of the individual array elements, while leading to stable near-field profiles, can give rise to random dynamical intensity fluctuations in the far-field. This can be traced to a phase instability across the array which is masked in the near-field intensity output but is converted into a strong amplitude modulation in the far-field.

We have recently extended the coupled mode theory in [18] to deal with very large arrays, by considering a continuum limit, which allows one to identify rather easily, new classes of stationary solutions . In the continuum limit, the coupled-mode equations can be reduced to a Riccati equation whose solutions can be identified with appropriate discrete array modes in the large N-limit. Here N refers to the number of lasers in the array. We find in fact that many of the continuum solutions have direct analogs in the discrete problem even for small N. Some of the most important features of these new solutions, their stability properties and relation to the discrete modes will be elaborated on briefly below.

Our main interest will focus on the injection-locking of the discrete array with an external optical field. We find further classes of robust injection-locked array output profiles, some of which exhibit interesting cooperative behavior as a function

of increasing array size. Some of these solutions should prove extremely useful in optimizing the output characteristics of laser diode arrays. By employing a combination of analytic and numerical stability techniques we have established that many of these solutions are stable attractors with large basins of attraction and are moreover robust to physical parameter variation and perturbation.

Chapter 2

BACKGROUND THEORY

The coupled mode equations appropriate to a one dimensional evanescently coupled laser diode array were derived in [18] and are extended here to include an external injection optical field. The details of this derivation can be found in appendix A These equations, when appropriately scaled, are given by

$$\begin{aligned} \dot{e}_j &= -\frac{1}{2}e_j + (1 - i\alpha)Z_j e_j \\ &\quad + i\eta(e_{j+1} + e_{j-1}) + a_j e^{i(\delta t - \frac{\pi}{2})} \qquad (2.1) \\ T\dot{Z}_j &= p_j - Z_j - 2Z_j|e_j|^2. \qquad (2.2) \end{aligned}$$

The linewidth enhancement factor α distinguishes semiconductor lasers from other laser systems and can range in magnitude from 4-6. This couples amplitude and phase across the array and is responsible for the observed chaotic outputs. Here e_j is the scaled complex amplitude of the j-th laser, Z_j is a normalized carrier density and p_j is proportional to the pumping current on the j-th laser. These equations describe the coupled semiconductor laser modes where the evanescent coupling is captured by the parameter η which couples nearest neighbors in the array. This latter parameter involves an overlap integral of single mode functions. The various physical parameters such as cavity damping time, carrier recombination time and

linear gain constant are absorbed in the scalings. The dimensionless parameter T is in fact the ratio of the carrier recombination to cavity decay time and typically has a magnitude of ≈ 2000. This makes the large coupled system of nonlinear ordinary differential equations stiff and has important consequences for their predicted bifurcation behavior . In contrast to reference [18] we must maintain an index on the current pump profile (p_j) in order to ensure stationary solutions for $N > 2$ in free-running mode . Equation (1) includes the external injection-locking optical field through the injection term a_j and we allow for a finite detuning of the latter from the cavity frequency via the detuning term δ. Equations (1) and (2) are central to our investigation.

Chapter 3

FREE-RUNNING MODE

This section contains a compressed version of our work on the free running laser arrays. An expanded version can be found in appendix B. A continuum model of the undriven array presented in appendix B, can be derived from a slightly rescaled version of (1) and (2). This provides a convenient theoretical framework within which more general classes of stationary solutions can be obtained beyond the well-known array supermodes. In particular we are interested in the limit of very large arrays and in solutions which tend to have uniform field profiles on the scale of the inter-element separation h. Under the assumption of slow variation of the field on the scale of the inter-element separation, we can reduce the above discrete dynamical model to the following coupled partial differential equations:

$$\begin{aligned} s_t &= zs - \eta h^2(2s_x\phi_x + s\phi_{xx}) \\ \phi_t &= -\alpha z + 2\eta + \eta h^2(s_{xx}/s - \phi_x^2) \\ Tz_t &= v(x) - z - (1+2z)s^2. \end{aligned}$$

Here we have written the real amplitude s and phase ϕ of the array explicitly. The restriction that the phase and amplitude cannot vary rapidly on the scale of h rules out the anti-locked states which are undesirable for applications anyhow.

The solutions for which s and Z are stationary, which, through $v(x)$, allow for an arbitrary current pumping profile, are obtained as solutions to the following Riccati equation,

$$\theta_x + f(x)\theta + \frac{1}{\alpha}\theta^2 + g(x) = 0.$$

The coefficients $f(x)$ and $g(x)$ are given by

$$f(x) = 2\frac{s_x}{s}, \qquad g(x) = \frac{(\Omega - 2\eta)}{\alpha\eta h^2} - \frac{1}{\alpha}\frac{s_{xx}}{s}.$$

The variable $\theta = \phi_x$ is the phase gradient across the array and Ω is a constant frequency offset. This equation admits a wide class of possible stationary profiles. We restrict our discussion to just two simple cases here.

Constant phase ($\theta = 0$) solutions require $g(x) = 0$ and consequently only sinusoidal ($s(x) = p\cos(kx+\tau)$) or hyperbolic ($s(x) = \cosh(kx)$ field profiles are allowed depending on whether $k = \sqrt{(2\eta - \Omega)/\eta h^2}$ is real or imaginary. The sinusoidal profiles correspond to the usual phase-locked supermode, while the hyberbolic profiles suggest peak intensities on the edge lasers, as observed transiently in experiments [25]. Constant intensity solutions are also possible and these require that $f(x) = 0$ and $g(x) = (\Omega - 2\eta)/\alpha\eta h^2$. The resulting equation for the phase gradient has the solution,

$$\theta = \sqrt{\frac{2\eta - \Omega}{\eta h^2}}\tanh\frac{1}{\alpha}\sqrt{\frac{2\eta - \Omega}{\eta h^2}}x + c$$

All of these solutions have direct counterparts in the discrete array problem as discussed in appendix B. A linear stability analysis shows that all of the solutions found so far are unstable except at very small output intensities, and bifurcation analysis shows that a symmetry breaking occurs as the pump current is increased beyond the first instability threshold. This symmetry breaking corresponds physically to

the individual laser elements slipping out of their locked states and it also manifests itself in the emergence of asymmetric intensity profiles across the array.

Chapter 4

INJECTION LOCKED MODE

Our analysis in the previous section and in appendix B has shown that whereas many novel stationary field amplitude profiles are possible for the undriven system ($a_j = 0$), essentially all such are intrinsically unstable in free-running mode except at very low powers. This theoretical conclusion is further supported by the elegant streak camera experiments of the Oregon group [17], [23], [24]. We now explore the possibility of stabilization of the array through injection-locking by an external optical field.An expanded version of the work described in this section can be found in appendix C. Stationary profiles for the driven array are obtained as solutions to the following coupled nonlinear difference equations.

$$s_{i+1} + s_{i-1} - \Delta s_i = \frac{a_i}{\eta}(\sin\phi_0 - \alpha\cos\phi_0) \tag{4.1}$$

$$p_i = (\frac{1}{2} - \frac{a_i\cos\phi_0}{s_i})(1 + 2s_i^2) \tag{4.2}$$

These equations follow directly from the original equations Eqs. (2.1) and (2.2) by substituting

$$e_j = s_j e^{i(\delta t - \pi/2 + \phi_0)},$$

where ϕ_0 is the phase lag between the laser and the injection field. The laser system is behaving as a coupled set of driven nonlinear oscillators. The generalized detuning

factor Δ is defined by $\Delta = (\alpha/2+\delta)/\eta$. We now seek phase-locked stationary profiles which yield the desirable single-lobed far-field pattern. Two cases of particular interest will be discussed.

4.1 Case 1: Uniform Pump Current Profile

This case, while it does not admit stationary profiles for the undriven array with $N > 2$, offers a very interesting class of stationary injection-locked profiles which can be analyzed via a simple Newtonian dynamical analog. The nonlinear difference equation yielding these solutions is,

$$s_{j+1} + s_{j-1} - 2s_j - \gamma_1 s_j = -\gamma_2 \frac{s-j}{1+2s_j^2}$$

where, $\gamma_1 = \Delta - 2 + R/2\cos\phi_0$, $\gamma_2 = pR/\cos\phi_0$ and $R = (\sin\phi_0 - \alpha\cos\phi_0)/\eta$. If we go to the continuum limit, this becomes

$$h^2 s_{xx} = -\frac{dU}{ds}$$

with

$$U(s) = -\frac{1}{2}(\gamma_1 - \gamma_2)s^2 - \frac{1}{2}\gamma_2 s^4$$

where, for simplicity we have assumed an unsaturated output field $s \ll 1$. The shapes of the laser field profiles for various cases can be inferred directly from the potential function $U(s)$. The case $(\gamma_1 - \gamma_2) < 0$ and $\gamma_2 > 0$ is particularly interesting. Figure 4.1 shows how the shape of the array output profile changes as a function of system size with $\eta = 1 \times 10^{-4}, p = 0.499, \Delta = 1.92$ and $\phi_0 = 1.3735$. The output profile flattens out as a function of increasing system size as shown for $N = 30, 40$ and 60 in the figure.

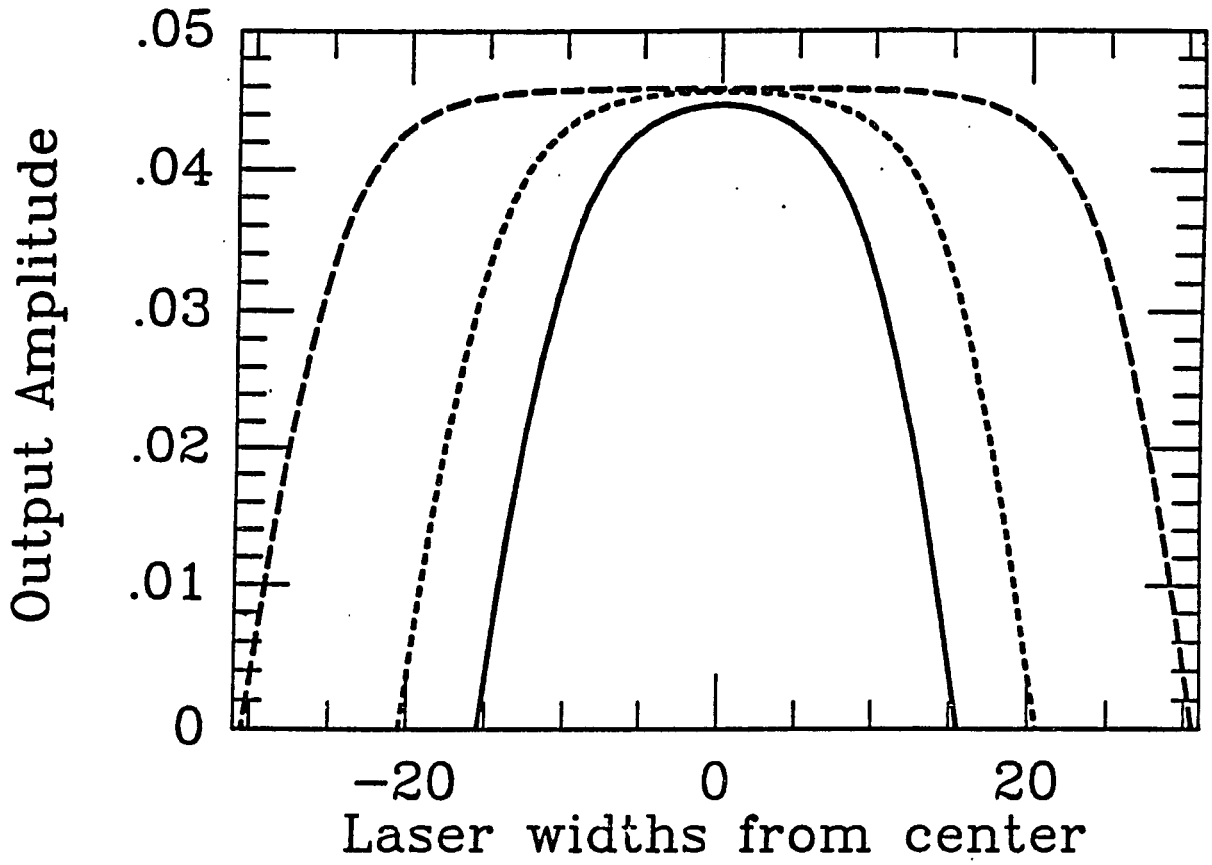

Figure 4.1: Laser array output amplitude profiles for case i) for $N = 30$, $N = 40$ and $N = 60$ and $\eta = 10^{-4}$, $p = 0.499$, $\Delta = 1.92$, $\phi_0 = 1.3735$.

Numerical studies have shown that these injection-locked profiles have large basins of attraction and are robust to detuning about the value $\Delta = 1.92$. Such array profiles should represent the most useful injection-locked states as, in the large N limit, each element in the array acquires the same intensity and the overall phase profile remains constant. Moreover, as a cooperative emission of the entire array, the system shows infinite gain as the pump current threshold ($p = 0.5$) is approached. Very large amplification of weak injected signals is achieved just below threshold for this array mode. (It is possible to run stably with pumping currents above threshold, but the injected locking field must experience two phase reversals as one scans across the array).

4.2 Case 2: Uniform Injected Optical Field

This case allows two further possibilities: (a) the righthand side of Eqn (4.1) is zero i.e. the relation $\phi_0 = \tan^{-1}\alpha$ is satisfied or, (b) the righthand side is nonzero. In both cases the two equations are decoupled, reducing to a linear problem. In (a), we need to solve a linear homogeneous difference equation for the real laser output field amplitudes s_j. Using the computed intensity profile in Eqn (4.2) we can determine the appropriate current pump profile (p_j) for the specified uniform injection a. This case is special as the array output intensity profile is uncoupled from the injection; however, the amplitude of the injection field does influence the stability of the injection-locked output. Once the current pump profile is established for a fixed detuning Δ we can consider tuning the external optical field about this fixed value. The discrete eigenvalue problem yields the following solutions,

$$\begin{aligned} s_i^l &= x \sin\tfrac{l\pi i}{N+1}, & \Delta_l &= 2\cos\tfrac{l\pi}{N+1} \\ s_i'^l &= x(-1)^i \sin\tfrac{l\pi i}{N+1}, & \Delta_l' &= -2\cos\tfrac{l\pi}{N+1} \end{aligned}$$

where l is an integer in the range $0 < l \leq \quad (N+1)/2$. We refer to these solutions as driven supermodes as they are identical to the old supermodes of the undriven array. Their frequencies are distributed in a narrow band about the single diode laser frequency $\omega_{cavity} - \alpha/2$. A condition for stability of these driven supermodes can be derived analytically for all N and an exact stability condition can be derived for the case $N = 2$.

These conditions have been verified numerically. The solutions are found to be stable and to have large domains of attraction for physical parameter values confined within the stable boundaries in (η, I) parameter space (I is the total output power). Stability of these solutions has been explored by perturbing the solution itself, the pumping current profile and the external detuning of the injection field.

If we relax the constraint $\phi_0 = \tan^{-1}\alpha$, one finds a novel type of injection-locked parabolic output profile representing a cooperative state of the laser array. This solution has the property that the maximum output power increases as N^5, where N is the number of elements in the array. In fact, if we consider the array of N lasers as an amplifier of the injected signal, and ignore for the moment the question of stability, the intensity gain g of that amplifier satisfies $g \propto a/\eta \times N^5$. This solution is found to be stable at very small powers, and for larger power it is weakly unstable in the sense that it collapses to a new stable solution in a time of the order of η^{-1}.

Chapter 5

CONCLUSIONS

Semiconductor laser diode arrays provide the ideal experimental structures for a systematic investigation of spatio-temporal complexity in extended nonlinear optical systems. An important point to emerge from the early streak camera experiments [17] is that slow time-integrated detection can mask the true spatio-temporal pulsations of the array output whose characteristic mean periods are on the order of a few hundred picoseconds [24]. Recent full scale simulations of both laser diode arrays and broad-stripe structures [26], including diffraction and carrier diffusion display many of the complex near- and far-field dynamical features alluded to above and observed experimentally. Future plans are to combine the powerful and flexible predictive capability of the above theory with realistic computer simulations in order to link directly to future experiments on free-running and injection-locked diode array and broad-stripe lasers.

Chapter 6

APPENDIX A

In this appendix we derive the laser array equations from Maxwell's equations using mode expansions. The idea is to expand the field in the array in translated single laser modes. Let a single mode of the field for a single laser cavity be

$$E_c = u_c(x,y,z)e^{i\omega_c t} + (*)$$

Where $(*)$ denote complex conjugate. The laser medium is assumed to be isotropic and the mode above is the amplitude of a plan polarized electric field. The functions u_c satisfy

$$(\nabla^2 + \epsilon_c \omega_c^2)u_c = 0$$

The above equation is assumed to be supplied with appropriate boundary conditions. The field is typically assumed to be zero at the mirrors and the mirror losses are added as a linear loss in the field equations. ϵ_c is the real dielectric constant of the background medium when no pumping or fixed index changes are introduced.

We will assume that the guiding of the optical field inside the array is achived by a combination of gain guiding and index guiding. The index guiding is assumed to consist of a series of index depressions. This arrangement will tend to focus the light between the depressions and thereby controlling the position of the individual

lasers in the array.

The field inside the array must satisfy the wave equation derived from Maxwells equations.

$$\frac{1}{v^2}\frac{\partial^2}{\partial t^2}E - \nabla^2 E = -\mu_0 \frac{\partial^2}{\partial t^2}P$$

Where v is the phase speed in the medium. P is the macroscopic polarization. We assume a linear isotropic response and write

$$P = \epsilon E$$

$$\epsilon = \delta\epsilon_i + \delta\epsilon_p$$

Where

- $\delta\epsilon_i$ is the real change in dielectric constant caused by the fixed index depressions.
- $\delta\epsilon_p$ is the complex change in the dielectric constant caused by the pumping of the medium.

Both of these quantities are assumed small as compared to the background dielectric constant ϵ_c

$$\frac{\delta\epsilon_i}{\epsilon_p} \ll 1$$

$$\frac{\delta\epsilon_c}{\epsilon_p} \ll 1$$

The first major assumption is that it is possible to expand the electric field inside the cavity as a sum of translated single cavity modes modes E_i.

$$E = \sum_{i=1}^{N} \mathcal{E}_i E_i + (*)$$

The second major assumption is that $\delta\epsilon_p$ and $\mathcal{E}_i$ vary slowly on the optical timescale $\frac{2\pi}{\omega_c}$.

$$\left|\frac{1}{\delta\epsilon_c}\frac{\partial\delta\epsilon_c}{\partial t}\right| \ll \omega_p$$
$$\left|\frac{1}{\mathcal{E}_i}\frac{\partial\mathcal{E}_i}{\partial t}\right| \ll \omega_p$$

Substitute the expansion for the electric field into the wave equation ,use assumptions outlined above, and keep first order terms. This gives

$$\sum_{i=1}^{N}\frac{d\mathcal{E}_i}{dt}E_i + (*) = -\imath b\sum_{i=1}^{N}\epsilon\mathcal{E}_i E_i + (*)$$

Where $b = \omega_p\mu_0/2$. Multiply this equation with E_j^* and integrate along the transverse dimension of the array. Lowest order terms give

$$\frac{d\mathcal{E}_j}{dt} = -\frac{1}{2\tau_{ph}}\mathcal{E}_j - \imath b[(\delta\epsilon_c + \kappa_1)\mathcal{E}_j - \kappa(\mathcal{E}_{j+1} + \mathcal{E}_{j-1})]$$

Where κ is the coupling constant and where κ_1 is the self coupling constant. τ_{ph} is a linear loss factor introduced in order to take care of loss at the mirrors.

$$\kappa_1 = \int_V \delta\epsilon_i E_j E_j^* dv$$
$$\kappa = \int_V \delta\epsilon_i E_{j+1} E_j^* dv$$

We will also consider the effect of injection the array with an external harmonic field E_{inject}.

$$E_{inject} = f(\vec{x})e^{\imath\omega_0 t}$$

This field adds another term to the polarization. So

$$P = \epsilon E + \epsilon_c E_{inject}$$

Under the same assumptions as above we get

$$\begin{aligned}\frac{d\mathcal{E}_j}{dt} &= -\frac{1}{2\tau_{ph}}\mathcal{E}_j - \imath b[(\delta\epsilon_c + \kappa_1)\mathcal{E}_j - \kappa(\mathcal{E}_{j+1} \\ &\quad +\mathcal{E}_{j-1})] + r_j e^{\imath\bar{\delta}t-\frac{\pi}{2}}\end{aligned}$$

Where r_j is determined by a overlap integral of E_{inject} with the mode $\mathcal{E}_j$ and $\bar{\delta}$ is the detuning.

$$\bar{\delta} = \omega_0 - \omega_p \tag{6.1}$$

The gain is assumed to depend linearly on the carrier density.

$$\delta\epsilon_c = \frac{1}{2}G(N - N_0)(\alpha + \imath)$$

Where α is the linewidth enhancement factor α and where G is a positive constant. N is the density of carriers induced by the pumping of the array. Writing down the above relation amounts to assuming that the real and imaginary part of the dielectric constant both are proportional to $N - N_0$ but with different constants of proportionality, α will then be the ratio between the real and imaginary parts of the complex dielectric constant. A key feature of semiconductor lasers is that this constant is not small, in fact for many experimental systems it varie between four and six [27]. In our numerical work we will use the value 5.

We model the evolution of the density of carriers with a rate equation. The equations for the coupled array can now be written

$$\begin{aligned}\frac{d\mathcal{E}_j}{dt} &= -\frac{1}{2\tau_{ph}}\mathcal{E}_j + \frac{1}{2}g(N_j - N_0)(1 - \imath\alpha)\mathcal{E}_j \\ &\quad +\imath b\kappa(\mathcal{E}_{j+1} + \mathcal{E}_{j-1}) + r_j e^{\imath\hat{\delta}t-\frac{\pi}{2}} \qquad (6.2)\\ \frac{dN_j}{dt} &= q_j - \frac{N_j}{\tau_s} - g(N_j - N_0)\left|\mathcal{E}_j\right|^2 \qquad (6.3)\end{aligned}$$

Where we have redefined $\mathcal{E}_i$ by a pure phase factor, $g = bG$ and $\hat{\delta} = \bar{\delta} - b\kappa_1$

It is convenient in the following to introduce dimensionless variables.

$$\begin{aligned} Z_i &= \frac{1}{2}g\tau_{ph}(N_i - N_0) \ , \ p_i = \frac{1}{2}g\tau_{ph}(\tau_s q_i - N_0) \\ e_i &= \sqrt{\frac{g\tau_s}{2}}\mathcal{E}_i \ , \ \eta = b\tau_{ph}\kappa \ , \ a_j = \tau_{ph}\sqrt{g\tau_s}r_j \\ T &= \frac{\tau_s}{\tau_{ph}} \ , \ \delta = \tau_{ph}\hat{\delta} \ , \ t \to \tau_{ph}t \end{aligned} \tag{6.4}$$

The model of the laser array in dimensionless form is

$$\begin{aligned} \frac{de_j}{dt} &= -\frac{1}{2}e_j + (1 - \imath\alpha)Z_j e_j \\ &\quad + \imath\eta(e_{j+1} + e_{j-1}) + ae^{\delta t - \frac{\pi}{2}} \end{aligned} \tag{6.5}$$

$$T\frac{dZ_j}{dt} = p_j - Z_j - 2Z_j|e_j|^2 \tag{6.6}$$

Chapter 7

APPENDIX B

This appendix contains an expanded version of our work on free running laser diode arrays that has been submitted for publication in Josa B.

Evanescently coupled diode laser diode arrays have been proposed as high power coherent light sources for many applications [23]. Experiments on a ten element array have indicated that the lasers are intrinsically unstable in free-running operation [17]. These observations have been further supported by the recent theoretical work of Wang and Winful [18] who have integrated the coupled mode equations for a ten element laser array using laser parameters appropriate to the experiment in reference [17]. Moreover, the latter authors were able to carry out a complete linear stability analysis for the two element array showing that the instability is ubiquitous in parameter space [19].

The main motivation for the present work is to provide a convenient theoretical framework within which more general classes of equilibrium array modes beyond the well-known supermodes [19], may be readily identified, in particular, for an array with a large number of elements N. Such large systems offer little hope of quantitative analysis using the discrete model derived from coupled mode analysis. It is natural therefore to seek a continuum model which will be accurate in the limit

$h/L << 1$, where h is the individual element spacing in the array and L the total array width. The continuum limit follows from the coupled mode equations of reference [18] by assuming that the envelopes of the laser field amplitude, phase and carriers vary slowly on the scale of the element separation. The envelope functions however, may undergo large excursions in these quantities across the array when many tens or hundreds of elements are involved. A disadvantage of the continuum model is that it cannot accommodate the usual higher order supermodes as these involve rapid phase jumps on the scale of the element separation h. A beating between these higher order modes is typically observed experimentally in the unstable oscillation of the arrays in free-running mode of operation. It is desirable therefore to explore pumping profiles which may yield single-lobed far-field profiles that are stable in some parameter range. We will show that the continuum model yields a Riccatti equation from which it is possible to generate a wide class of solutions, some of which may be physically realizable. The solutions that we have found so far have analogs in the discrete model and the latter solutions tend in the limit $h/L \rightarrow 0$ to these continuous ones.

The model equations describing an N-element array of evanescently coupled lasers is derived from coupled mode analysis following [18].

$$\begin{aligned} \dot{s_j} &= z_j s_j - \eta s_{j+1}\sin(\phi_{j+1}-\phi_j) - \eta s_{j-1}\sin(\phi_{j-1}-\phi_j) \\ \dot{\phi_j} &= -\alpha z_j + \eta\frac{s_{j+1}}{s_j}\cos(\phi_{j+1}-\phi_j) + \eta\frac{s_{j-1}}{s_j}\cos(\phi_{j-1}-\phi_j) \qquad (7.1) \\ T\dot{z_j} &= P_j - z_j - (1+2z_j)s_j^2 \\ & \text{for} \quad j = 1,\ldots,n \qquad x_0 = x_{N+1} = 0 \end{aligned}$$

Where s_j is proportional to the field mode amplitude, z_j is the excess carrier

density above threshold, and ϕ_j is the phase of the field in the j^{th} laser. The constants are: α, the antiguiding coefficient, η, the coupling coefficient and P_j, a multiple of the excess of the pumping current for laser j above threshold. Further details of the derivation of this model are contained in [18]. We note here that it is essential to allow the pumping current to vary across the array in order to get consistent equilibrium solutions. Because we are modeling semiconductor lasers, the frequency at which the single laser oscillates will not coincide with the cavity resonance frequency. The antiguiding parameter α causes a shift in the operating frequency of the laser. In our investigations of the coupled array, we will find solutions that oscillate at frequencies that vary slightly from the frequency of the single laser. We introduce a "detuning" term δ into the equation. Instead of using an envelope function $e_j = s_j e^{i\phi_j}$ we will use $e_j = s_j e^{i(\phi_j + \delta t)}$. The equations (7.1) now become

$$\begin{aligned} \dot{s_j} &= z_j s_j - \eta s_{j+1}\sin(\phi_{j+1} - \phi_j) - \eta s_{j-1}\sin(\phi_{j-1} - \phi_j) \\ \dot{\phi_j} + \delta &= -\alpha z_j + \eta\frac{s_{j+1}}{s_j}\cos(\phi_{j+1} - \phi_j) + \eta\frac{s_{j-1}}{s_j}\cos(\phi_{j-1} - \phi_j) \qquad (7.2) \\ T\dot{z_j} &= P_j - z_j - (1 + 2z_j)s_j^2 \end{aligned}$$

(7.3)

The Continuum Limit

The continuum limit follows by expanding the amplitude, phase and carrier density in the above set of $3N - 1$ coupled ordinary differential equations in a Taylor series about s_j, ϕ_j, z_j. We are assuming that the field envelope, phase and carrier density do not vary much from one laser to the next in the array. The system of ordinary differential equations can then be considered to be a discretized version of

the following system of partial differential equations.

$$\begin{aligned} s_t &= zs - \eta h^2(2s_x\phi_x + s\phi_{xx}) \\ \phi_t + \delta &= -\alpha z + 2\eta + \eta h^2(s_{xx}/s - \phi_x^2) \\ Tz_t &= v(x) - z - (1+2z)s^2 \end{aligned} \tag{7.4}$$

Here h is the transverse width of each laser. In these expressions we have only retained terms to order h^2. The function $s(x)$ now represents amplitude, $\phi(x)$ phase, and $z(x)$ carrier density. The potential $v(x)$ now plays the role of the variable pumping current in the discrete equations.

We now seek time invariant solutions to the partial differential equations. The spatial variation of these equilibrium solutions is then determined by the following system of equations.

$$\begin{aligned} 0 &= zs - \eta h^2(2s_x\theta + s\theta_x) \\ \delta - 2\eta &= -\alpha z + \eta h^2(s_{xx}/s - \theta^2) \\ 0 &= v(x) - z - (1+2z)s^2 \end{aligned} \tag{7.5}$$

In this problem we use the last equation to determine the pumping. We are then left with two equations and three variables, so one of these variables must be prescribed. We assume that the field amplitude s is the prescribed variable. The two unknowns are then z and θ, and their behavior is determined by

$$zs - \eta h^2(2s_x\theta + s\theta_x) = 0 \tag{7.6}$$

$$-\alpha z + \eta h^2(s_{xx}/s - \theta^2) = \delta - 2\eta \tag{7.7}$$

Where $\theta = \phi_x$ is the phase gradient. From (7.7) we get

$$z = -\frac{\delta - 2\eta}{\alpha} + \frac{\eta h^2}{\alpha}(s_{xx}/s - \theta^2)$$

If we substitute this expression for z into (7.6), we get an equation for the phase gradient.

$$\theta_x + f(x)\theta + \frac{1}{\alpha}\theta^2 + g(x) = 0 \tag{7.8}$$

This is a Riccatti equation where the coefficients $f(x)$ and $g(x)$ depends on the assumed form of $s(x)$, and are given by

$$\begin{aligned} f(x) &= 2s_x/s \\ g(x) &= \frac{\delta - 2\eta}{\alpha\eta h^2} - \frac{1}{\alpha}\frac{s_{xx}}{s} \end{aligned}$$

This equation can yield a wide class of potentially interesting solutions. We consider two of the simplest cases here. The most interesting solutions physically are those that are phase locked. There are two kinds of phase locked solutions in this system, one with constant phase across the array, the other with constant intensity.

Constant Phase

For these solutions the phase gradient is identically zero. We observe that $\theta = 0$ is a solution of (7.8) only if $g(x) = 0$. From the definition of $g(x)$ we have

$$s_{xx} = \frac{\delta - 2\eta}{\eta h^2} s$$

There are two different types of solutions depending on the sign of the coefficient multiplying s. If this multiplier is negative the solutions are

$$s(x) = p\cos(kx + \tau)$$

Where p and τ are arbitrary and k is defined by

$$k^2 = \frac{2\eta - \delta}{\eta h^2}$$

The other class of solutions are found when the multiplier is positive

$$s(x) = \sinh(\bar{k}x), \cosh(\bar{k}x)$$

Where $\bar{k}$ now is defined by

$$k^2 = \frac{\delta - 2\eta}{\eta h^2}$$

In Figure 7.1, we sketch a typical sinusoidal (solid curve) and hyperbolic (dashed curve) field envelope for the continum model. We will elaborate further on the envelope profiles after we discuss their discrete analogs. The hyperbolic profile does not belong to the usual class of supermode solutions and there is experimental evidence that intensity profiles of this shape can be observed.

Constant intensity

Solutions with constant intensity across the array, $s(x) =$ constant give

$$\begin{aligned} f(x) &= 0 \\ g(x) &= \frac{\delta - 2\eta}{\alpha\eta h^2} \end{aligned}$$

so the equation for the phase gradient reduces to

$$\theta_x + \frac{1}{\alpha}\theta^2 + \frac{\delta - 2\eta}{\alpha\eta h^2} = 0 \tag{7.9}$$

This equation is separable. The solution [1] is

$$\theta = \sqrt{\frac{2\eta - \delta}{\eta h^2}} \tanh\left(\frac{1}{\alpha}\sqrt{\frac{2\eta - \delta}{\eta h^2}}x + c\right).$$

[1] There are actually two other types of solution, depending on the sign of $\delta - 2\eta$ and boundary values. If $\delta < 2\eta$ the solution involves the tangent. Some boundary values lead to a hyperbolic cotangent solution. These solution's discrete analogues have singularities, and so we do not explore them here.

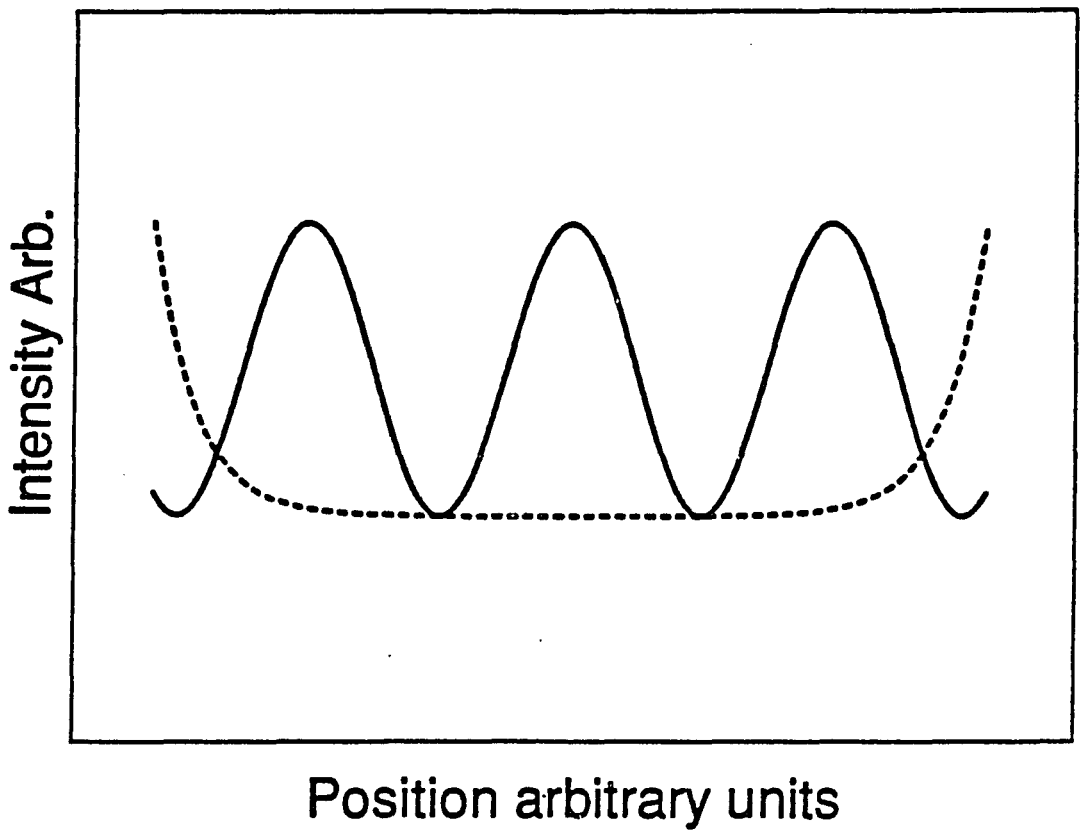

Figure 7.1: Intensity profiles for the sinusoidal (solid line) and hyperbolic (dashed line) phase-locked solutions to the continuum model.

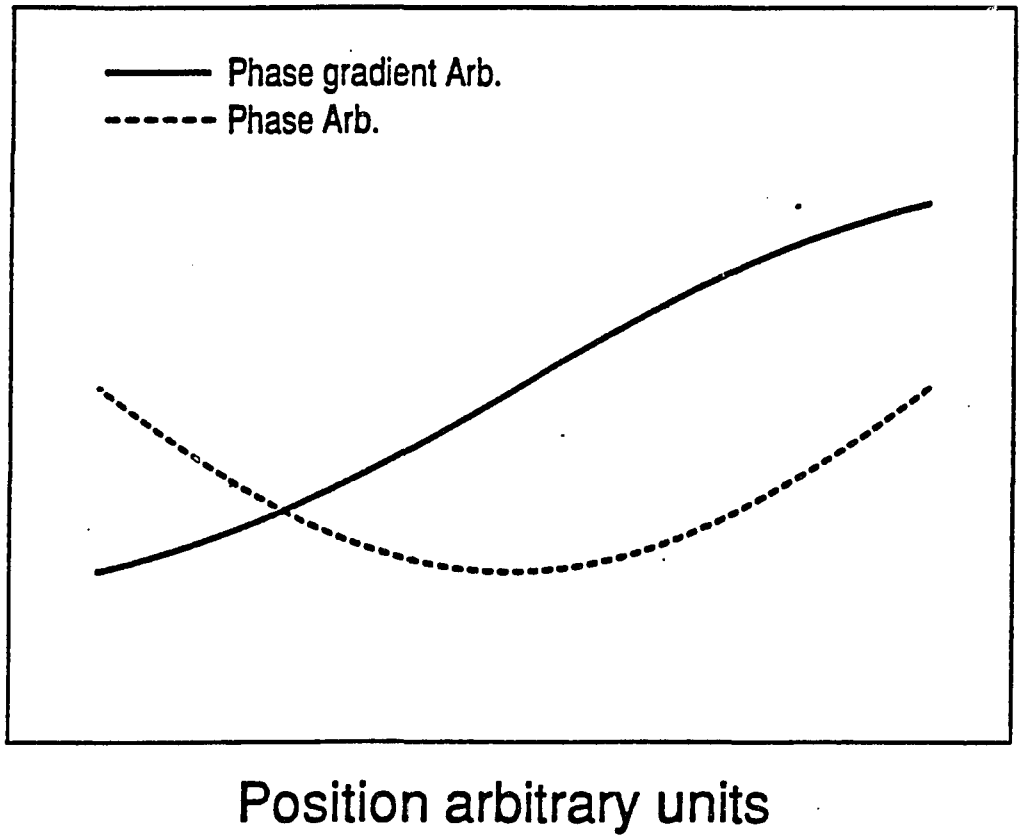

Figure 7.2: Phase and phase gradient profiles for a constant intensity solution for the continuum model.

The phase and phase gradient of the constant intensity solution are sketched in Figure 7.2. We will see shortly that this solution has a direct counterpart in the discrete array problem. These two simple cases illustrate the ease with which field envelope, carrier density and pumping profiles can be derived from the continum model.

Discrete array

The solutions for the continuum limit are readily accessible since they come from a Riccatti equation. It remains now to derive analogous solutions for the discrete array and establish in what sense these tend to the continuum solutions in the limit

$N \to \infty$.

Constant Phase

In the discrete model we look for equilibrium solutions with ϕ_i independent of i. From the equations for the discrete model we find that we must have $z_i = 0$ for all i and s_i must satisfy

$$\frac{s_{i+1}}{s_i} + \frac{s_{i-1}}{s_i} = \frac{\delta}{\eta}$$

The index i ranges from 2 to $N-1$ assuming that there are N lasers numbered from 1 to N. For $i = 1, N$ we get the equations

$$\begin{aligned} \frac{s_2}{s_1} &= \frac{\delta}{\eta} \\ \frac{s_{N-1}}{s_n} &= \frac{\delta}{\eta} \end{aligned}$$

We may think of these two last equations as supplying boundary conditions to the difference equation for the sequence s_i. We observe that these two last equations follow immediately from the difference equation by extending the sequence s_i to include s_0 and s_{N+1} and then enforcing the boundary conditions $s_0 = 0$ and $s_{N+1} = 0$.

The difference equation is solved by assuming $s_i = r^i$. Then r must satisfy the equation

$$r + \frac{1}{r} = \frac{\delta}{\eta}$$

The possible solutions to this equation are

$$r = \frac{1}{2}(\frac{\delta}{\eta} + -((\frac{\delta}{\eta})^2 - 4)^{\frac{1}{2}})$$

Observe that the roots always are reciprocals of each other, so that for a given value of r two linearly independent solutions of the recursive relation are $s_i = r^i$ and $s_i = r^{-i}$.

Let us first consider the case of complex solutions for r. This is the case if $\delta/\eta < 2$. Remembering the connection between δ and k in the continuum limit we observe that this corresponds to the case $k < 0$. We therefore expect periodic solutions. By taking linear combinations we find indeed that a linear independent pair of solutions in this case is

$$s_i = \sin(ki), s_i = \cos(ki).$$

Here k is determined by the boundary conditions $s_0 = s_{N+1} = 0$ for a laser array consisting of N lasers to be

$$k = \frac{2\pi}{N+1}m$$

for any integer m. These are the so called super-modes. Figure 7.3 and 7.4 show the near- and far-field intensity patterns for the lowest order supermode. The far-field profile shows the characteristic single lobed profile.

Second let us consider the case of real solutions for r. This is the case if $\delta/\eta > 2$. This corresponds to the case $k > 0$ in the continuum limit. Taking linear combinations as before we get the following set of linearly independent solutions.

$$s_i = \sinh(ki), s_i = \cosh(ki)$$

These solutions, cannot satisfy zero boundary conditions. In order to find solutions of this form, we must assume that $s_0 = a_1, s_{N+1} = a_2$ with $a_1, a_2 > 0$. With these conditions we can find solutions for every k. These solutions are clearly different

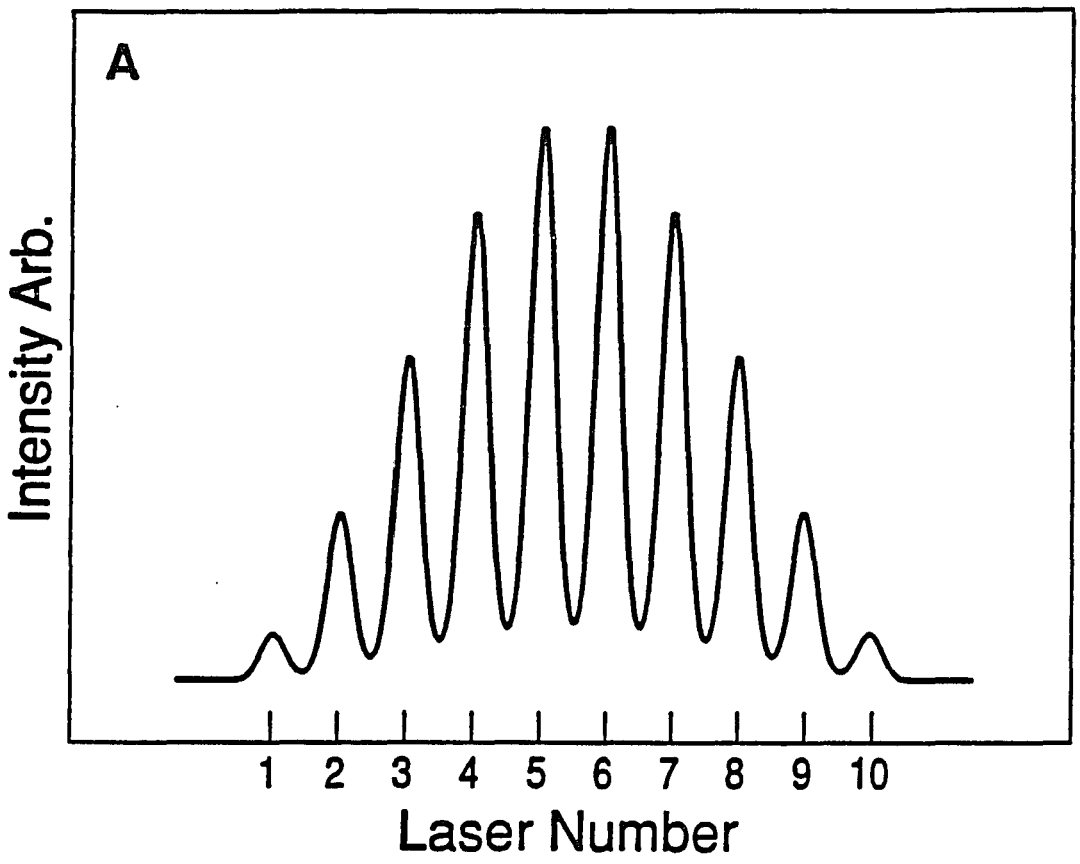

Figure 7.3: Near field intensity profile for constant phase solution

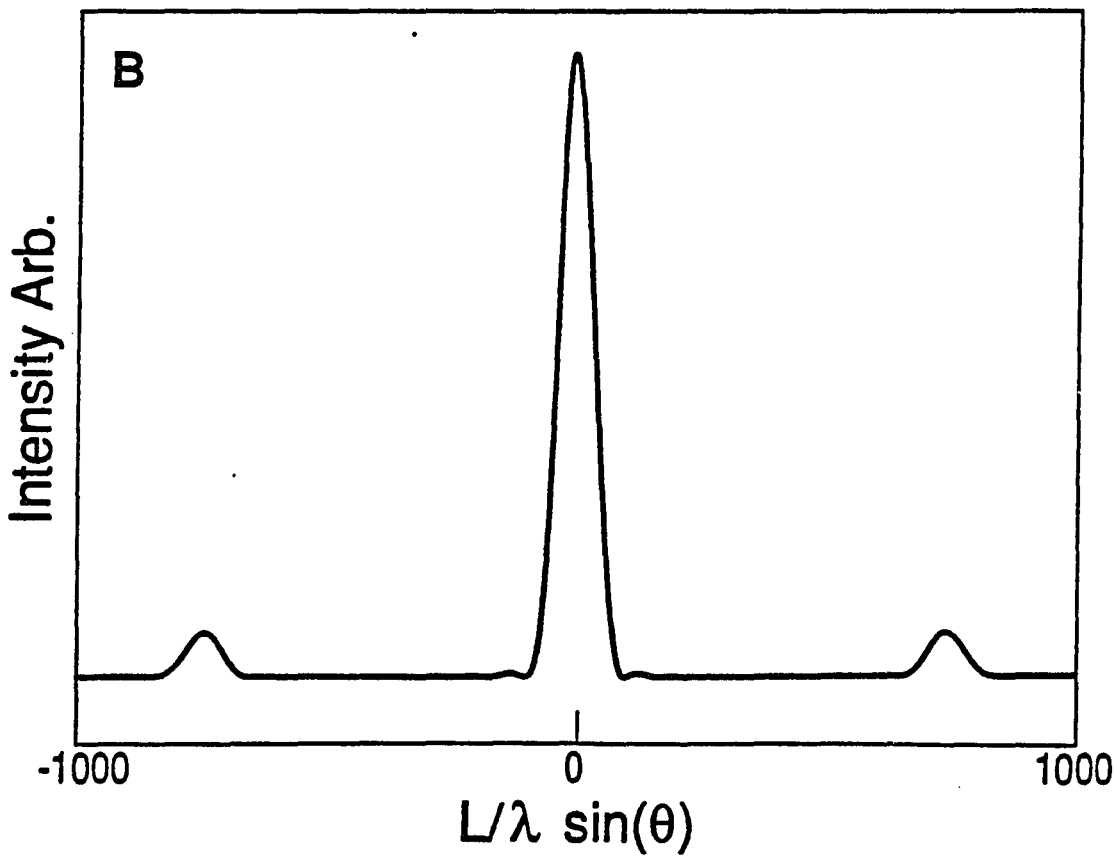

Figure 7.4: Far field intensity profile for constant phase solution

from the supermodes exibiting strong emmision at both ends of the array. Interestingly modes having qualitatively similar shapes have been observed experimentally. Moreover this class of array solutions allow for assymetric profiles by adjusting the boundary amplitudes a1 and a2. We note that the mode frequency is also adjustable depending on the boundary amplitudes a1 and a2. The phase-locked condition that requires that $s_i \geq 0$, restricts the solutions that we consider in this case only in that we consider only positive boundary values. In particular, if we impose the boundary conditions $s_0 = s_{N+1} = a$, we find the solution

$$s_i = A\cosh(k(i - (N+1)/2))$$

where A is an arbitary amplitude, and $k = 2cosh^{-1}(a/A)/(N+1)$.

Constant intensity

Let us look for solutions where $s_i = s$ and $\phi_i = \phi_i(0) + \delta t$. Writing $\theta_i = \phi_{i+1} - \phi_i$ we find from the first and second equations of (7.2) that

$$z_i = \eta\sin(\theta_i) - \eta\sin(\theta_{i-1}) \tag{7.10}$$

$$\alpha z_i = \eta\cos(\theta_i) + \eta\cos(\theta_{i-1}) - \delta \tag{7.11}$$

From these two equations we find that the phase gradient θ_i must satisfy the following relation

$$\sin(\theta_i - c) = \sin(\theta_{i-1} + c) - \frac{\delta}{\alpha\eta}\cos(c) \tag{7.12}$$

where $c = \tan^{-1}(1/\alpha)$.

In this recursive relation i goes from 2 to $N-1$. There are two more equations that determine θ_1 and θ_N. The same conditions that yield (7.10) and (7.11) in the

middle of the array, yield

$$z_1 = \eta \sin(\theta_1) \tag{7.13}$$

$$\alpha z_1 = \eta \cos(\theta_1) - \delta \tag{7.14}$$

and

$$z_N = -\eta \sin(\theta_N) \tag{7.15}$$

$$\alpha z_N = \eta \cos(\theta_N) - \delta \tag{7.16}$$

at the ends of the array. These yield the boundary conditions

$$\theta_1 = c - sin^{-1}(\delta \cos(c)/\alpha\eta)$$

$$\theta_N = -c + sin^{-1}(\delta \cos(c)/\alpha\eta)$$

It is convenient and equivalent to introduce θ_0 and θ_{N+1}, and to require that equations (7.10) and (7.11) be satisfied for $i = 1, \ldots, N$, while requiring the boundary conditions

$$\theta_0 = -c$$

$$\theta_{N+1} = c$$

These two equations together with (7.12) will determine for each N which δ if any gives a solution for the phase. As an example , for $N = 3$, $y = \delta/\alpha\eta \cos(c)$ must satisfy

$$y = \sin(\sin^{-1}(\sin(2c - \sin^{-1}(y)) - y) + 2c)$$

This equation has a solution, so there exists a phase profile for the case $N = 3$. We have not proved that a solution exists for any N, but by numerical means we

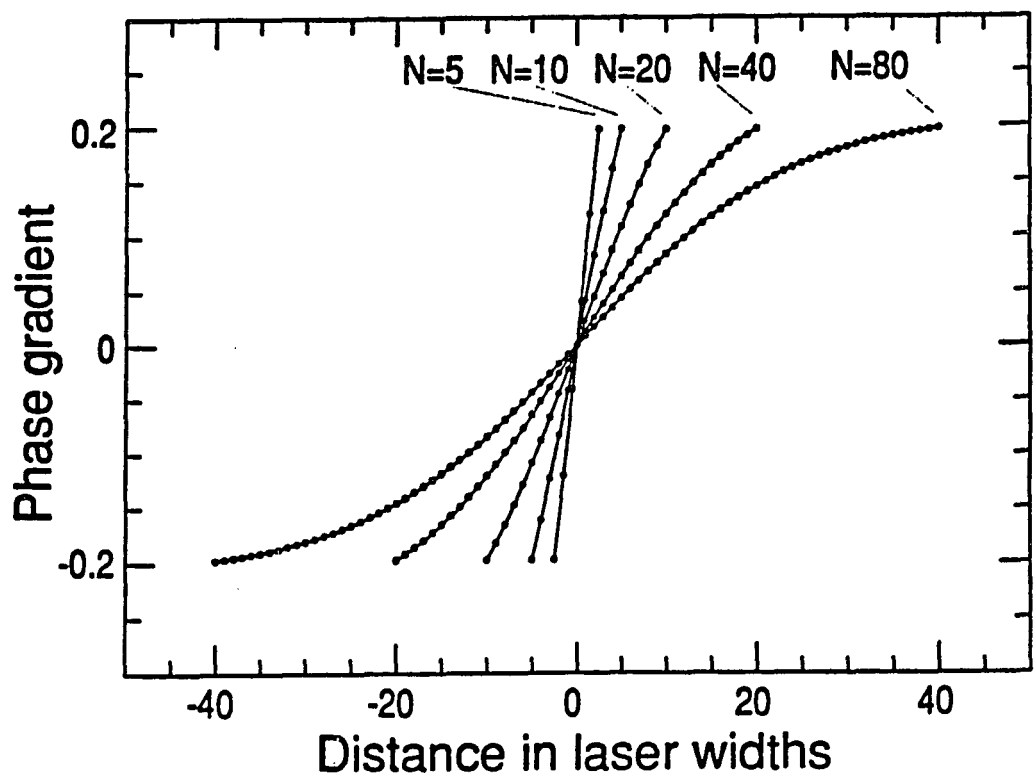

Figure 7.5: Comparison of discrete and continuous constant intensity phase gradient profiles for different numbers of lasers. The points are the discrete values, the curves are the continuous solutions.

have found the solution up to $N = 150$. Figure 7.5 shows the phase gradient across the array computed numerically for the discrete problem as points, and from the continuum model as curves for N =5, 10, 20, 40, and 80. The solution from the discrete model has two parameters, c a translation factor, and δ the detuning which can be adjusted. The translation was chosen to give symmetric solutions, and the detuning was chosen to match the boundary value. The agreement is strikingly good. We have as yet not understood why the agreement is so close to perfect. Figure 7.6 and 7.7 shows both near- and far-field intensity profiles for the case of a ten-stripe laser. This again shows a single lobed far-field profile.

We note in passing, that considerable care must be exercised when introducing

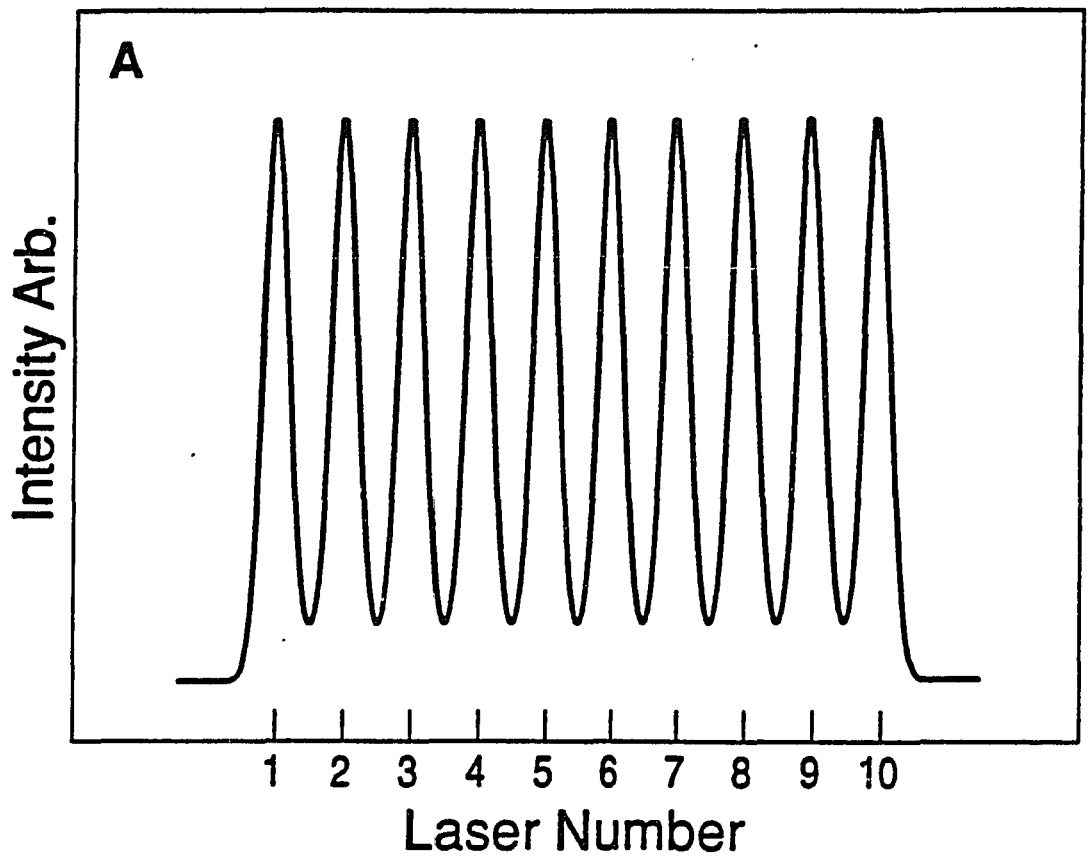

Figure 7.6: Near field intensity profile for constant intensity solution.

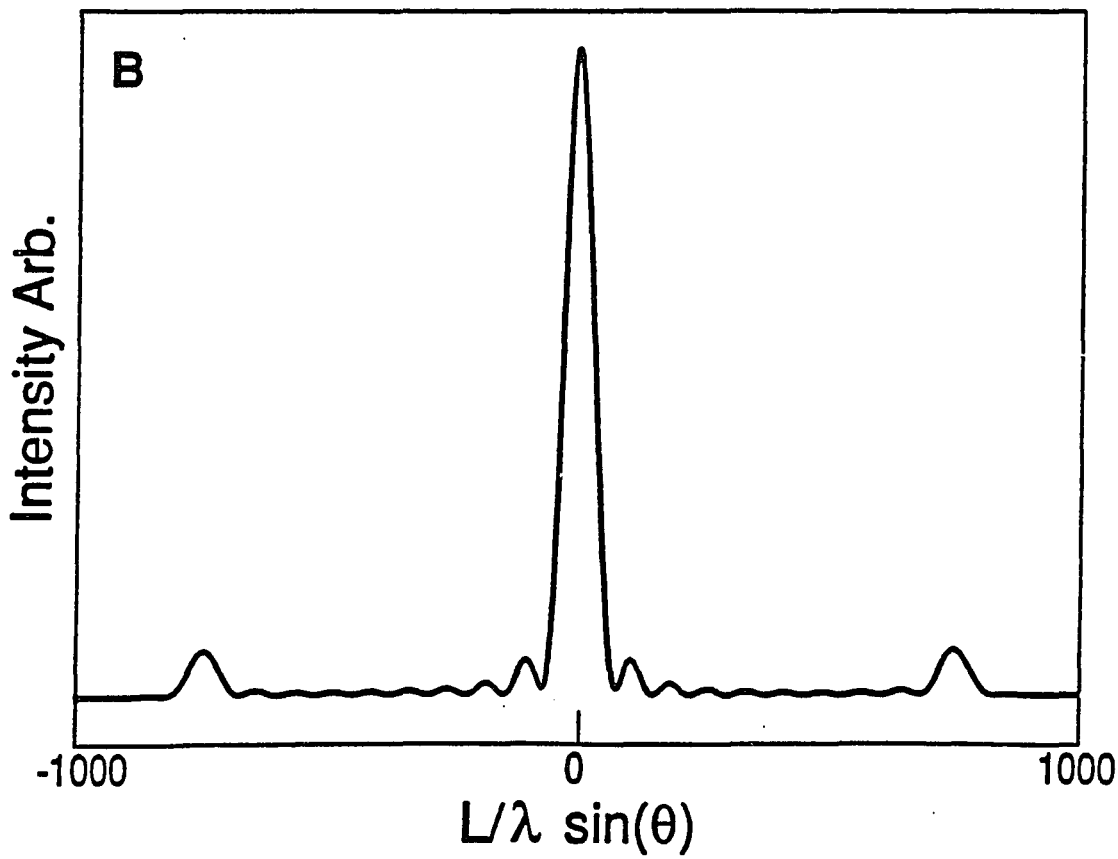

Figure 7.7: Far field intensity profile for constant intensity solution.

boundary conditions in the continum model that yields solutions consistent with the discrete array. This can be appreciated from the fact that, in going to the continous limit, higher order spatial derivatives appear in the model. Detailed analysis of the boundary conditions in the limit $\frac{h}{L} \rightarrow 0$ for both phase locked and constant intensity continum solutions shows that solutions to both models are self-consistent in the large N limit.

Linear stability

An important consideration from a practical viewpoint is whether these array mode profiles, whether discrete or continuous, are stable to perturbations. Previous stability analysis was restricted to the case $N = 2$ for the constant phase solution, although numerical solutions for a 10 element array suggest that the laser system should be intrinsically unstable. We have extended the stability analysis of the fundamental supermode and constant intensity solution to higher N using a combination of analytical and numerical methods. Figure 7.8 is a sequence of pictures showing the global behaviour of the instability boundary of the fundamental supermode as N increases.

Using asymptotic methods we have derived an expression for the value of the pumping where the fundamental supermode loses stability. We are using the numerical observation that the stability is lost for very small values of the pumping when the coupling is in the physical regime and that the bifurcation at this point is a pitchfork. The resulting formula is

$$p = \sqrt{\frac{\eta}{2\alpha}} \lambda^{\frac{1}{2}} .$$

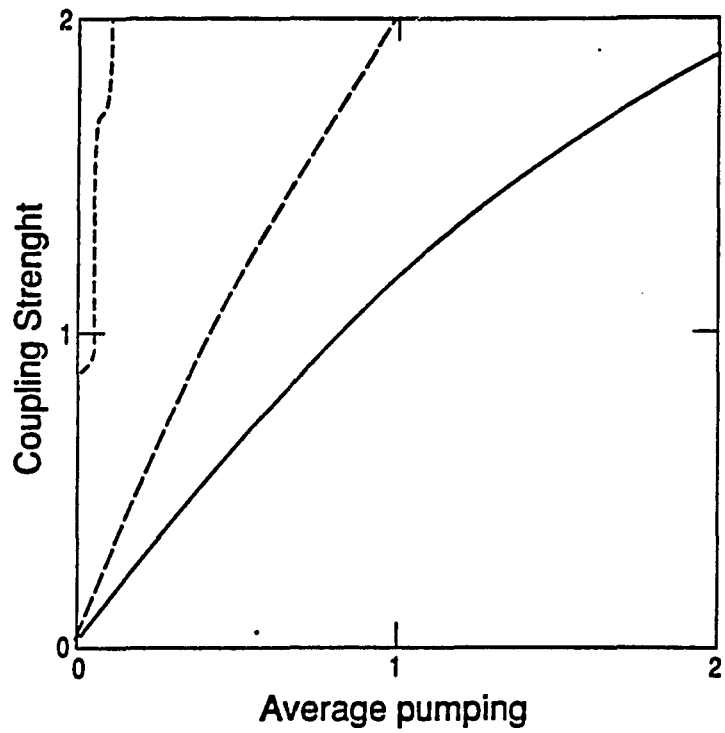

Figure 7.8: Stability curves for $N = 2$ (solid line), $N = 4$ (long dash), $N = 10$ (short dash) constant phase. The solution is stable above the curve

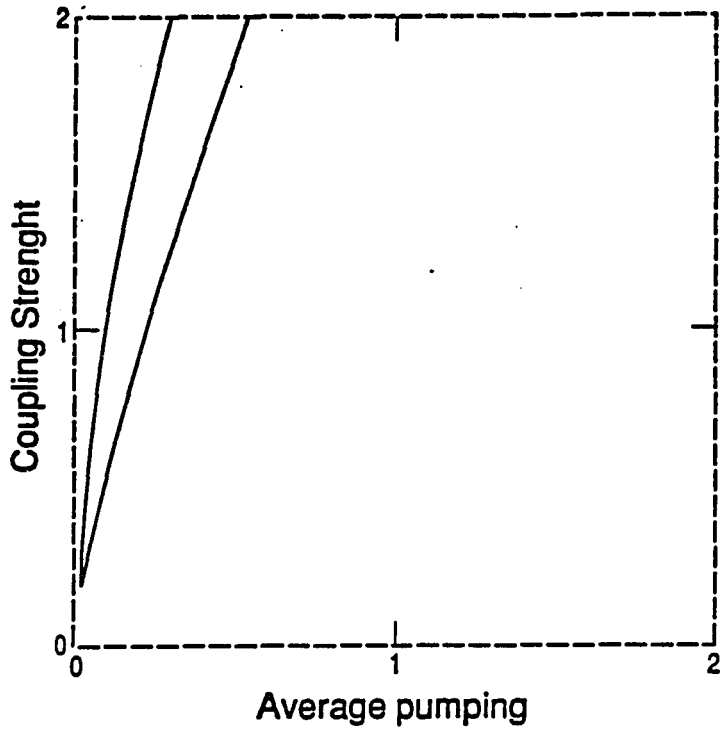

Figure 7.9: Stability boundary for constant intensity solution $N = 4$. The solution is stable above the curve. For $N = 2$ the constant intensity solution is identical to the constant phase solution and for $N = 10$ the solution is unstable in the whole domain in the picture

where λ depends only on N and is the eigenvalue of a N dimensional square matrix. The details of this derivation can be found in appendix A. The function λ stay finite as N increases. All the plots were calculated with $\alpha = 5$ and $T = 1$. The general trend is that at fixed average pumping level p, the instability domain shifts to higher η as a function of N. We note in particular that for physically reasonable values ($\eta \approx 10^{-3} - 10^{-4}, T = 2000$) both types of solution are intrinsically unstable. Figure 7.9 is a picture of the stability as a function of coupling and average pumping for the constant intensity solution when $N = 4$. The system is stable above the single curve.

Bifurcation Analyses

We have used the AUTO [6] bifurcation package to track branches of equilibrium solutions up to $N = 10$ for both types of solution discussed above. It is readily apparent from our study that the stiffness of the problem for physically realistic parameter values ($T = \tau_s/\tau_p \approx 2000$) causes the Hopf bifurcation responsible for the onset of dynamic pulsations to nearly coincide with the pitchfork bifurcation on the lowest threshold instability boundary. The branch of periodic solutions emanating from the Hopf bifurcation point becomes essentially vertical as a function of increasing pumping and terminates on a homoclinic orbit. The sharp transition to large amplitude pulsations on crossing the instability boundary is consistent with homoclinic excursions in phase space. We find that in the limit $T \rightarrow 1$, the Hopf bifurcation migrates away from the pitchfork bifurcation to higher pump values. There now exists a pitchfork bifurcation from a phase-locked state to a stable state with $\theta \neq 0$ but small. With further increase in the pumping, the laser output can now break into stable periodic oscillations representing a small modulation about the constant phase gradient solution. This exercise proves useful when considering injection locking of the array in a work now in progress. Our overall conclusions here are that the physically accessible solutions (discrete and continuous) are intrinsically unstable in a free-running mode of operation.

Figure 7.10 shows bifurcations diagrams generated from AUTO for N =2 and 4, for both the lowest-order supermode and the constant intensity solution. All bifurcation plots were calculated with $\eta = 0.5$, $T = 1$ and $\alpha = 5$. In each diagram, the initial bifurcation at zero (normalized) average pumping current, which represents the laser array turning on, is followed at higher pumping levels by a secondary

symmetry breaking bifurcation (Label 1 in each diagram). In Figures 7.10a and 7.10b corresponding to the N =2 and 4, phase-locked lowest-order supermode, the phase-locking is destroyed and the relative disposition of intensities of each element is represented by the fixed labels 2 or 3 in both diagrams. The solid line represent stable solutions and the dashed ones unstable solutions. Even though the phase-locking is destroyed, the laser array output remains constant for increasing pumping up to the Hopf bifurcation (Label 4) point as shown in figure 7.10b. Beyond this point the array becomes dynamically unstable and undergoes periodic oscillations which eventually lead to chaotic outputs. The situation in Figure 7.10c is essentially similar except that the constant intensity solution is initially dynamically unstable up to the point labelled 1. We reiterate that these parameter values are not physically realistic for existing evanesently coupled laser arrays. However the underlying equlibrium branches do not change as $T \rightarrow 2000$ but their stability characteristics do. The equilibrium solutions while unstable, provide important information with regard to analysis of the dynamics of the array.

Conclusion

In conclusion, we have presented a continuum model of the discrete array derived from coupled mode analysis, that allows one to derive new types of diode laser array mode solutions in a simple fashion. Our stability analysis of some of these solutions shows that all are intrinsically dynamically unstable under free-running mode of operation. Recent experiments with a streak camera [24] shows that unusual spatio-temporal profiles can appear transiently in the laser array near-field output. It is important therefore to be able to isolate the broadest classes of allowed solu-

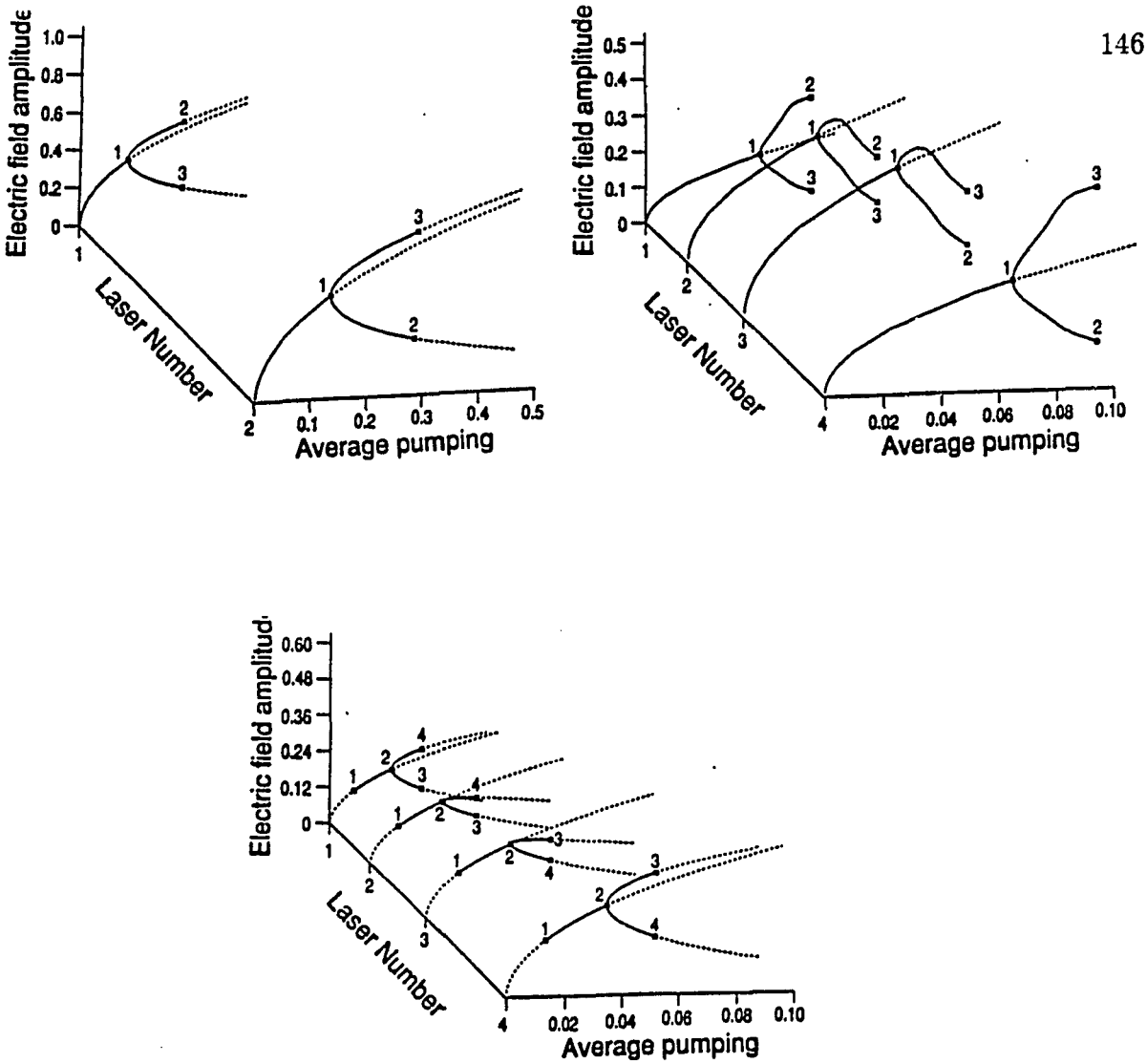

Figure 7.10: Bifurcation diagrams for a) $N = 2$, b) $N = 4$ constant phase, and c) $N = 4$ constant intensity. Note for $N = 2$ the constant phase and constant intensity solutions are identical.

tions to the discrete array problem. For example, the hyperbolic profile identified as a solution to the continuum model suggests that output pulsations with most of the energy confined to the edge lasers may be possible. Pulsations of this type have been observed experimentally. The continuum model should prove particularly powerful when analyzing injection-locking of these arrays as the underlying partial differential equation is more amenable to analytic investigation. The effect of injection-locking on the array and its continuum representation will be the subject of a future publication.

Chapter 8

APPENDIX C

We will look for phaselocked solutions with constant phase across the array. Solutions of this type are desirable because they will produce a time invariant single lobed far field, and all the energy will be consentrated in a single spot. The carrier densities Z_j will be assumed to be time invariant. From (6.6) we find that the time invariant carrier densities are given by

$$Z_j = \frac{p_j}{1+2|e_j|^2} \tag{8.1}$$

Substituting (8.1) into (6.5) we find

$$\begin{aligned} \frac{de_j}{dt} &= -\frac{1}{2}e_j + (1-\imath\alpha)\frac{p_j}{1+2|e_j|^2}e_j + \imath\eta(e_{j+1} \\ &\quad +e_{j-1}) + ae^{\delta t-\frac{\pi}{2}} \end{aligned} \tag{8.2}$$

(8.3)

For the field we will assume the following form

$$e_j = s_j e^{\delta t-\frac{\pi}{2}+\phi_0} \tag{8.4}$$

(8.5)

Where s_j will be assumed to be real and s_j are timeinvariant. The parameter ϕ_0 is the phaselag between the injection and the response of the array.It will determine how much energy is transferred to the array through the injection. As for a driven pendulum there is no energy transfered if $\phi_0 = \frac{\pi}{2}$. This is pretty obvious since the laser array model it nothing else that a coupled set of driven oscillators. Energy relations for the driven array are derived in appendix G.

Upon substitution of (8.4) into equation (8.2) we get the following

$$p_i = (\frac{1}{2} - \frac{a_i \cos\phi_0}{s_i})(1 + 2s_i^2) \tag{8.6}$$

$$s_{i+1} + s_{i-1} - \Delta s_i = \frac{a}{\eta}(\sin(\phi_0) - \alpha\cos(\phi_0)) \tag{8.7}$$

Where we have defined

$$\Delta = \frac{\frac{1}{2}\alpha + \delta}{\eta} \tag{8.8}$$

The array is not infinite so the above recursion relation (8.7) for s_i must be supplied with boundary conditions. Since the first laser has no left neighbour and the right laser has no right neighbour the boundary conditions must be taken as

$$s_0 = s_{N+1} = 0 \tag{8.9}$$

Where N is the number of lasers in the array. Equation (8.6) is an energy balance for laser No. j. Since the amplitude of each laser is a constant the energy in each laser is also a constant and equation (8.6) is a balance between gain and loss. Mathematically speaking the equation (8.6) is a result of over constraining the

system of equations by forcing constant phase profile across the array. Since there are two equations to satisfy, equation (8.6) follows. Both the injection profile a_j and the pumping profile p_j can be manipulated experimentally. We will in the following investigate the case of constant injection profile and the case of constant pumping profile.

Constant injection

In the case of constant injection profile ($a_j = a$ for all j) we will investigate two different cases. In the first case the right hand side of equation (8.7) is zero but a is not zero. In the second case the right hand side is not zero.

The driven supermode

We will in this section investigate the particular case when the right hand side of the recursion relation is zero and a different from zero. The recursion relation for the amplitude s_j reduce to the equation for the supermodes in the case of free running conditions. This can only happen when the phaseshift ϕ_0 is given by

$$\phi_0 = \arctan \alpha \tag{8.10}$$

Specifying this value for the phase corresponds, through equation (8.6), to choosing a current pumping profile. The recursion relation (8.7) with boundary conditions (8.9) is solved by (appendix K)

$$s_i^l = x \sin \frac{l\pi i}{N+1} \tag{8.11}$$

at

$$\Delta_l = 2 \cos \frac{l\pi}{N+1} \tag{8.12}$$

and

$$s_i^l = x(-1)^i \sin \frac{l\pi i}{N+1} \tag{8.13}$$

at

$$\Delta_l = -2\cos\frac{l\pi}{N+1} \tag{8.14}$$

Where l is an integer in the range $0 < l < \frac{N+1}{2}$. The values of Δ give a discrete set of values for the detuning δ corresponding to the fact that the supermodes has frequencies distributed in a narrow domain around the single laser frequency $\omega_0 - \frac{1}{2}\alpha$.

Linear stability of driven supermodes

We will in this section study the linear stability of the driven supermodes. The linearized laser array equations are derived in appendix D. We will first investigate the case of a two element array $N = 2$. For this case the linear stability is determined by the eigenvalues of a 6x6 matrix. This eigenvalue problem is studied in detail in appendix E. Because of a reflection symmetry in the problem we reduce the eigenvalue problem to two uncoupled 3x3 problems, using sum and difference variables. Each of these problems can then be analysed in detail. We do not find analytic expressions for the eigenvalues, but using graphical techniques find analytic expressions determining the domain of stability in parameter space. We find that some sufficient conditions for stability in this case are

$$a < \frac{\bar{s}(1+2\bar{s})}{\cos\phi_0 T(1+\alpha^2)} \tag{8.15}$$

$$\eta < \frac{1}{2}(\alpha + \frac{1}{\alpha})\frac{a\cos\phi_0}{\bar{s}} \tag{8.16}$$

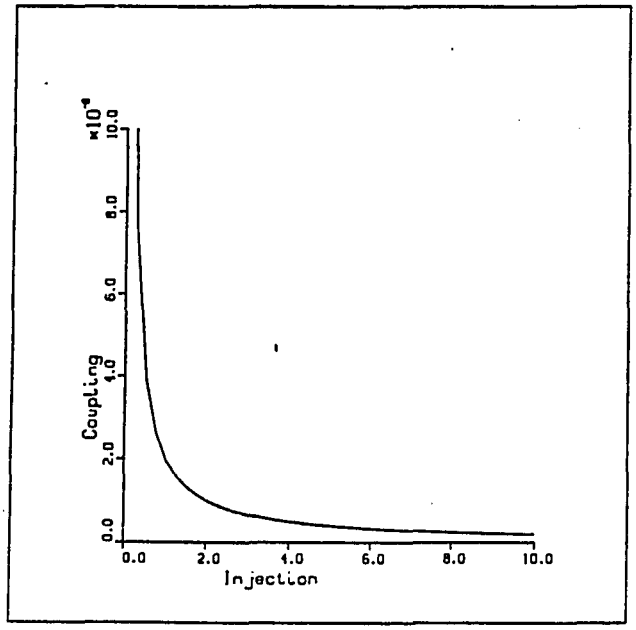

Figure 8.1: The domain of stability of the injection locked fundamental supermode as a function of coupling and injection. The solution is unstable to the right of the single curve. Parameter values are $N = 2$, $\alpha = 5$, $T = 10^4$ and $a = 1$.

Where $\bar{s}$ is the common amplitude of the two lasers. In addition we have stability if η is big enough as in the case of no injection. Figure 8.1 shows the domain of stability as a function of η and average amplitude computed numerically.

It is interesting to note the if a is choosen small enough so that (8.15) is satisfied then we will have stability if

$$\eta < \frac{1 + 2\bar{s}}{2\alpha T} \tag{8.17}$$

This is exactly the condition for stability of the highest order supermode in the case of no injection. We also observe that the supermode is stable even for zero coupling . The above result means that a two element laser array can be stabilized

by injection the array with a common frequency if the elements do not couple to strongly. This is important since you typically want to put a lot of lasing elements in a small space so that coupling is hard to avoid. From the above considerations we can conclude that one way to stabilize a laser array is to use an outside master laser and to minimize coupling. For the case $N > 2$ use a continuity argument on the linear stability results for a single laser (appendix E) to prove that the any constant phase solution of the driven is stable for weak enough coupling. Figure 8.2 shows the stability boundary as a function of coupling and average electric field amplitude across the array. The parameter values are $N = 10, T = 10^4, \alpha = 5$ and $a = 10^{-5}$. The system is unstable above the single curve.

There are of course several other properties that we would like the solution to have. Among these are a large domain of attraction and structural stability. We have addressed these questions by solving the array equations numerically with perturbations. We have in these investigations used the values $T = 10^4$, $\alpha = 5$, $a = 0.001$ and average amplitude 0.01. Figure 8.3 shows the time evolution when we perturb the first supermode for a 10 element array in the stable regime. It is clearly attracted to the supermode, so the fundamental supermode is locally attracting at least for some initial conditions.

The domain of attraction is further investigated in Figure 8.4, where we are starting a 30 element array from zero initial condition and let it evolve. Again we see that the fundamental supermode is attracting the initial condition. From these and similar numerical runs we conclude that the fundamental supermode has a very large basin of attraction.

We have however also the question of stability with respect to variation of the

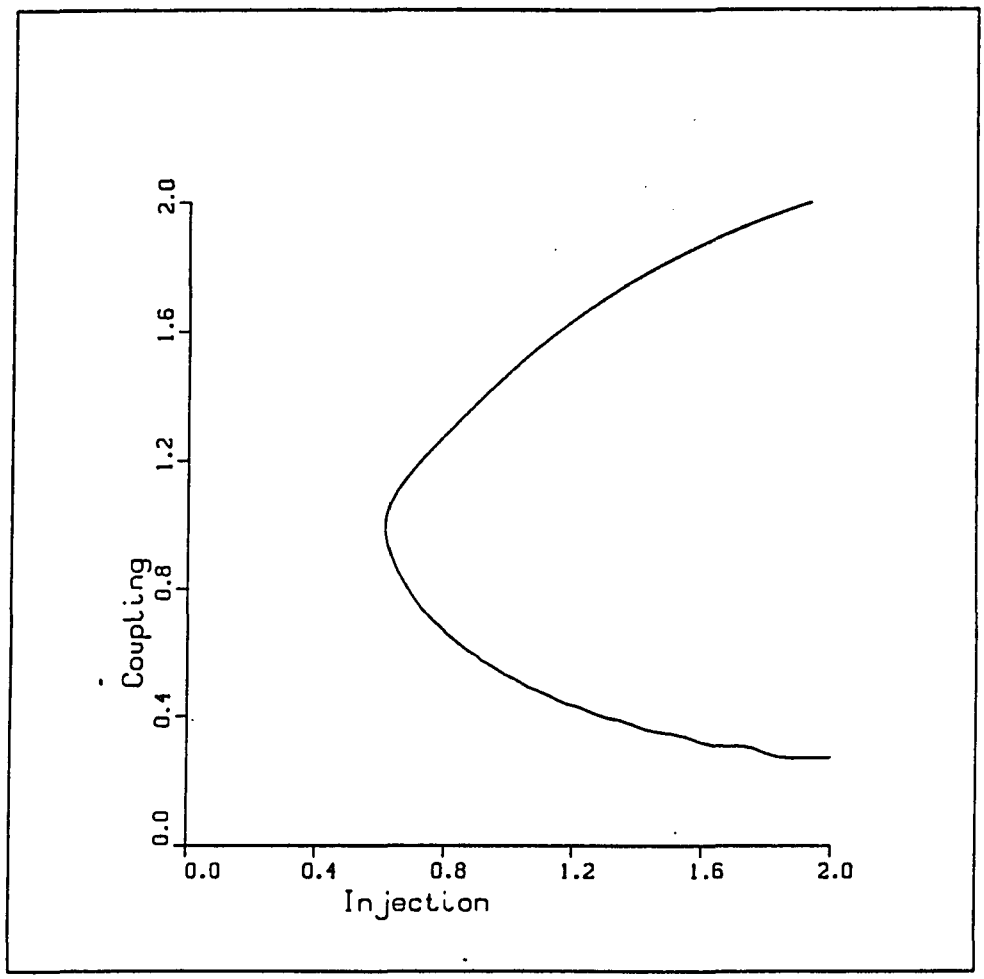

Figure 8.2: The domain of stability of the injection locked fundamental supermode as a function of coupling and injection. The solution is unstable to the right of the single curve. Parameter values are $N = 10$, $\alpha = 5$, $T = 10^4$ and $a = 1$.

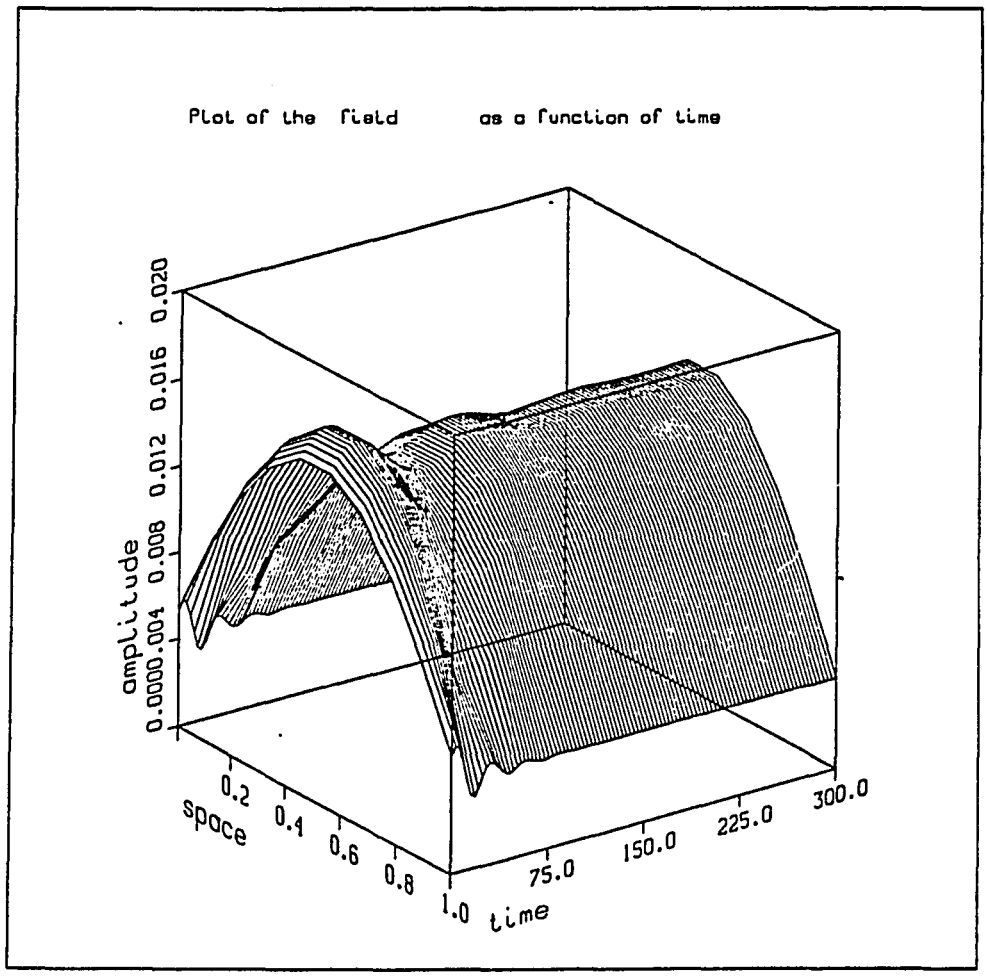

Figure 8.3: The time evolution of a perturbation of the first fundamental supermode for a 10 element array in the stable regime. Parameter values are $T = 10^4$, $\alpha = 5$, $a = 0.001$ and $N = 10$.

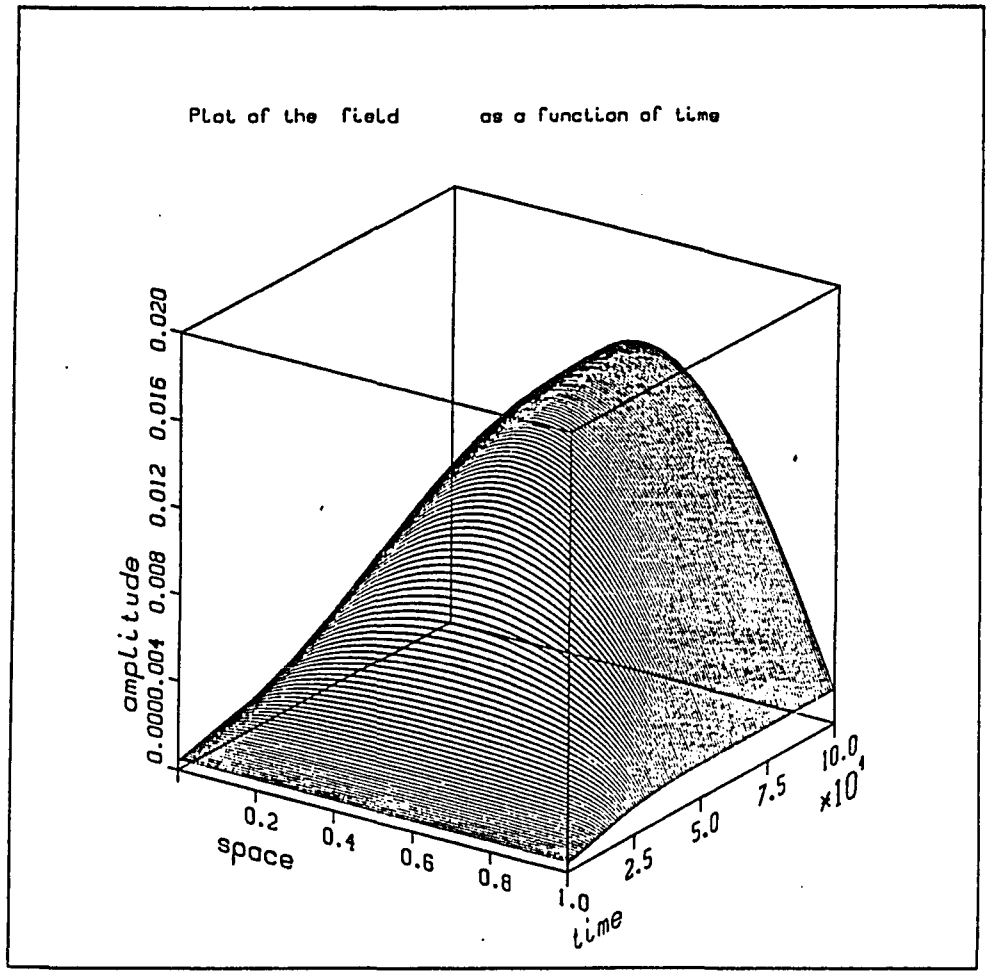

Figure 8.4: The time evolution of the electric field for a 30 element array starting from zero with current pumping corresponding to the first funcdamental supermode. Parameter values are $T = 10^4$, $\alpha = 5$, $a = 0.001$ and $N = 30$.

pumping profile from the shape determined by equation (8.6). This is an important point because it is experimentally impossible to control the pumping profile in such detail that equation (8.6) is exactly satisfied. Mathematically the phase locked solutions exist only if (8.6) is exactly satisfied. If it is not exactly satisfied the real part of the laser array field equation is not zero. From the equations one can see that one could still have phaselocked solutions in this case if the phase varied across the array. We have run the 30 element laser array equations numerically with a slightly perturbed pumping profile (0.1% of average) for 10^6 time units and, as Figure 8.5 indicate, the amplitude profile converges to a new time invariant shape. The phase is not constant across the array anymore. Figure 8.6 shows the phase profile across the array at $t = 10^6$.

Finally we have adressed the question of what happens when the detuning is not exactly at the correct value determined from equation (8.12). Figure 8.7 show the phase profile across the array at $t = 10^6$ when the value of Δ is perturbed by a small amount (10%). We can not prove by numerical means that the field shape at $t = 10^6$ is stable. It could be a hyperbolic type fixpoint with very slow unstable manifold. With a perturbation of Δ of the size we are using the laser array equations will experience a perturbation on the order of 10^{-4}, so a natural timescale for the evolution should be 10^4. Since we are running the system up to $t = 10^6$ we feel confident that what we see are a stable attracting solution of the array equations.

The driven arraymode

In this section we consider the case when the right hand side of (8.7) is nonzero. We must now solve a second order linear recursion equation with a constant injection

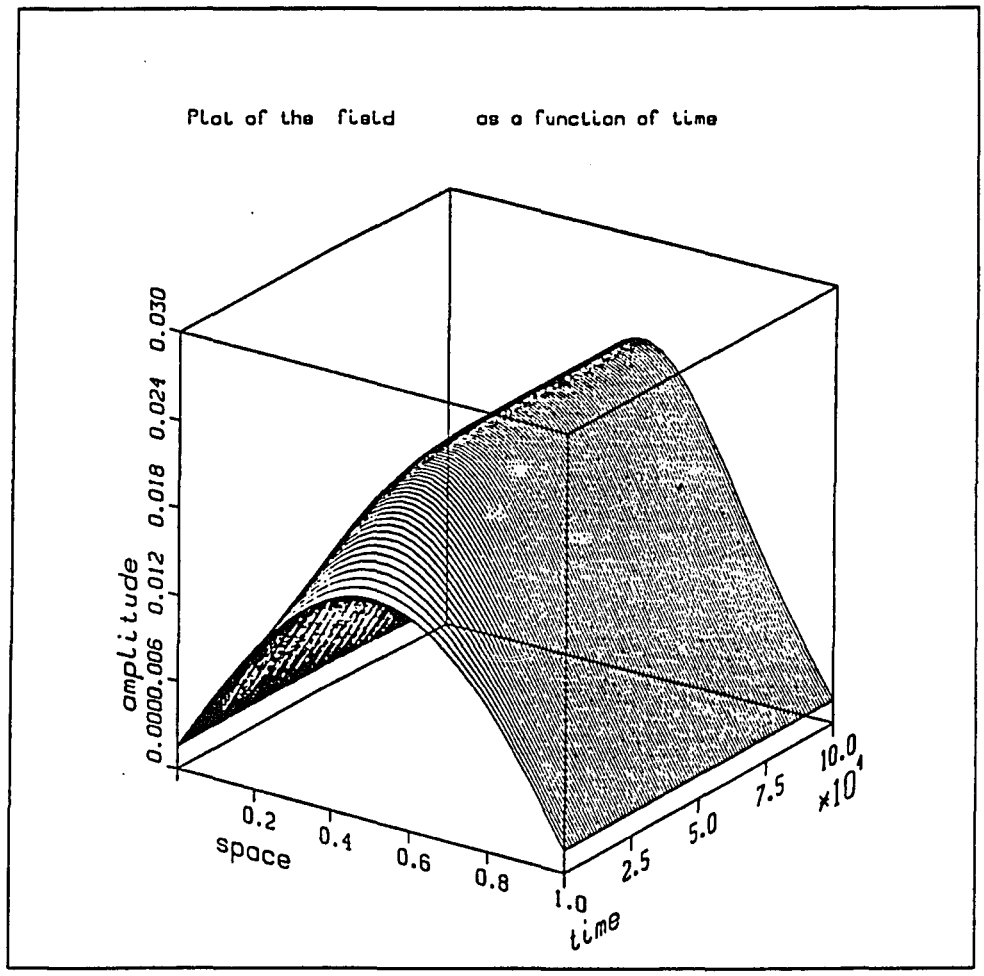

Figure 8.5: The time evolution of the electric field amplitude for a 30 element array when the pumping profile is perturbed by 0.1% of average. Parameter values are $T = 10^4$, $\alpha = 5$, $a = 0.001$, $N = 30$.

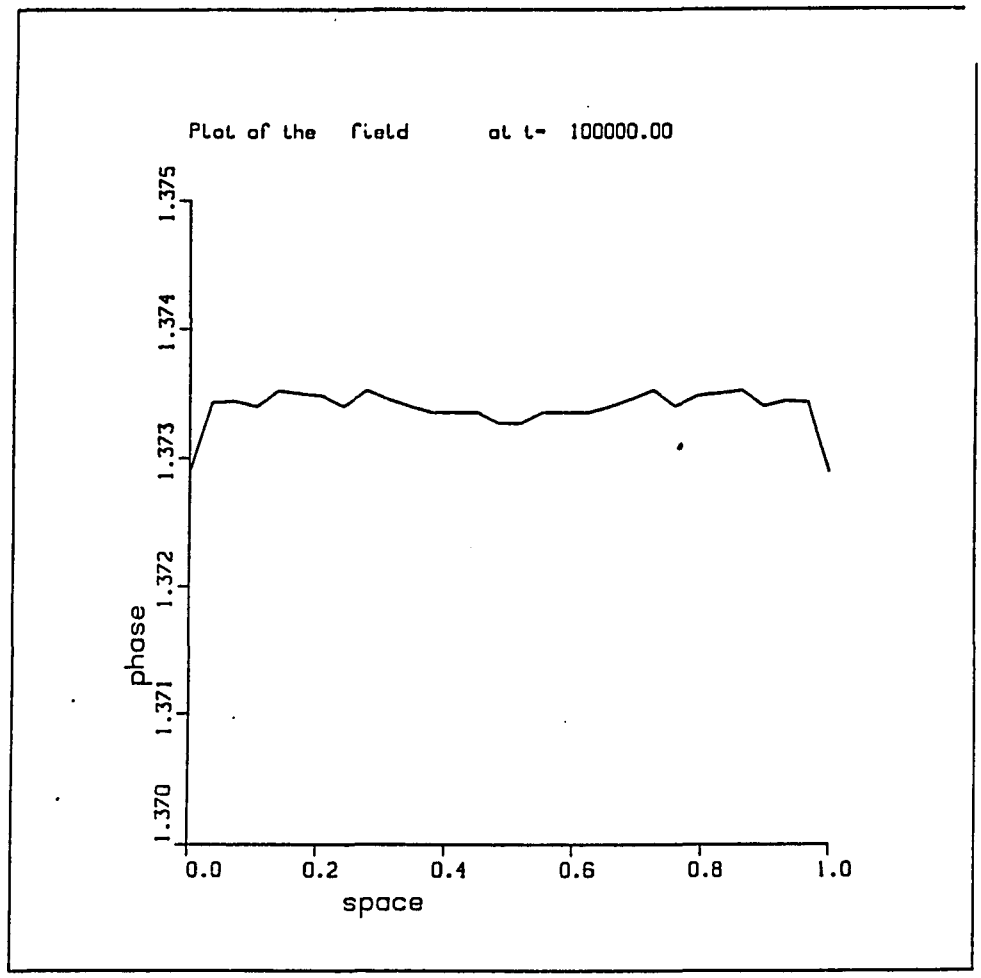

Figure 8.6: The phase profile across the array at $t = 10^6$ when the pumping profile is perturbed by 0.1% above average.The parameter values are $T = 10^4$, $\alpha = 5$, $a = 0.001$, $N = 30$.

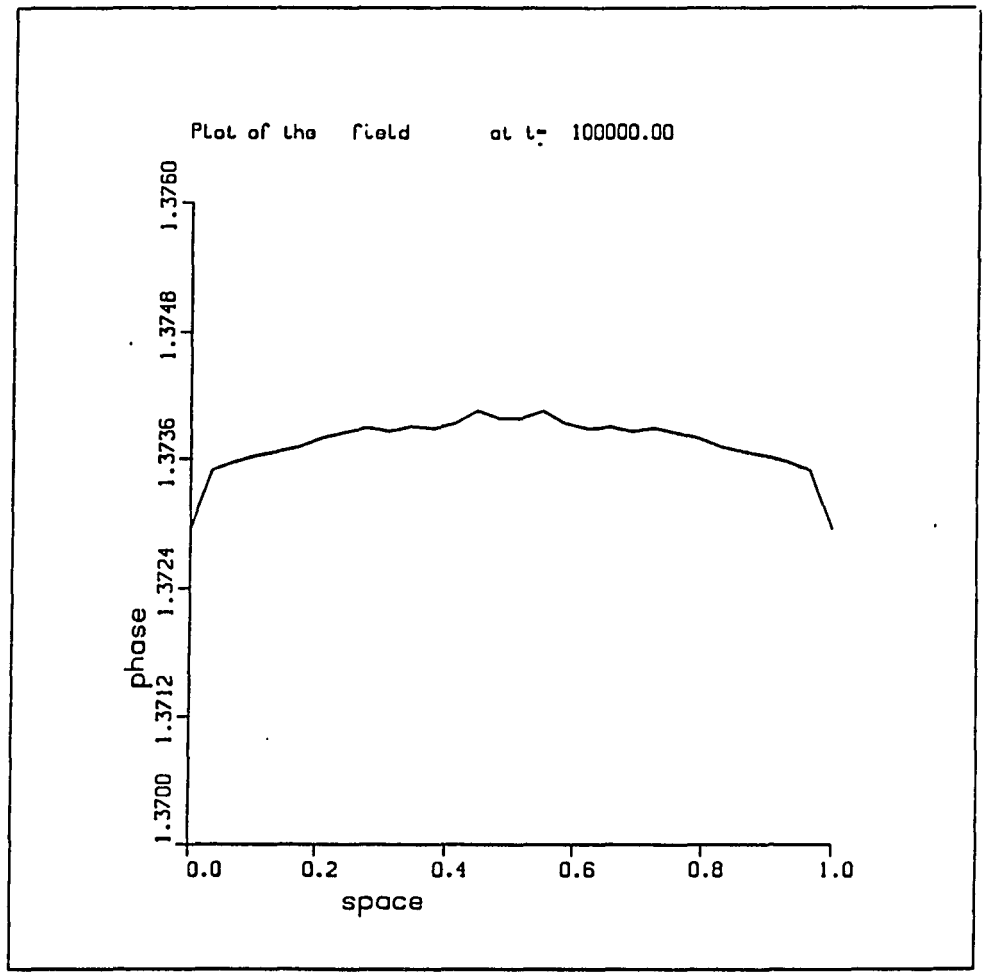

Figure 8.7: The phase profile across the array at $t = 10^6$ when the detuning is perturbed by 10%. Parameter values are $T = 10^4$, $\alpha = 5$, $a = 0.001$, $N = 30$.

term. The type of solution depends on the value of the parameter Δ. As we see in appendix L there are many different cases depending on the values of the parameters and on whether the number of elements in the array is even and odd. None of these appear to be more stable than the driven supermode. Some of them have however interesting cooperative properties. We will only discuss the case $\Delta = 2$. This solution is both positive and stable for low enough amplitude. The formula derived in appendix L is

$$s_j = Aj(j - (N+1)) \tag{8.18}$$

Where $A = \frac{aR}{2}$. The amplitude profile is just a parabola. Figure 8.8 is a picture of this profile for a 10 element array when $\eta = 10^{-3}$, $\alpha = 5$ and the average amplitude is 10^{-5}.

It is interesting to note that the total intensity for this solution increase as the fifth power of the number of elements in the array. This should be compared to a linear increase for the supermode solutions of the undriven array. So this parabolic solution takes much more advantage of the array than the supermodes. It is however difficult to make use of this N^5 dependence since it will require more and more power as N increases, quickly passing beyond any practical limits. If you require that the current pumping supplied to any element in the array stay below a certain fixed limit when N increases, the total intensity will only increase linearly with the size of the array.

There is also the issue of stability of the solution. Figure 8.9 is a picture displaying the stability as a function of coupling η and average amplitude of the solution. We observe that this solution is much less stable than the solution investigated in

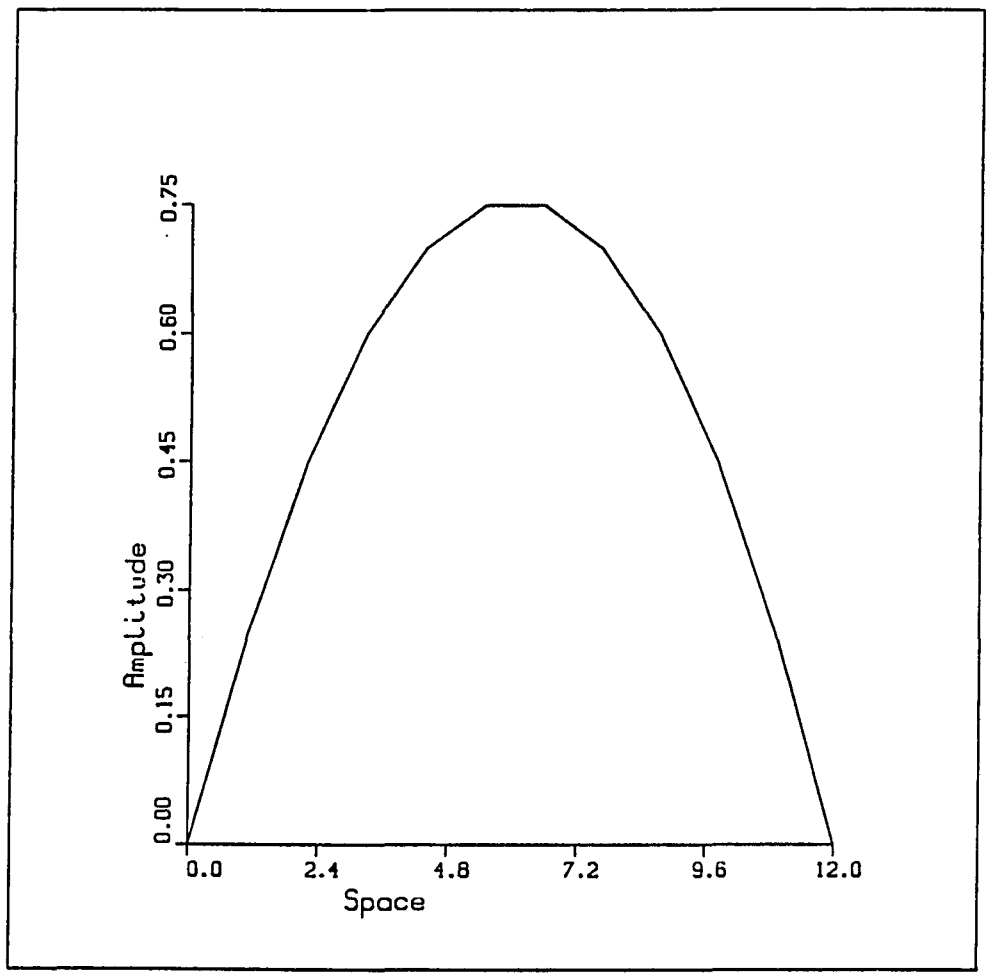

Figure 8.8: The amplitude of the electric field for the parabolic array mode across a 10 element array. Parameter values are $\eta = 10^{-3}$, $\alpha = 5$, $\phi_0 = 0$, $\Delta = 2$ and the average amplitude of the solution is 10^{-5}.

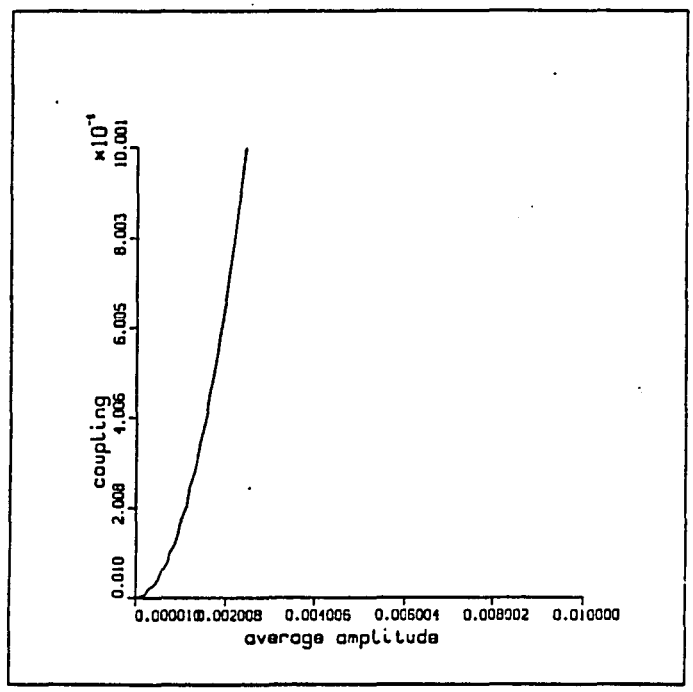

Figure 8.9: The stability of the parabolic array mode as a function of coupling and average amplitude. The solution is unstable to the right of the single curve. Parameter values are $\alpha = 5$, $T = 10^4$, $\Delta = 2$ and $\phi_0 = 0$.

the last section.

In the stable region it is however attracting when starting at zero. Figure 8.10, 8.11 are pictures of the time evolution of the amplitude and phase starting at zero for a 10 element array.The parameter values are $\Delta = 2$, $\alpha = 5$,$T = 10^4$ and $\eta = 0.0002$.

Constant pumping

We will in the following investigate the case where the current pumping is constant across the array. Equation (8.6) then will determine the injection profile a_j as a

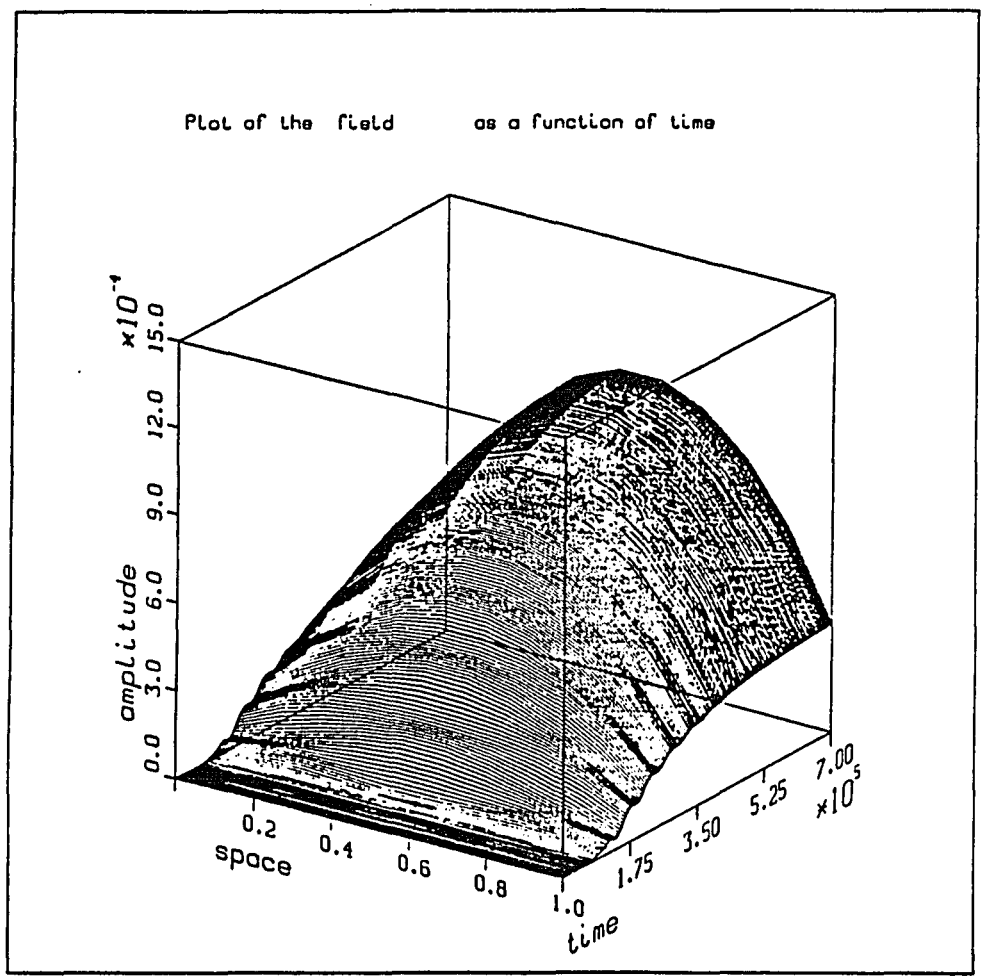

Figure 8.10: The time evolution of the electric field amplitude starting from zero in the stable regime for the parabolic array mode. Parameter values are $\Delta = 2$, $\alpha = 5$, $T = 10^4$, $N = 10$ and $\eta = 0.0002$.

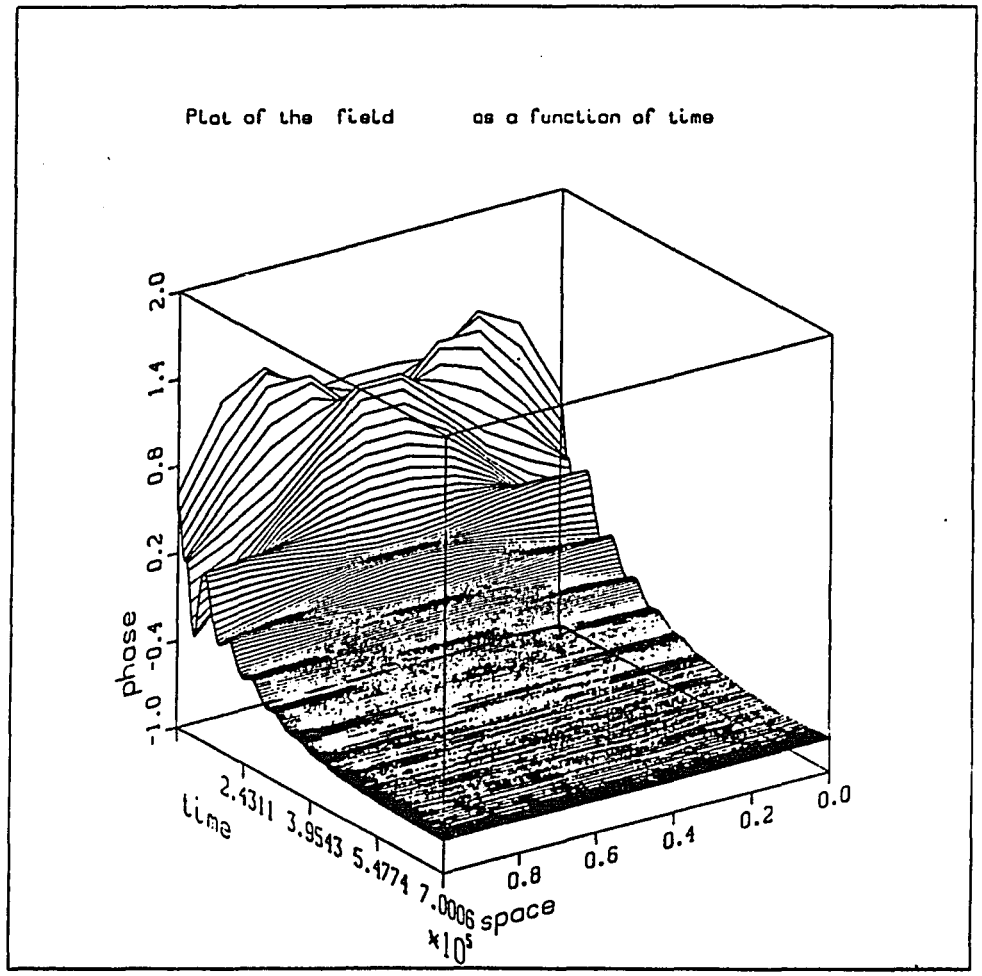

Figure 8.11: The time evolution of the electric field phase starting from zero in the stable regime for the parabolic array mode. Parameter values are $\Delta = 2$, $\alpha = 5$, $T = 10^4$, $N = 10$ and $\eta = 0.0002$.

function of the amplitude s_j and the pumping p. We find

$$a_j = \frac{s_j}{\cos\phi_0}(\frac{1}{2} - \frac{p}{1+2s_j^2}) \tag{8.19}$$

We will assume in the following that the dimensionless intensity s_j^2 is much smaller than 1. This is, (appendix F) a realistic assumption. Substitute (8.19) into (8.7). This gives a closed equation for the field amplitude profile s_j.

$$s_{j+1} + s_{j-1} - 2s_j - \gamma_1 s_j = -\gamma_2 \frac{s_j}{1+2s_j^2} \tag{8.20}$$

Where we have defined

$$\gamma_1 = \Delta - 2 + \frac{R}{2\cos\phi_0} \tag{8.21}$$

$$\gamma_2 = \frac{pR}{\cos\phi_0} \tag{8.22}$$

$$R = \frac{\sin\phi_0 - \alpha\cos\phi_0}{\eta} \tag{8.23}$$

We will solve this nonlinear discrete boundary value problem numerically, but first we will investigate the continous version of the above discrete model in order to find what sort of solutions we might expect to find. Using h as mesh parameter, we can consider equation (8.20) to be a discretization of the following nonlinear ordinary differential equation.

$$h^2 s_{xx} - \gamma_1 s = -\gamma_2 \frac{s}{1+2s^2} \tag{8.24}$$

We will as mentioned earlier only consider this equation in the limit $s^2 \ll 1$. We can then expand the ratio and find the following approximation

$$h^2 s_{xx} + (\gamma_2 - \gamma_1)s = 2\gamma_2 s^3 \tag{8.25}$$

This equation can be analyzed qualitatively using the fact that it is Newton's equation for the motion of a particle in a potential U.

$$h^2 s_{xx} = -\frac{dU}{ds} \tag{8.26}$$

The potential is

$$U(s) = -\frac{1}{2}(\gamma_1 - \gamma_2)s^2 - \frac{1}{2}\gamma_2 s^4 \tag{8.27}$$

The Newton equation is supplied with boundary conditions $s(0) = s(L) = 0$, where L is the length of the array. There are three quite different cases that will arise when we vary the parameters γ_1 and γ_2. We will in the following investigate all three cases.

Case 1

This case is defined by $\gamma_1 - \gamma_2 < 0$ and $\gamma_2 < 0$. The potential has a shape as displayed in Figure 8.12. Figure 8.13 displays a picture of a numerical solution of the original difference equations for parameter values corresponding to Case 1. The values of parameters used were $\eta = 0.0001, \Delta = 1.95, N = 30, p = 0.7$ and $\phi_0 = 1.3734$.

The solution behave as we should expect from the shape of the potential.Let us reintroduce the original parameters from equations (8.21),(8.22). The current case is then found to characterized by

$$\delta < -\frac{1}{2}\alpha + 2\eta - (p - \frac{1}{2})|\tan\phi_0 - \alpha| \tag{8.28}$$

$$\tan\phi_0 < \alpha \tag{8.29}$$

We will later compare these relations with similar relations derived for case 2 and case 3.

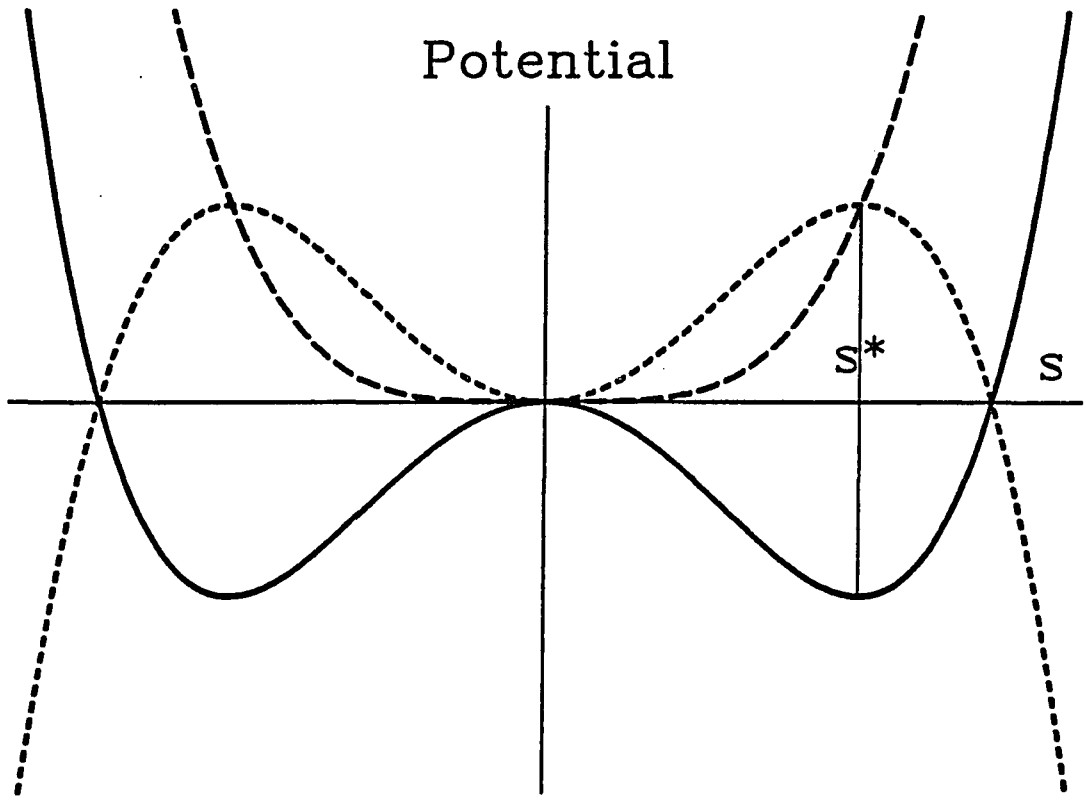

Figure 8.12: This figure shows the potential U for case 1 (long dots), case 2 (continous line) and case 3 (short dots).

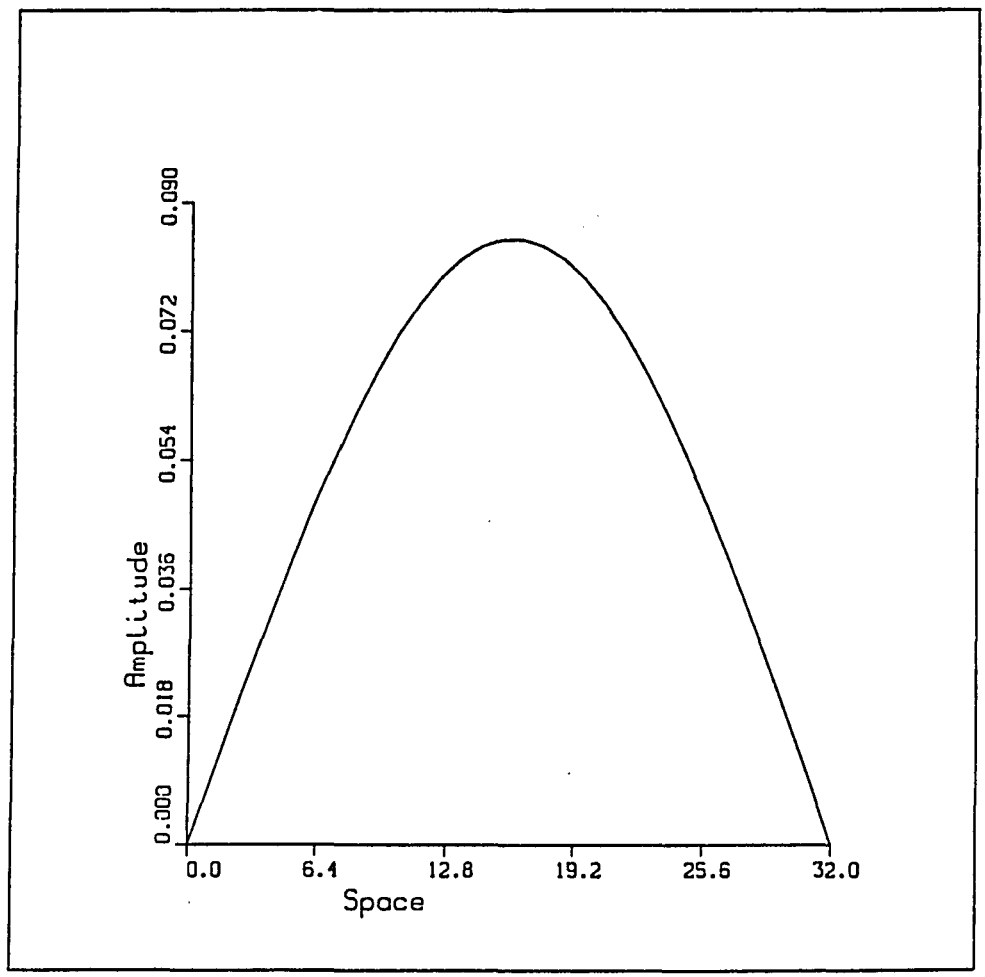

Figure 8.13: The electric field amplitude across the array when the pumping is uniform (case 1). Parameter valus are $\eta = 0.0001, \Delta = 1.95, N = 30, p = 0.7$ and $\phi_0 = 1.3734$.

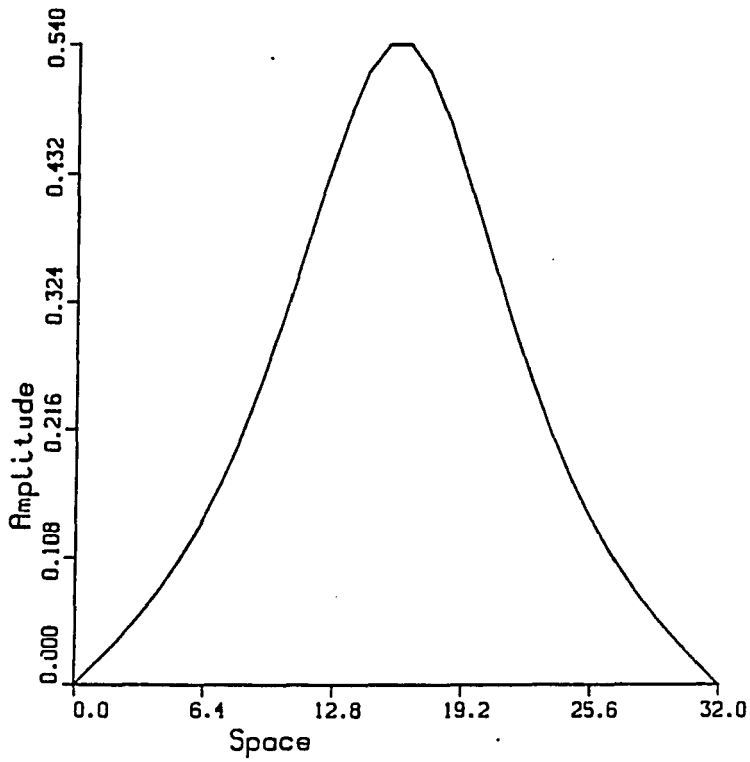

Figure 8.14: The electric field amplitude across the array when the pumping is uniform (case 2). Parameter valus are $\eta = 0.0001, \Delta = 2, N = 30, p = 0.7$, $\phi_0 = 1.3734$

Case 2

This case is defined by $\gamma_1 - \gamma_2 > 0$ and $\gamma_2 < 0$. The potential for this case is displayed in Figure 8.12. Figure 8.14 display an amplitude profile computed for the difference equation in this parameter regime. The values of the various parameters are $\eta = 0.0001, \Delta = 2, N = 30, p = 0.7$ and $\phi_0 = 1.3734$.

In order to be consistent with the assumption $s \ll 1$ we must assume that the nonzero critical point for $U(s)$ is small. The critical point s^* is

$$s^* = \frac{\gamma_1 + |\gamma_2|}{2|\gamma_2|} \tag{8.30}$$

Reintroducing the original parameters we find

$$\delta > -\frac{1}{2}\alpha + 2 - (p - \frac{1}{2})|\tan\phi_0 - \alpha| \tag{8.31}$$

$$\frac{\delta + \frac{1}{2}\alpha - 2\eta + (p - \frac{1}{2})|\tan\phi_0 - \alpha|}{\tan\phi_0 - \alpha} \ll 1 \tag{8.32}$$

The last inequality can be written as

$$\delta \ll -\frac{1}{2}\alpha + 2\eta - (p - \frac{1}{2})|\tan\phi_0 - \alpha| + |\tan\phi_0 - \alpha| \tag{8.33}$$

Case 3

This case is characterized by $\gamma_1 - \gamma_2 < 0$ and $\gamma_2 > 0$. Figure 8.12 displays the shape of the potential for this case.

Let s^* be the location of the critical point of the potential as under case 2. When the amplitude of the oscillation is much smaller than s^* the intensity profile for the array should look very much as in case 1. Figure 8.15 show a numerical solution of the difference equation for this case. The parameters used were $\eta = 0.0001$,$p = 0.7$,$\triangle = 2$,$N = 30$ and $\phi_0 = 1.373401$.

If s^* is much smaller than 1 we have the possibility of another type of solution. Figure 8.16 show a numerical solution of the difference equation for this case.

The parameter values are the same but the size of the array is now $N = 60$. The solution corresponds to a particle that almost has enough energy to escape from the potential well. It will spend most of its time close to the critical point s^* of the potential. This will produce an array profile that is uniform except for a short section of variation close to the edges. In appendix H we prove that the functional form close to the boundaries in the large array limit is in fact a hyperbolic tangent. Figure 4.1 shows the near field amplitude profile for increasing size of the array.

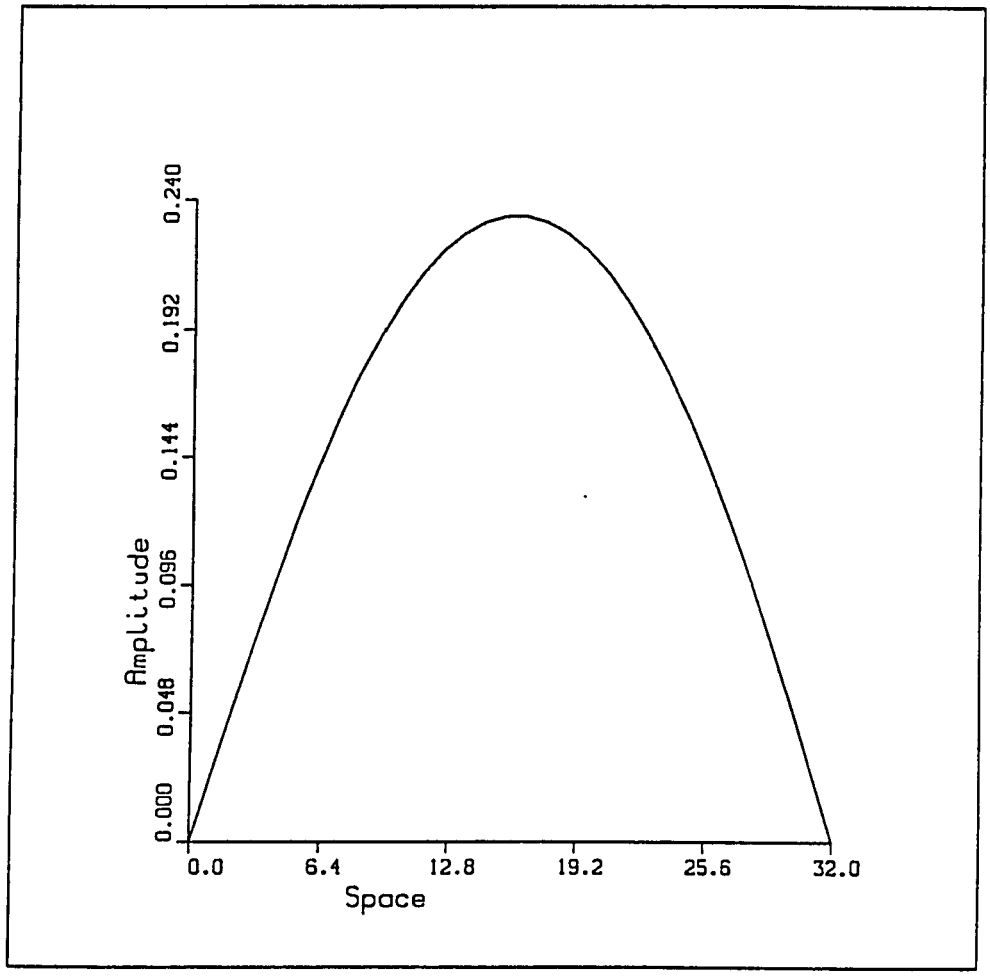

Figure 8.15: The electric field amplitude across the array when the pumping is uniform (case 3). Parameter valus are $\eta = 0.0001, \Delta = 2, N = 30, p = 0.7$, $\phi_0 = 1.373401$.

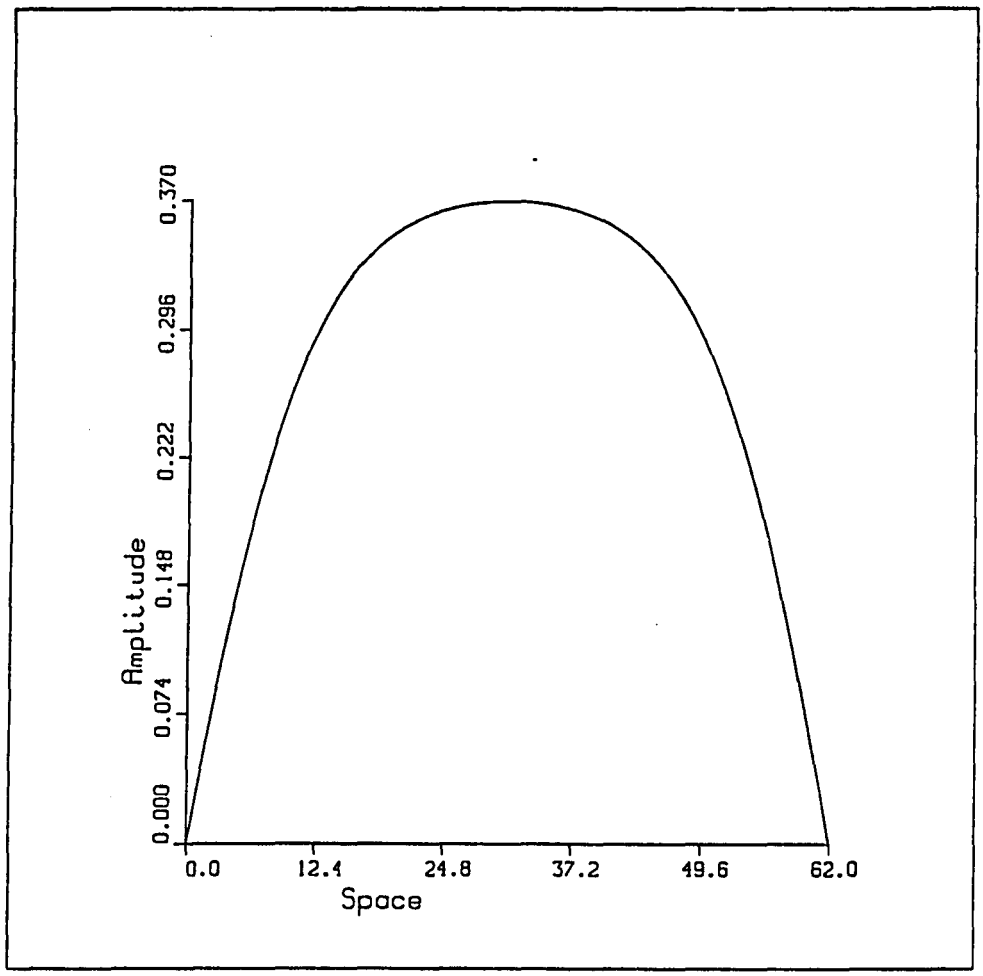

Figure 8.16: The electric field amplitude across the array when the pumping is uniform (case 3). Parameter valus are $\eta = 0.0001, \Delta = 2, N = 60, p = 0.7$, $\phi_0 = 1.373401$.

Introducing the original parameters as in case 1 and case 2 we find that solution of the type displayed in Figure 8.15 will be realised when

$$\delta < -\frac{1}{2}\alpha + 2\eta + (p - \frac{1}{2})|\tan\phi_0 - \alpha| \tag{8.34}$$

$$\tan\phi_0 - \alpha > 0 \tag{8.35}$$

In order for solutions of the form displayed in Figure 8.16 to exist we must in addition to (8.34) assume ($s^* \ll 1$)

$$\delta \gg -\frac{1}{2}\alpha + 2\eta + (p - \frac{1}{2})|\tan\phi_0 - \alpha| - |\tan\phi_0 - \alpha| \tag{8.36}$$

Discussion

We will now make some comments on the results derived in the three last sections and address the question of stability. Let us first restate the conditions on the parameters corresponding to the different cases. First define

$$\delta_0 = -\frac{1}{2}\alpha + 2\eta - (p - \frac{1}{2})|\tan\phi_0 - \alpha| \tag{8.37}$$

$$\delta_1 = -\frac{1}{2}\alpha + 2\eta + (p - \frac{1}{2})|\tan\phi_0 - \alpha| \tag{8.38}$$

We then have

Case 1:

$$\tan\phi_0 - \alpha < 0 \tag{8.39}$$

$$\delta < \delta_0 \tag{8.40}$$

Case 2:

$$\tan\phi_0 - \alpha < 0 \tag{8.41}$$

$$\delta > \delta_0 \tag{8.42}$$

$$\delta \ll \delta_0 + |\tan\phi_0 - \alpha| \tag{8.43}$$

Case 3:

$$\tan\phi_0 - \alpha > 0 \tag{8.44}$$

$$\delta < \delta_1 \tag{8.45}$$

$$\delta \gg \delta_1 - |\tan\phi_0 - \alpha| \tag{8.46}$$

We observe that amplitude profiles from case 1 and case 2 should connect smoothly at $\delta = \delta_0$ cross the value . Figures 8.17a, 8.17b and 8.17c display the numerical solutions of the difference equation as a function of δ. The parameter values used were $\eta = 0.0001$,$N = 30$,$p = 0.7$ and $\phi_0 = 1.3734$ and $\Delta = 1.95,\ 1.97,\ 2.0$.

The profiles connect smoothly across the value δ_0 as expected. For $\tan\phi_0 = \alpha$ equation (8.20) reduces to the equation for the driven supermode. If $\delta < \delta_0$ the amplitude profile for case 1 and case 3 connect to the driven supermode at $\tan\phi_0 = \alpha$. We know that the driven supermode is stable for small coupling η. We therefore expect that the solutions for case 1 and case 3 that connect to the supermode should be stable also, at least for $\tan\phi_0 \approx \alpha$.Approximations to the spectrum of the continum model has been computed in appendix I. The spectrum will give an approximation to the values for the detuning δ where the solutions in case 1 and case 3 will be found. From appendix I we have.

Case 1:

$$\delta^l = -\frac{1}{2}\alpha + 2\eta - \eta(\frac{2\pi l}{L})^2 - (p - \frac{1}{2})|\tan\phi_0 - \alpha|(1 - 4a^3) \tag{8.47}$$

Case 3:

$$\delta^l = -\frac{1}{2}\alpha + 2\eta - \eta(\frac{2\pi l^2}{L}) + (p - \frac{1}{2})|\tan\phi_0 - \alpha|(1 - 4a^3) \tag{8.48}$$

These relations are very useful when choosing parameter values for the numerical solution of the bounadry value problem. At the crossover point $\tan\phi_0 = \alpha$ the

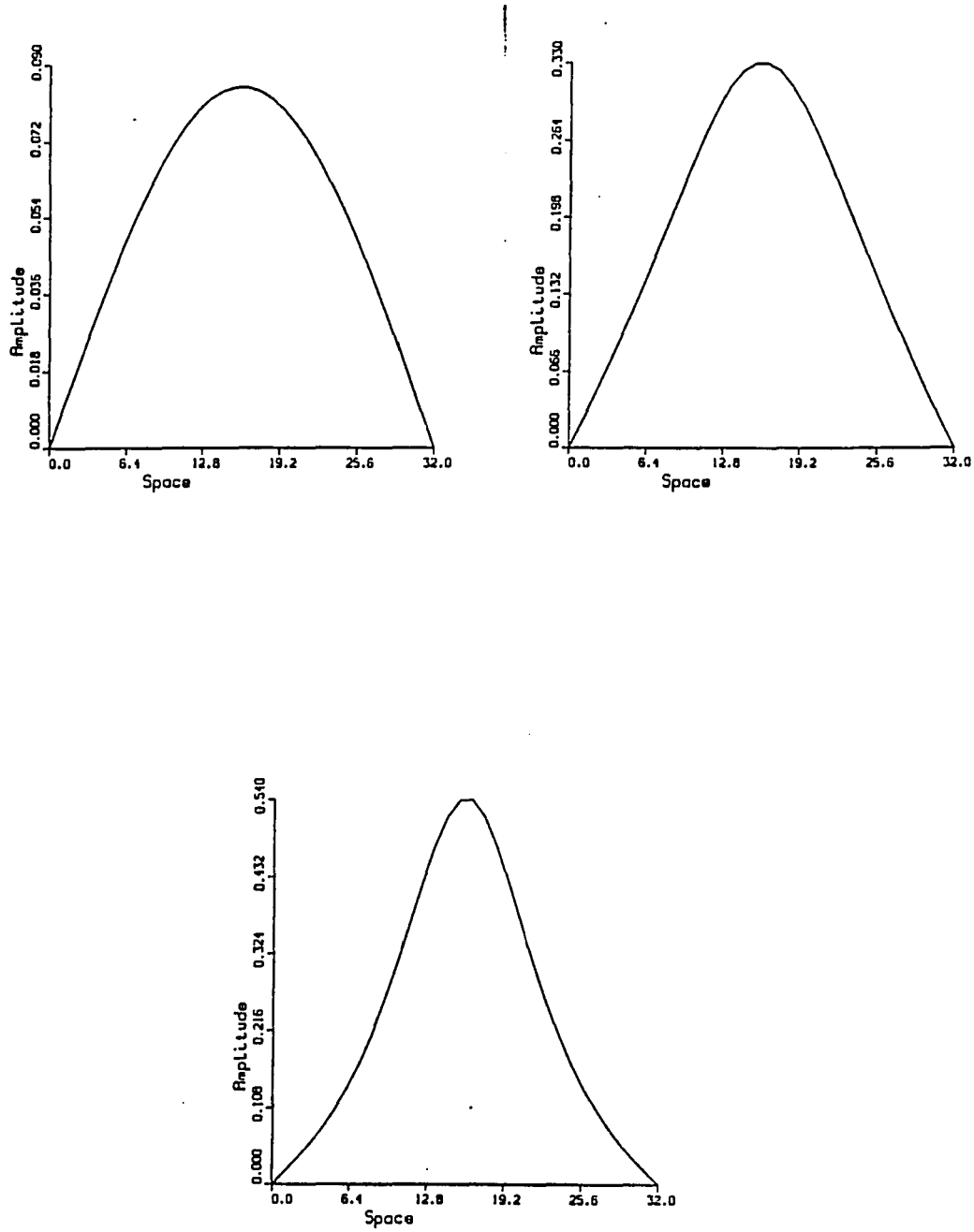

Figure 8.17: The electric field amplitude across the array for increasing value of the detuning. Parameter values are $\eta = 0.0001$,$N = 30$,$p = 0.7$ and $\phi_0 = 1.3734$ and a) $\Delta = 1.95$, b) 1.97 and c) 2.0

expressions for the spectrum reduce to the large array limit expression for the spectrum of the driven supermode. When we move away from this point the spectrum for case 1 will be shifted down and the spectrum for case 3 will be shifted up as compared to the spectrum of the driven supermode assuming we are above threshold $p > \frac{1}{2}$. The exact solutions of the continuum model can be found in all cases using elliptic functions. These solutions can be found in appendix H.

Assuming that the parameters are chosen in such a manner that the relevant solutions are stable, the various solutions will be seen experimentally by varying the detuning. To be more specific,we pick values for ϕ_0, p and $\delta = \delta^*$. We then use these values to compute the amplitude profile s_j. From this profile we find the injection profile a_j from equation (8.19). Fix this injection profile and current pumping experimentally. When you vary the detuning δ, you should expect to lock into a phaselocked solution with amplitude profile s_j when $\delta = \delta^*$.

We have adressed the question of linear stability and structural stability by numerical methods, both solving the linear eigenvalue problem numerically and simulating the time evolution of the array under various perturbations. Figures 8.18a and 8.18b are pictures of the solution and the corresponding injection profile when $\eta = 0.0001$, $p = 0.499$, $\phi_0 = 1.3733$, $\Delta = 2.1$ and $N = 30$.

These values of the parameters correspond to what we have called case 2 above. Figure 8.19 is a picture of the time evolution of the array when the solution is perturbed slightly.

The solution is locally attracting. This confirms the results of the linear stability calculations that predict the solution to be stable. The solution has a very large basin of attraction. This is explored in Figure 8.20 where we are using the same

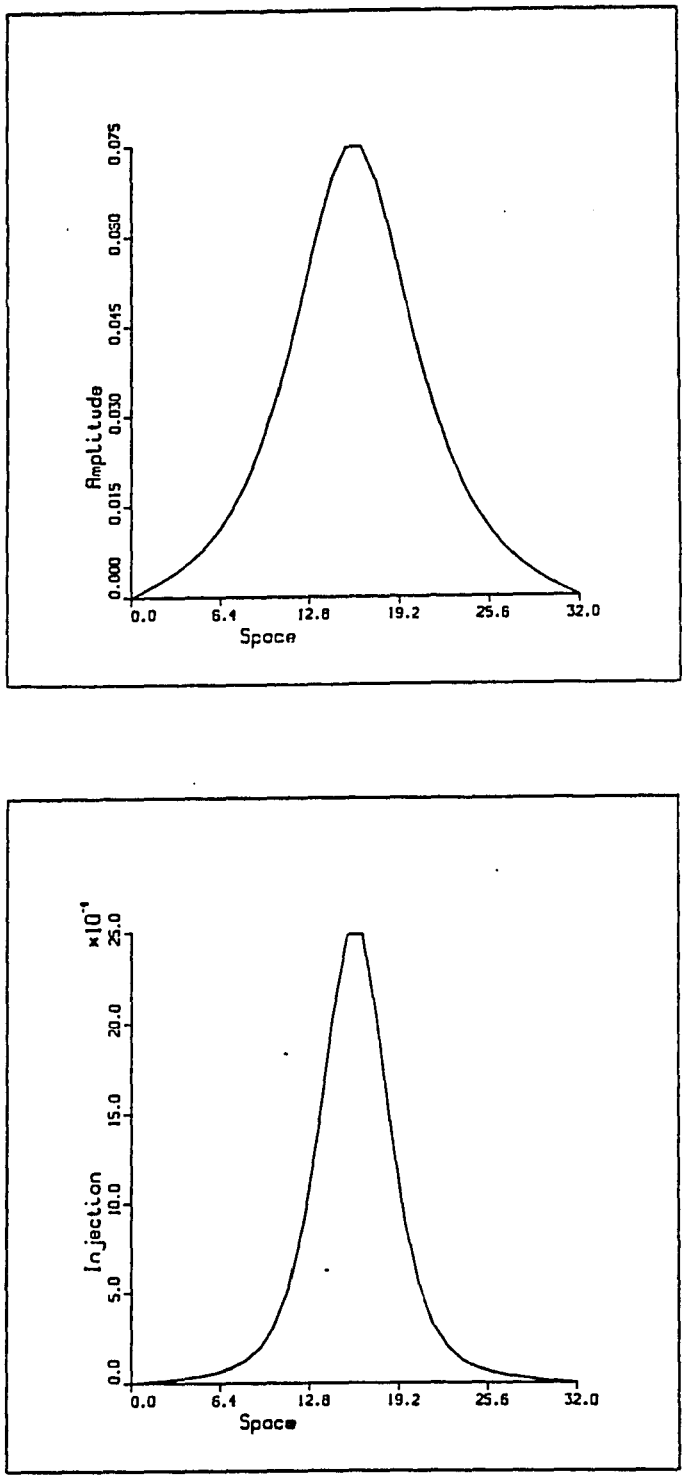

Figure 8.18: The electric field amplitude a) and injection b) across the array for case 2. The parameter values are $\eta = 0.0001$, $p = 0.499$, $\phi_0 = 1.3733$, $\Delta = 2.1$ and $N = 30$.

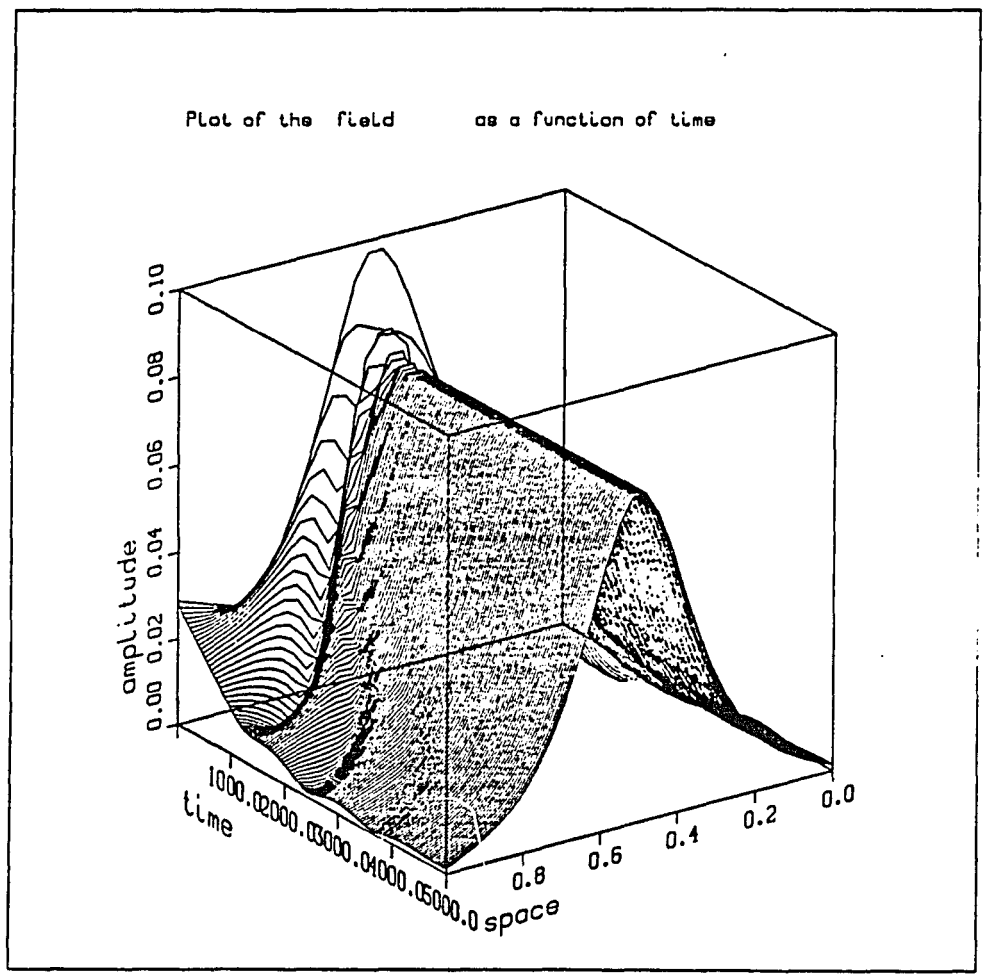

Figure 8.19: The time evolution of a perturbation to the solution from 8.18. Parameter values are $\eta = 0.0001$, $p = 0.499$, $\phi_0 = 1.3733$, $\Delta = 2.1$ and $N = 30$.

parameter values as in Figure 8.19 but starting from zero initial condition.

This picture shosw the time evolution of the amplitude. We have also investigated the phase and find it to be converging to a flat state, so the final state displayed in Figure 8.20 is really the constant phase solution from Figure 8.18.

We have also investigated what happends when the detuning or injection profile is not exactly right so that the phaselocked solution does not exist as a solution for the laser array equations. This is the question of structural stability. In Figure 8.21 we explore what happend to the solution from Figure 8.18 when we perturb the normalized detuning Δ by a small amount (10%). The amplitude is essentially unchanged but the phase developes a small variation across the array. Figure 8.21 shows the phase as a function of time. We have run the time evolution up to 10^6 and the final stage in Figure 8.21 is stable on this timescale. In Figure 8.22 we explore the effect of a small (0.1% of average) perturbation to the pumping profile. Figure 8.22 shows the time evolution of the amplitude. It relaxes to a new time invariant state. We have studied the time evolution up to 10^6 and the final state in Figure 8.22 appears to be stable. The phase developes a small time invariant profile across the array just as in the previous case.

From a practical point of view the solutions with flat top discussed in case 3 are most interesting since for large arrays almost all lasers are shining with the same intensity.Such a solution will give larger integrated intensity as compared to the solutions from case 1 and case 2. These solutions are also stable for parameter values of practical interest. Figures 8.23a and 8.23b show the amplitude profile and the corresponding injection profile when $\phi 0 = 1.3735$, $\eta = 0.0001$, $\Delta = 1.92$, $T = 10000$, $p = 0.499$ and $N = 60$.

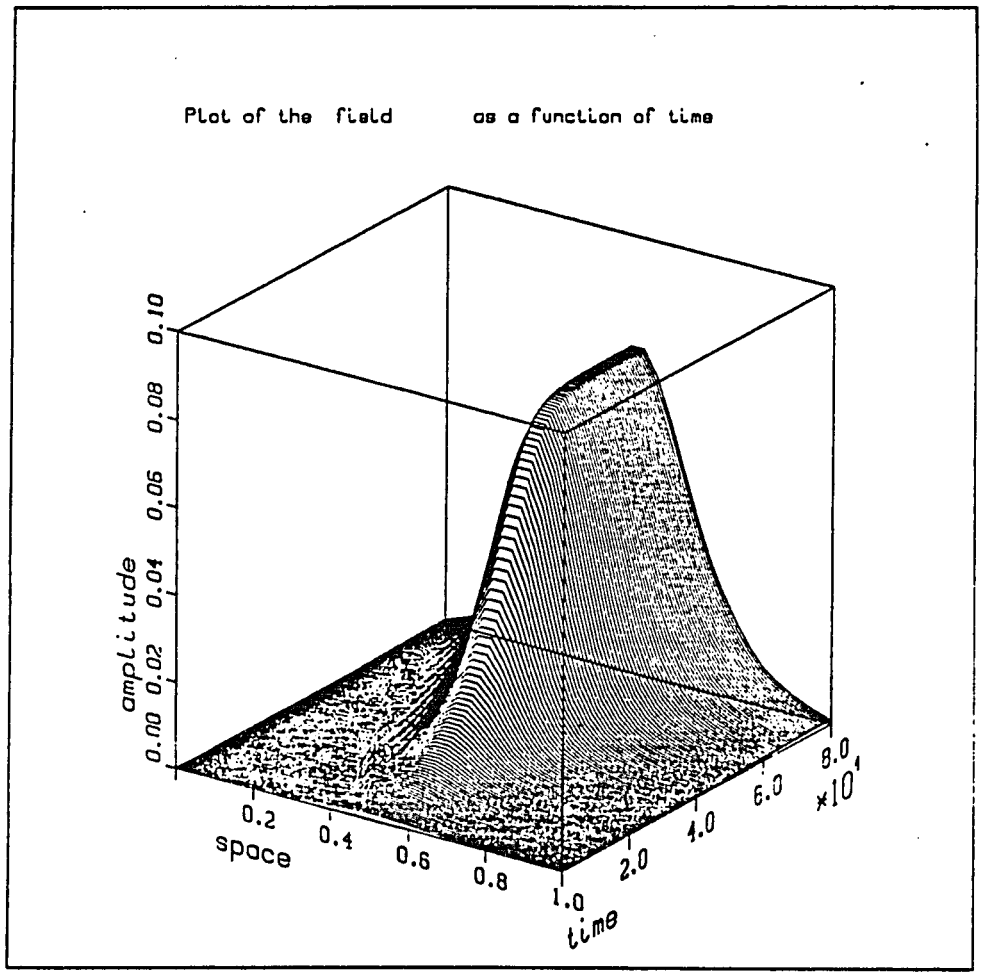

Figure 8.20: The time evolution of the electric field amplitude starting from zero when the injection field is the one from Figure 8.18. Parameter values are $\eta = 0.0001$, $p = 0.499$, $\phi_0 = 1.3733$, $\Delta = 2.1$ and $N = 30$.

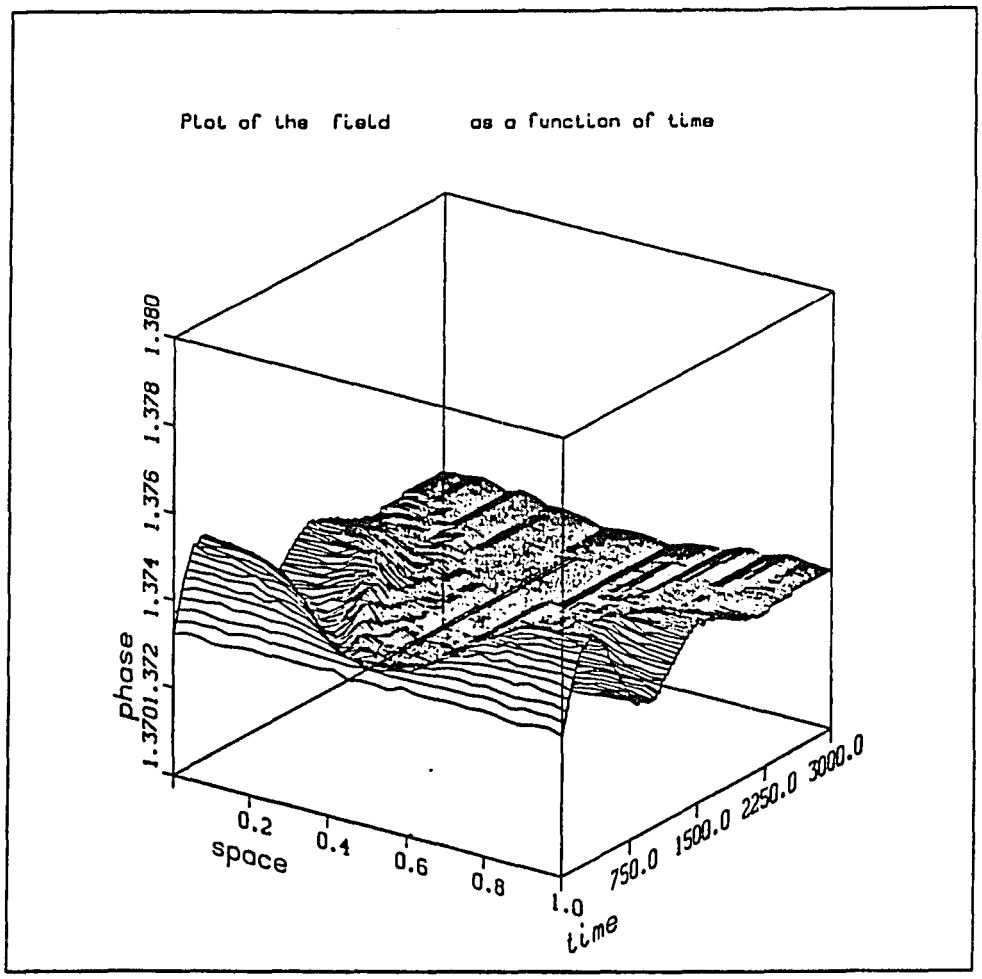

Figure 8.21: The time evolution of the phase of the electric field across the array when the detuning by 10%. Parameter values are $\eta = 0.0001$, $p = 0.499$, $\phi_0 = 1.3733$, $\Delta = 2.1$ and $N = 30$.

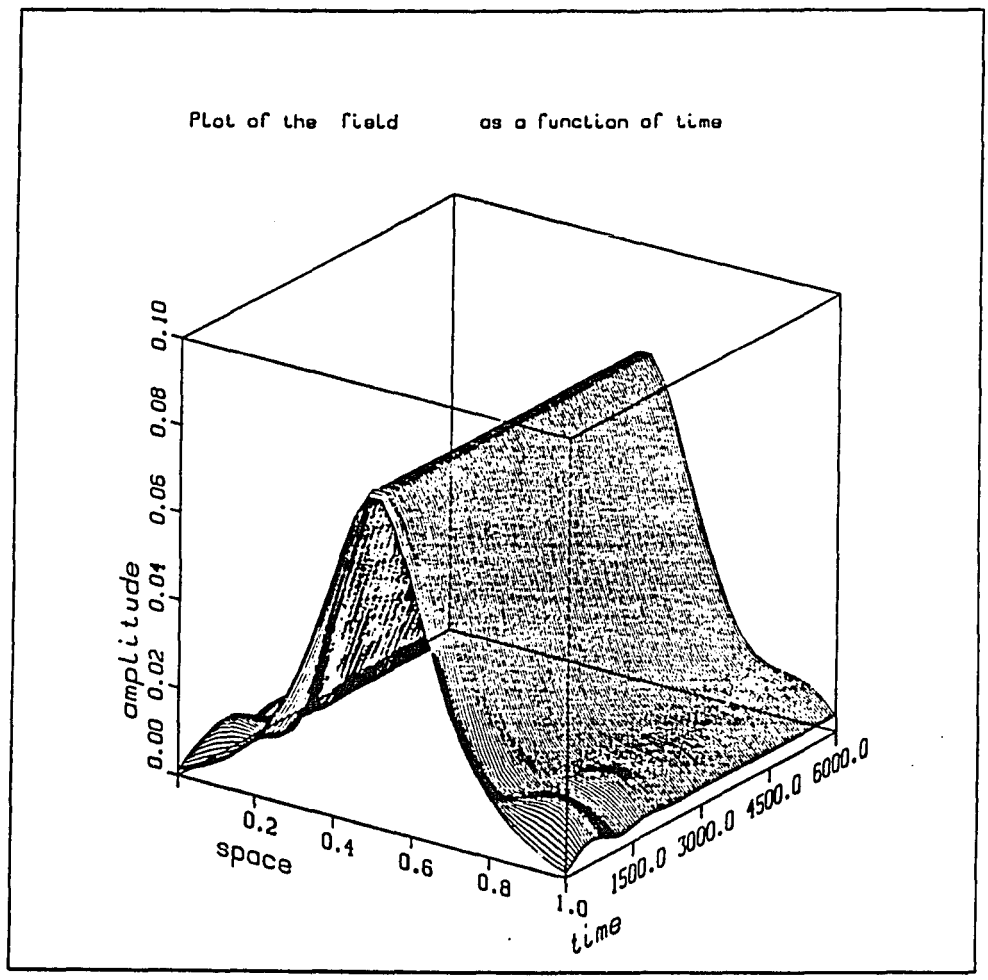

Figure 8.22: The time evolution of the amplitude of the electric field across the array when the pumping is perturbed 0.1% of average. Parameter values are $\eta = 0.0001$, $p = 0.499$, $\phi_0 = 1.3733$, $\Delta = 2.1$ and $N = 30$.

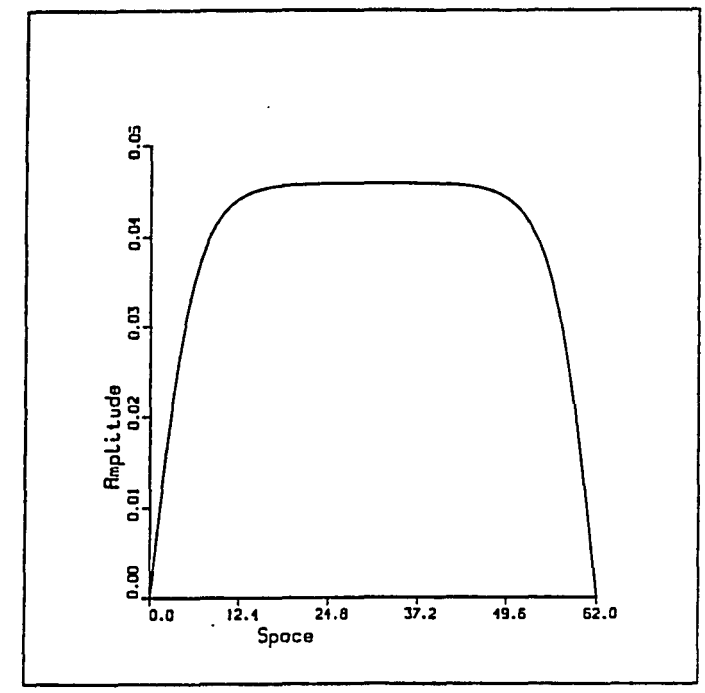

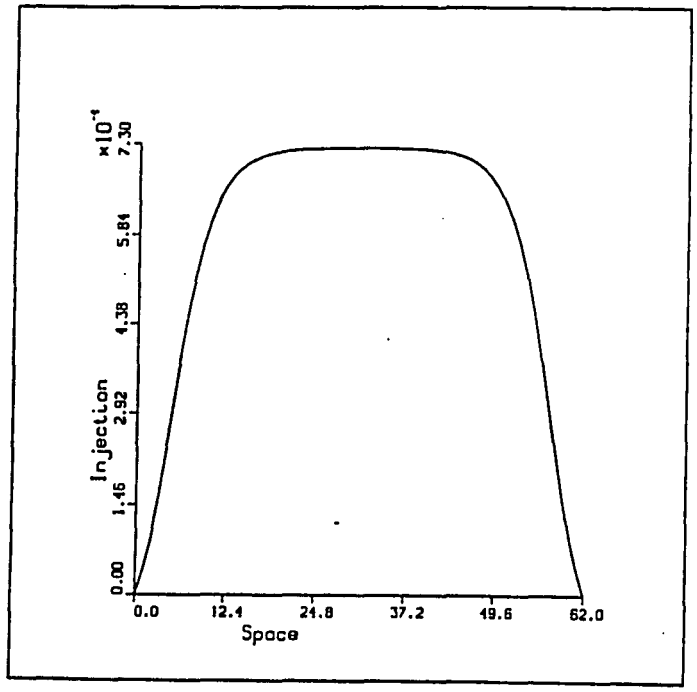

Figure 8.23: This Figure shows the electric field amplitude a) and injection field b) across the array in case 3. Parameter values are $\phi 0 = 1.3735$, $\eta = 0.0001$, $\Delta = 1.92$, $T = 10000$, $p = 0.499$ and $N = 60$.

Numerical solutions of the linear stability problem for these parameter values show that the solution is in fact stable to small perturbations. In order to explore the basin of attraction we did a simulation of the array starting at zero and injection it with the profile from Figure 8.23a. Figure 8.24 show the result of this simulation. The solution from Figure 8.23a clearly has a large basin of attraction. Also observe that the amplification of the input signal a_j is of the order of 10^2. In fact from the relation (8.19) we see that the laser array will act like a saturable amplifier. The rate of amplification of weak input signals goes to infinity as we approach the threshold value $p = \frac{1}{2}$.

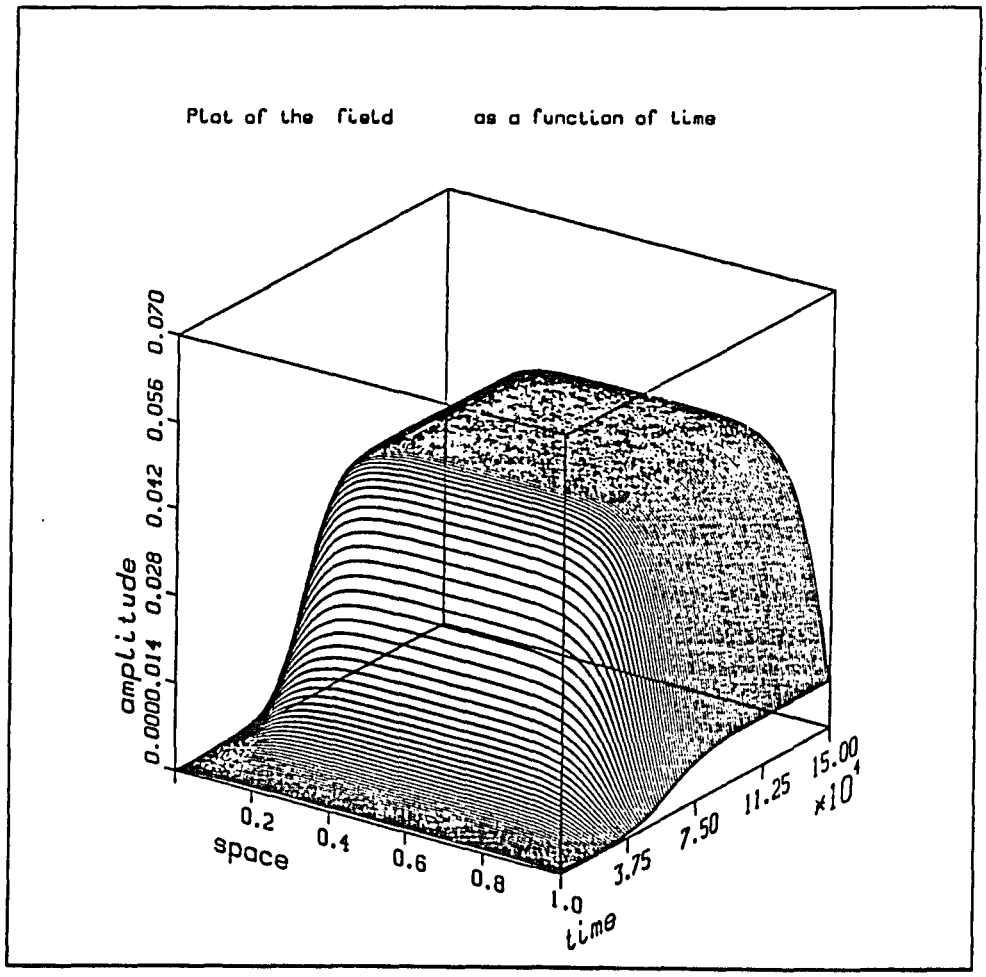

Figure 8.24: The time evolution of the electric field amplitude across the array starting from zero with the injection field as given in Figure 8.23b. Parameter values are $\phi 0 = 1.3735$, $\eta = 0.0001$, $\Delta = 1.92$, $T = 10000$, $p = 0.499$ and $N = 60$.

Chapter 9

APPENDIX D

In this appendix we derive the linearized laser array equations. The equations will be derived in general without assuming any particular shape for pumping p_j or injection a_j. We will be linearizing around a solution of the form

$$e_j = s_j e^{\imath(\delta t - \frac{\pi}{2})} \tag{9.1}$$

$$z_j^0 = \frac{p_j}{1+2s_j^2} \tag{9.2}$$

Where s_j and z_j are time independent. For the linearization assume that e_j and z_j are of the form

$$E_j = (s_j + e_j)e^{\delta t - \frac{\pi}{2} + \phi_0} \tag{9.3}$$

$$z_j = z_j^0 + n_j \tag{9.4}$$

The quantities e_j and n_j are small perturbations. Insert (9.3) ,(9.4) into the laser array equations

$$\frac{dE_j}{dt} = -\frac{1}{2}E_j + (1-\imath\alpha)Z_jE_j + \imath\eta(E_{j+1} + E_{j-1}) + ae^{\delta t - \frac{\pi}{2}} \tag{9.5}$$

$$T\frac{dZ_j}{dt} = p_j - Z_j - 2Z_j|E_j|^2 \tag{9.6}$$

We then get

$$\frac{de_j}{dt} = -\imath\delta(s_j + e_j) - \frac{1}{2}(s_j + e_j) \tag{9.7}$$

$$+(1 - \imath\alpha)(s_j + e_j)(z_j^0 + n_j) \tag{9.8}$$

$$+\imath\eta(s_{j+1} + s_{j-1} + e_{j+1} + e_{j-1}) + a_j e^{-\imath\phi_0} \tag{9.9}$$

$$\frac{dn_j}{dt} = p_j - (z_j^0 + n_j) - 2(z_j^0 + n_j)(s_j + e_j)(s_j + e_j^*) \tag{9.10}$$

Collecting terms we get from (9.9)

$$\frac{de_j}{dt} = \imath\eta e_{j-1} + [(1 - \imath\alpha)z_j^0 \tag{9.11}$$

$$-(\frac{1}{2} + \imath\delta)]e_j + \imath\eta e_{j+1} \tag{9.12}$$

$$+(1 - \imath\alpha)s_j n_j \tag{9.13}$$

But p_j is a function of s_j and a_j through

$$p_j = (1 + 2s_j^2)(\frac{1}{2} - \frac{a_j \cos\phi_0}{s_j}) \tag{9.14}$$

So the term in front of e_j in (9.13) can be written as

$$(1 - \imath\alpha)z_j^0 - (\frac{1}{2} + \imath\delta) = \tag{9.15}$$

$$-\frac{a_j \cos\phi_0}{s_j} + \imath(\eta\triangle - \frac{a_j \cos\phi_0}{s_j}) \tag{9.16}$$

Where $\triangle$ is defined as

$$\triangle = \frac{\delta + \frac{1}{2}\alpha}{\eta} \tag{9.17}$$

The equation (9.10) for the perturbation n_j to the carrier consentration is in linearized form

$$\frac{dn_j}{dt} = -\frac{2z_j^0 s_j}{T}(e_j + e_j^*) - \frac{1+2s_j^2}{T}n_j \tag{9.18}$$

Write the complex electrix field amplitude as a sum of real and imaginary parts $e_j = e_j^r + \imath e_j^i$. The linearized laser array equations can then be written as

$$\frac{de_j^r}{dt} = -\frac{a_j \cos\phi_0}{s_j}e_j^r - \eta e_{j-1}^i \tag{9.19}$$

$$+(\eta\triangle - \frac{\alpha a_j \cos\phi_0}{s_j})e_j^i - \eta e_{j+1}^i \tag{9.20}$$

$$+s_j n_j \tag{9.21}$$

$$\frac{de_j^i}{dt} = -\frac{a_j \cos\phi_0}{s_j}e_j^i + \eta e_{j-1}^r \tag{9.22}$$

$$-(\eta\triangle - \frac{\alpha a_j \cos\phi_0}{s_j})e_j^i + \eta e_{j+1}^i \tag{9.23}$$

$$-\alpha s_j n_j \tag{9.24}$$

$$\frac{dn_j}{dt} = -\frac{4z_j^0 s_j}{T}e_j^r - \frac{1+2s_j^2}{T}n_j \tag{9.25}$$

The matrix of the linear system can be written as

$$A = \begin{pmatrix} D_1 & TR+\alpha D_1 & D_2 \\ -TR-\alpha D_1 & D_1 & -\alpha D_2 \\ D_4 & 0 & D_5 \end{pmatrix} \tag{9.26}$$

Where D_i are diagonal matrices and TR is a tridiagonal matrix. The matrices are defined as follows.

$$D_1 = diag(-\frac{a_j \cos\phi_0}{s_j}) \tag{9.27}$$

$$D_2 = diag(s_j) \tag{9.28}$$

$$D_3 = diag(-\frac{4z_j^0 s_j}{T}) \tag{9.29}$$

$$D_4 = diag(-\frac{1+2s_j^2}{T}) \tag{9.30}$$

TR is a tridiagonal matrix with $\eta\Delta$ on the diagonal and $-\eta$ on the sub and super diagonal. This completes the derivation of the linearized laser array equations.

Chapter 10

APPENDIX E

We will in this appendix first do the linear stability of the driven supermode for the case of a two element array. We will then discuss the stability of arbitrary profiles and for arbitrary large arrays. From appendix D we find that the linear system for this case is

$$\frac{de_1^r}{dt} = (z-\frac{1}{2})e_1^r + (\delta+\alpha z)e_1^i + sn_1 - \eta e_2^i \quad (10.1)$$

$$\frac{de_2^r}{dt} = (z-\frac{1}{2})e_2^r + (\delta+\alpha z)e_2^i + sn_2 - \eta e_1^i \quad (10.2)$$

$$\frac{de_1^i}{dt} = (z-\frac{1}{2})e_1^i - (\delta+\alpha z)e_1^r - \alpha s n_1 + \eta e_2^r \quad (10.3)$$

$$\frac{de_2^i}{dt} = (z-\frac{1}{2})e_2^i - (\delta+\alpha z)e_2^r - \alpha s n_2 + \eta e_1^r \quad (10.4)$$

$$\frac{n_1}{dt} = -\frac{4zs}{T}e_1^r - \frac{1+2s^2}{T}n_1 \quad (10.5)$$

$$\frac{n_2}{dt} = -\frac{4zs}{T}e_2^r - \frac{1+2s^2}{T}n_2 \quad (10.6)$$

Where $s_1 = s_2 = s$ and $z_1 = z_2 = z$. This six dimensional linear system can be split into two three dimensional systems. Define

$$X = e_1^r + e_2^r$$

$$
\begin{aligned}
Y &= e_1^i + e_2^i \\
Z &= n_1 + n_2 \\
U &= e_1^r - e_2^r \\
V &= e_1^i - e_2^i \\
W &= n_1 - n_2
\end{aligned}
$$

The linear system is in these variables reduced to two uncoupled systems

$$
\frac{d}{dt}\begin{pmatrix} X \\ Y \\ Z \end{pmatrix} =
\begin{pmatrix} z-\frac{1}{2} & \delta+\alpha z-\eta & s \\ -(\delta+\alpha z-\eta) & z-\frac{1}{2} & -\alpha s \\ -\frac{4zs}{T} & 0 & -\frac{1+2s^2}{T} \end{pmatrix}
\begin{pmatrix} X \\ Y \\ Z \end{pmatrix} \tag{10.7}
$$

and

$$
\frac{d}{dt}\begin{pmatrix} U \\ V \\ W \end{pmatrix} =
\begin{pmatrix} z-\frac{1}{2} & \delta+\alpha z+\eta & s \\ -(\delta+\alpha z+\eta) & z-\frac{1}{2} & -\alpha s \\ -\frac{4zs}{T} & 0 & -\frac{1+2s^2}{T} \end{pmatrix}
\begin{pmatrix} U \\ V \\ W \end{pmatrix} \tag{10.8}
$$

The two linear problems are very similar. Define $\theta = \delta + \alpha z - \eta$ in (10.7) and $\theta = \delta + \alpha z + \eta$ in (10.8). The linear problems are then identical with common matrix A defined as

$$
A = \begin{pmatrix} z-\frac{1}{2} & \theta & s \\ -\theta & z-\frac{1}{2} & -\alpha s \\ -\frac{4sz}{T} & 0 & -\frac{1+2s^2}{T} \end{pmatrix} \tag{10.9}
$$

The characteristic polynomial for this matrix is

$$\begin{aligned}(\lambda + \frac{1+2s^2}{T})((\lambda+\gamma)^2+\theta^2) \\ +\frac{4zs^2}{T}((\lambda+\gamma)-\alpha\theta) &= 0 \end{aligned} \tag{10.10}$$

Where $\gamma = \frac{a\cos\phi_0}{s}$. Observe that for reasonable values of the injection a, z is positive. We can now imidiately say that a sufficient condition for no positive real roots is $\gamma - \alpha\theta > 0$. We will call this the condition for real stability.

From equation (8.1),(8.6) and (8.8) we find

$$\delta + \alpha z = \eta\Delta - \alpha\gamma$$

For the first supermode we find from equation (8.12) that $\Delta = 1$. We can now compute θ for the two linear systems (10.7) and (10.8)

$$\begin{aligned}\theta &= -\alpha\gamma \\ \theta &= 2\eta - \alpha\gamma\end{aligned}$$

Where the upper value refer to system (10.7) and the lower value refer to (10.8) The sufficient condition applied with $\theta = -\alpha\gamma$ gives no restriction on η so the linear system (10.7) has no real instability. The sufficient condition applied with $\theta = 2\eta - \alpha\gamma$ gives the following sufficient condition for real stability

$$\eta < \frac{1}{2}(\alpha + \frac{1}{\alpha})\gamma \tag{10.11}$$

Neccesary and sufficient conditions for real stability can be found by considering the graph of the characteristic polynomial and its value at zero. We have real stability if

$$\eta < \frac{1}{2}\alpha\gamma + \frac{1}{4}\left\{\frac{4\alpha z s^2}{1+2s^2} - \sqrt{(\frac{4\alpha z s^2}{1+2s^2})^2 - 4\gamma^2 - \frac{16\gamma z s^2}{1+2s^2}}\right\} \tag{10.12}$$

or

$$\eta > \frac{1}{2}\alpha\gamma + \frac{1}{4}\left\{\frac{4\alpha z s^2}{1+2s^2} + \sqrt{(\frac{4\alpha z s^2}{1+2s^2})^2 - 4\gamma^2 - \frac{16\gamma z s^2}{1+2s^2}}\right\} \tag{10.13}$$

We must now consider the posibility of complex roots. These will give rise to what we might call complex stability/instability. In the characteristic polynomial write $\lambda = x + \imath y$. Solve for y as a function of x and write down an equation for x alone. The resulting equation is

$$\begin{aligned} -((x+\gamma)^2 + \theta^2) = (x+P)(3x+P+2\gamma) + Q \\ +Q\frac{P-\gamma+\alpha\theta}{2(x+\gamma)} \end{aligned} \tag{10.14}$$

Where we have defined

$$P = \frac{1+2s^2}{T} \tag{10.15}$$

$$Q = \frac{4zs^2}{T} \tag{10.16}$$

Complex stability will exist if (10.14) has no positive real roots. A sufficient condition for this is clearly $P - \gamma + \alpha\theta > 0$. For the system (10.7) we get the condition

$$\gamma < \frac{P}{1+\alpha^2} \tag{10.17}$$

and for the system (10.8) we get the condition

$$\eta > \frac{1}{2\alpha}(\gamma(1+\alpha^2) - P) \tag{10.18}$$

Since η must be positive we clearly have that (10.17) implies (10.18). Using the definition (10.15) of P in (10.17) we find a sufficient condition for complex stability as

$$a < \frac{s}{\cos\phi_0}\frac{1+2s^2}{T(1+\alpha^2)} \tag{10.19}$$

A neccesary and sufficient condition for complex stability is rather complicated and will not be written down. For physical values of the parameters the above sufficient condition is fairly sharp.

Let us now turn to the case of arbitrary N and profiles . We will argue that the condition (10.19) is sufficient to assure stability for any N if η is small enough and s is replaced with the minimum of s_j. The argument is simply to investigate the case $\eta = 0$ and then do a continuity argument. Let $\eta = 0$ in the matrix (9.26) for the linearized laser array equations. The linear system then decouples into N 3x3 blocks. Each of the blocks is structurally identical to the matric (10.9) with the same value of θ as for the case of complex instability discussed ealier in this appendix. Each of the blocks will have a different value of $\bar{s}$. In fact the j'th block will have $\bar{s} = s_j$. Assume that the condition (10.19) holds for each of the N blocks. This is clearly true if

$$a < \frac{s_{min}}{\cos\phi_0}\frac{1+2s_{min}^2}{T(1+\alpha^2)} \tag{10.20}$$

Where s_{min} is the smallest value for the amplitude of any element in the array. If (10.20) is true then by definition all eigenvalues of the matrix (10.9) is in the left halfplan or purely imaginary when $\eta = 0$. From equation (10.10) and (10.14) we observe that none of the N 3x3 blocks can have eigenvalues with zero real part as long as the injection a is nonzero. So all eigenvalues are in fact in the left halfplan when $\eta = 0$The position of the eigenvalues depends continously on the parameter η so we can now conclude that all eigenvalues stay in the left halfplane up to some unknown but positive value of η. The above argument clearly does not depend on the particular shape of the amplitude profile s_j so the condition (10.20) is enough to ensure stability for weak coupling for any amplitude profile as long as the array is driven.($a \neq 0$) Note that for the case of driven supermodes we have $s_{min} = \sin(\pi/(N+1))$ so s_{min} goes to zero as the size of the array increase. This means that the range of values for a that stabilize the fundamental supermode decrease as a function of N. stability become smaller and smaller as N increase

Chapter 11

APPENDIX F

We will in this appendix give some approximate values and ranges for the dimensionless quantities defined by equations (6.4). From [18],[28] we find that values for the gain g vary from $10^{-12}m^3s^{-1}$ to $10^{-14}m^3s^{-1}$. We will take these as representative values for the gain. From the same references we also find $\tau_s \approx 10^{-9}s$ and $\tau_{ph} \approx 10^{-12}s$ Typically [28],the photon density is $10^{21}m^{-3}$. Equation (6.4) then give that the field amplitude in each channel is not larger than 1. In [29] we find that the injection current I for a diode laser has a range of $0.1A$. The variable q_i in (6.4) is defined by the current through $q_i = \frac{I}{eV}$ where e is the electronic charge and V is the volume of the active region. From (6.4) we find

$$\delta p_i = \frac{g\tau_s \tau ph}{eV}\delta I_i$$

Using values for V from [28] we find $\delta p_i \approx 10^{-3}$. The threshold pumping for a single laser is $p_i = \frac{1}{2}$. So realistic values for p_i are very close to the threshold value $\frac{1}{2}$ The dimensionless coupling η will be assumed to be so small that a coupled mode theory is appropriate. Realistic values are $10^{-3} - 10^{-4}$.

Chapter 12

APPENDIX G

In this appendix we derive an energy relation for the laser array system. The laser array equations are.

$$\frac{de_j}{dt} = -\frac{1}{2}e_j + (1-\imath\alpha)Z_j e_j + \imath\eta(e_{j+1} \tag{12.1}$$

$$+e_{j-1}) + ae^{\delta t - \frac{\pi}{2}} \tag{12.2}$$

$$T\frac{dZ_j}{dt} = p_j - Z_j - 2Z_j|e_j|^2 \tag{12.3}$$

Multiply (12.2) with e_j^* and add this to the complex conjugate of (12.2) multiplied by e_j. This give the system

$$\frac{d|e_j|^2}{dt} = -\frac{1}{2}|e_j|^2 + 2Z_j|e_j|^2 + \imath\eta(e_j^*(e_{j+1}+e_{j-1}) \tag{12.4}$$

$$-e_j(e_{j+1}^* + e_{j-1}^*)) + a_j e_j^* e^{\imath(\delta t - \frac{\pi}{2})} \tag{12.5}$$

$$+a_j e_j e^{-\imath(\delta t + \frac{\pi}{2})} \tag{12.6}$$

$$T\frac{dZ_j}{dt} = p_j - Z_j - 2Z_j|e_j|^2 \tag{12.7}$$

Write e_j in phase amplitude form

$$e_j = \sqrt{I_j} e^{i(\delta t + \frac{\pi}{2})} e^{\phi} \tag{12.8}$$

Define the energy H, total pumping P ,total intensity I and total material inversion Z as

$$\begin{aligned} I &= \sum_{j=1}^{N} I_j \\ Z &= \sum_{j=1}^{N} Z_j \\ P &= \sum_{j=1}^{N} p_j \\ H &= I + TZ \end{aligned}$$

We then find the following equation for the quantity H

$$\frac{dH}{dt} = P - Z - I + 2\cos\phi \sum_{j=1}^{N} a_j \sqrt{I_j} \tag{12.9}$$

Where we have used the zero boundary conditions to elliminate the integrated flux term. The time variation of H is determined by the difference between the energy put in by pumping and the energy lost by material and field plus a term that is a loss or gain depending on the phase relation between the injection and the response of the array.

Chapter 13

APPENDIX H

We will in this appendix compute the exact solution to the Newton equation (8.26) for all three cases using elliptic functions. For all three cases we can write equation (8.26) as

$$\int_0^s \frac{dt}{\sqrt{2(E-U)}} = x \tag{13.1}$$

Where E is an arbitrary constant of integration that is the total erergy for the particle moving in the potential $U(s)$. For the array this energy would be determined by giving the initial sloop of the intensity profile. We will integrate (13.1) in all three cases discussed in the main text.

Case 1

This case is as we have seen defined by $-\gamma_1 + \gamma_2 > 0$ and $\gamma_2 < 0$. Define ω_0 by $\omega_0^2 = -\gamma_1 + \gamma_2$. Equation (13.1) become

$$\int_0^s \frac{dt}{\sqrt{2E - \omega_0^2 t^2 - |\gamma_2| t^4}} = x \tag{13.2}$$

The expression inside the square root can be factored as

$$2E - \omega_0^2 t^2 - |\gamma_2| t^4 = |\gamma_2|(t_1^2 + t^2)(t_0^2 - t^2) \tag{13.3}$$

Where t_0 and t_1 are defined by

$$t_0 = \sqrt{\frac{1}{2|\gamma_2|}[\sqrt{\omega_0^4 + 8E|\gamma_2|} - \omega_0^2]} \tag{13.4}$$

$$t_1 = \sqrt{\frac{1}{2|\gamma_2|}[\sqrt{\omega_0^4 + 8E|\gamma_2|} + \omega_0^2]} \tag{13.5}$$

So (13.3) can be written as

$$\int_0^s \frac{dt}{(t_1^2 + t^2)(t_0^2 - t^2)} = \sqrt{|\gamma_2|}x \tag{13.6}$$

The integral above can be solved and inverted using the elliptic function $sd(y|m)$ [30].

$$s(x) = \frac{t_0 t_1}{\sqrt{t_1^2 + t_0^2}} sd(\sqrt{|\gamma_2|(t_0^2 + t_1^2)}x | \frac{t_0^2}{t_1^2 + t_0^2}) \tag{13.7}$$

The condition $s(L) = 0$ and the requirement that the solution for the array should have constant phase ($s(x) > 0$) give the following condition on the parameters of the problem.

$$K(\frac{t_0^2}{t_1^2 + t_0^2}) = \frac{1}{2}L \tag{13.8}$$

Where K is the complete elliptic integral of the first kind.

Case 2

This case we have defined by $\gamma_1 - \gamma_2 > 0$ and $\gamma_2 < 0$. Define ω_0 by $\omega_0^2 = \gamma_1 - \gamma_2$. Equation (13.1) now become

$$\int_0^s \frac{dt}{\sqrt{2E + \omega_0^2 t^2 - |\gamma_2| t^4}} = x \tag{13.9}$$

By using the same notation as in last section we find imidiately that

$$s(x) = \frac{t_0 t_1}{\sqrt{t_1^2 + t_0^2}} sd(\sqrt{|\gamma_2|(t_0^2 + t_1^2)}x | \frac{t_1^2}{t_1^2 + t_0^2}) \tag{13.10}$$

Where t_0 and t_1 are defined as in equations (13.4),(13.5). Equation (13.8) applies also in this case.

Case 3

This case is defined by $-\gamma_1 + \gamma_2 > 0$ and $\gamma_2 > 0$. Define ω_0 as in caseI $\omega_0^2 = -\gamma_1 + \gamma_2$. Factoring the polynomial inside the square root we can write equation (13.1) for this case as

$$\int_0^s \frac{dt}{(t_1^2 - t^2)(t_0^2 - t^2)} = \sqrt{|\gamma_2|}x \tag{13.11}$$

Where we now have defined

$$t_0 = \sqrt{\frac{1}{2|\gamma_2|}[\omega_0^2 + \sqrt{\omega_0^4 - 8E|\gamma_2|}]} \tag{13.12}$$

$$t_1 = \sqrt{\frac{1}{2|\gamma_2|}[\omega_0^2 - \sqrt{\omega_0^4 - 8E|\gamma_2|}]} \tag{13.13}$$

In the above expressions for t_0 and t_1 we assume that the square root is real. We observe that this is equivalent to assuming

$$E < E^* = \frac{\omega_0^4}{8|\gamma_2|} \tag{13.14}$$

In the Newton picture this corresponds to the energy of the particle beeing so small that it does not move out of the potential well. When the energy approaches the limiting energy E^* the particle spend a larger and larger fraction of its time close to the edge of the potential well. In the array picture this will produce a intensity profile that is uniform across most of the array. The equation (13.11) cas be inverted using the elliptic function $sn(x|m)$ [30].

$$s(x) = t_1 sn(t_0\sqrt{|\gamma_2|}x|\frac{t_1}{t_0}) \tag{13.15}$$

The condition on the parameters for giving a constant phase solution for the array is now

$$K(\frac{{t_1}^2}{t_0}) = \frac{1}{2}L \tag{13.16}$$

Observe that when $E \to E^*$, $\frac{{t_1}^2}{t_0} \to 1$. This implies that $K \to \infty$, so the period goes to infinity as indicated earlier. In fact $sn(x|1) = \tanh x$ so in the large array limit the intensity profile is uniform over most of the array and at the edges it will have the shape of a hyperbolic tangent.

Chapter 14

APPENDIX I

We will in this appendix compute approximations to the spectrum for case 1 and case 3. The spectrum will be computed under the assumption of small amplitude. In both cases we can write the equation for the profile as

$$s_{xx} + \omega_0^2 s = 2\gamma_2 s^3 \tag{14.1}$$

This is clearly just the equation for a nonlinear oscillator, and the problem consist of computing an approximate expression for the frequency of the oscillator. This can be done using standard asymptotic methods [31]. The result is

$$\omega = \omega_0 - \frac{3\gamma_2 a^3}{4\omega_0} \tag{14.2}$$

Where a is an approximation to the amplitude of the solution. At this level approximation the solution for $s(x)$ is just $a \sin \omega x$. An approximation to the spectrum is found by imposing the boundary condition $s(L) = 0$. This give

$$\omega^l = \frac{2\pi l}{L} \tag{14.3}$$

Reintroducing the original parameters into the expression for ω and using the assumption that a is small we find

Case1:

$$\delta' = -\frac{1}{2}\alpha + 2\eta - \eta(\frac{2\pi l}{L})^2 - (p - \frac{1}{2})|\tan\phi_0 - \alpha|(1 - 4a^3) \tag{14.4}$$

Case 3:

$$\delta' = -\frac{1}{2}\alpha + 2\eta - \eta(\frac{2\pi l}{L})^2 + (p - \frac{1}{2})|\tan\phi_0 - \alpha|(1 - 4a^3) \tag{14.5}$$

Chapter 15

APPENDIX J

In this appendix we will derive the phaselocked solutions for the driven array in the case of constant injection and variable pumping.

From (8.7) we have the following equation for the amplitude s_j

$$s_{i+1} + s_{i-1} - \Delta s_i = aR \tag{15.1}$$

Where we have defined $R = (\sin\phi_0 - \alpha\cos\phi_0)/\eta$. The general solution of (15.1) depends on what range of values Δ occupy. We will discuss five different cases depending on the values of Δ. The equation (15.1) is a inhomogenous second order linear difference equation so the general solution will in all cases be the sum of a particular solution of the inhomogenous equation and the general solution of the homogenous equation.

Case 1

Let us first assume that $|\Delta| < 2$ or $|\Delta| > 2$ and later subdivide this case. The particular solution is clearly just the constant $s^1 = \frac{aR}{2-\Delta}$. Let us look for a solution to the homogenous solution of the form.

$$s_j = e^{kj} \tag{15.2}$$

Where k can be any complex number, since we can always from solutions of type (15.2) produce a real solution by linear combination. Upon insertion of (15.2) into equation (15.2) we find

$$e^k = \frac{1}{2}(\Delta \stackrel{+}{-} \sqrt{\Delta^2 - 4}) \tag{15.3}$$

So a set of two linear independent solutions is e^{kj} and e^{-kj}. Both solutions (15.3) produce the same independent set so we can choose k to be any of the two. We will now subdivide the current case into three subcases.

Case 1a

Assume $\Delta > 2$. From equation (15.3) and the discussion that follows it we find by linear combination that a basis of real solutions is $\sinh \hat{k}j$ and $\cosh \hat{k}j$. So the general solution for this case is

$$s_j = s^1 + A \sinh \hat{k}j + B \cosh \hat{k}j \tag{15.4}$$

$$\hat{k} = \ln \frac{1}{2}(|\Delta| + \sqrt{\Delta^2 - 4}) \tag{15.5}$$

Where A and B are free constants

Case 1b

Assume $0 < \Delta < 2$. We now find that a basis of real solutions is $\sin \bar{k}j$ and $\cosh \bar{k}j$. So the general solution for this case is

$$s_j = s^1 + x\sin(kj + \psi) \tag{15.6}$$

$$\bar{k} = \arctan\frac{\sqrt{4-\Delta^2}}{|\Delta|} \tag{15.7}$$

Where x and ψ are free constants.

Case 1c

Assume $-2 < \Delta < 0$. From equation (15.3) we now find that we must choose $k = \bar{k} - \pi$. So a basis of independent solutions for this case is $\sin(\bar{k} - \pi)j$ and $\cos(\bar{k} - \pi)j$. The general solution for this case is then

$$s_j = s^1 + x\sin((\bar{k} - \pi)j + \psi) \tag{15.8}$$

Where x and ψ are free constants.

Case 1d

Assume $\Delta < -2$. From equation (15.3) we find that a basis of solutions for this case is $(-1)^j \sinh \hat{k}j$ and $(-1)^j \cosh \hat{k}j$. So a general solution for this case is

$$s_j = s^1 + (-1)^j(A\sinh \hat{k}j + B\cosh \hat{k}j) \tag{15.9}$$

Where A and B are free constant.

Case 2

Assume $\Delta = 2$. For this case we will seek a particular solution of the form $s_j = Aj^2$, where A is a free constant to be determined. Insert this ansatz into (15.1). This

gives

$$A(j+1)^2 + A(j-1)^2 - 2Aj^2 = aR \tag{15.10}$$

So we find that $A = \frac{aR}{2}$. Call this value s^2. The general solution of the homogenous equation is a general linear expression in j. So the general solution of equation (15.1) is for this case

$$s_j = s^2 j^2 + Aj + B \tag{15.11}$$

In summary the phase locked solutions for the case of uniform injection are

$$s_j = s^1 + (-1)^j (A \sinh \hat{k} j + B \cosh \hat{k} j) \tag{15.12}$$

for $\Delta < -2$

$$s_j = s^1 + x \sin((\bar{k} - \pi) j + \psi) \tag{15.13}$$

for $-2 < \Delta < 0$

$$s_j = s^1 + x \sin(\bar{k} j + \psi) \tag{15.14}$$

for $0 < \Delta < 2$

$$s_j = s^2 j^2 + Aj + B \tag{15.15}$$

for $\Delta = 2$

$$s_j = s^1 + A \sinh \hat{k} j + B \cosh \hat{k} j \tag{15.16}$$

for $\Delta > 2$

$$\bar{k} = \arctan \frac{\sqrt{4 - \Delta^2}}{|\Delta|} \tag{15.17}$$

$$\hat{k} = \ln \frac{1}{2}(|\Delta| + \sqrt{\Delta^2 - 4}) \tag{15.18}$$

$$s^1 = \frac{aR}{2 - \Delta} \tag{15.19}$$

$$s^2 = \frac{aR}{2} \tag{15.20}$$

(15.21)

Chapter 16

APPENDIX K

We will in this appendix we will investigate the solutions of the uniformly driven array in the special case $R = 0$. In appendix J we deriven the solutions for the uniformly driven array for different values of Δ. We will now apply the boundary conditions $s_0 = s_{N+1} = 0$ to the solutions from appendix J. It is immidiately clear that when $R = 0$ only case 1b,1c will give a nontrivial solution since the hyperbolic functions can not be fitted to the zero boundary conditions. Using the fact that $\cos \pi j = (-1)^j$ we find when the boundary conditions are applied that both case 1b and 1c give

$$\sin \psi = 0 \tag{16.1}$$

$$\sin (\bar{k}(N+1) + \psi) = 0 \tag{16.2}$$

From this we find

$$k = \frac{\pi l}{N+1} \tag{16.3}$$

Where $1 \leq l \leq 2N+1$. Let us first concider the case $0 < \Delta < 2$. Introducing the expression for $k(\Delta)$ we find

$$\Delta_l = 2\cos\frac{\pi l}{N+1} \tag{16.4}$$

Since we require $\Delta > 0$ we must clearly have $1 \leq l \leq \frac{N+1}{2}$ or $\frac{3N+3}{2} \leq l \leq 2N+1$. But using the periodicity of cos we have $\Delta_{2N+2-l} = \Delta_l$, so the second interval only reproduce the values in the first interval. So for $0 < \Delta < 2$ we have supermodes at

$$\Delta_l = 2\cos\frac{\pi l}{N+1} \text{ for } 1 \leq l \leq \frac{N+1}{2} \tag{16.5}$$

A similar argument gives for the case $-2 < \Delta < 0$

$$\Delta_l = -2\cos\frac{\pi l}{N+1} \text{ for } 1 \leq l \leq \frac{N+1}{2} \tag{16.6}$$

The supermodes on the two sides of $\Delta = 0$ only differ by a factor $(-1)^j$. That is we have

$$s_j = x(-1)^j \sin \bar{k}j \tag{16.7}$$

$$\text{for } -2 < \Delta < 0$$

$$s_j = x \sin \bar{k}j \tag{16.8}$$

$$\text{for } 0 < \Delta < 2$$

This concludes the calculation of the phase locked modes for the case $R = 0$

Chapter 17

APPENDIX L

We will in this appendix apply the boundary conditions $s_0 = s_{N+1} = 0$ to the solutions of the recursion relation (8.7) when $R \neq 0$. We will separate the discussion into several different cases depending on the value of the variable $\triangle$.

Case 1a

This is the case defined by $\triangle < -2$. From (15.12) we have that the general solution for this case is

$$s_j = s^1 + (-1)^j (A \sinh \hat{k} j + B \cosh \hat{k} j) \tag{17.1}$$

Applying the boundary conditions $s_0 = s_{N+1} = 0$ we find

$$s^1 + B = 0 \tag{17.2}$$

$$s^1 + (-1)^j (A \sinh \hat{k}(N+1) + B \cosh \hat{k}(N+1)) = 0 \tag{17.3}$$

Solving for A and B we find immediately

$$B = -s^1 \tag{17.4}$$

$$A = -s^1(-1)^{N+1}\frac{1-(-1)^{N+1}\cosh\hat{k}(N+1)}{\sinh\hat{k}(N+1)} \tag{17.5}$$

Substitute these expressions for A and B into equation (17.1). We then find, after using a hyperbolic identity that

$$s_j = s^1(1-(-1)^j\left[\frac{(-1)^{N+1}\sinh\hat{k}j - \sinh\hat{k}(j-(N+1))}{\sinh\hat{k}(N+1)}\right]) \tag{17.6}$$

By using some more hyperbolic identities and distinguising between even and odd N we find that the solution that satisfy the boundary conditions is

$$s_j = s^1(1+(-1)^j\frac{\sinh\hat{k}(j-\frac{N+1}{2})}{\sinh\hat{k}\frac{N+1}{2}}) \tag{17.7}$$

for N even

$$s_j = s^1(1-(-1)^j\frac{\cosh\hat{k}(j-\frac{N+1}{2})}{\cosh\hat{k}\frac{N+1}{2}}) \tag{17.8}$$

for N odd

(17.9)

Case 1b

This case is defined by $-2 < \triangle < 0$. From appendix J equation (15.13) we have that the general solution for this case is

$$s_j = s^1 + x\sin((\bar{k}-\pi)j+\psi) \tag{17.10}$$

Applying the boundary conditions we now find that

$$s^1 + x \sin \psi = 0 \tag{17.11}$$

$$s^1 + x \sin ((\bar{k} - \pi)(N+1) + \psi) \;\; = \;\; 0 \tag{17.12}$$

So we find that $x = -\frac{s^1}{\sin \psi}$ and

$$\sin ((\bar{k} - \pi)(N+1) + \psi) = \sin \psi \tag{17.13}$$

We will now distinguise between the cases N even and N odd.

N even

Equation has two different types of solutions since $\sin x = \sin y$ if $x = y$ or $x = \pi - y$.

(i)

For this case we find

$$(\bar{k} - \pi)(N+1) + \psi \;\; = \;\; \psi + 2\pi l \tag{17.14}$$

So ψ is any real number and

$$\bar{k} = \frac{(2l+1)\pi}{N+1} \tag{17.15}$$

Where l is any integer. So these solutions have the same positions in detuning as the odd supermodes when $R = 0$ The modes can be written as

$$s_j = s^1(1 - (-1)^j \frac{\sin (\frac{(2l+1)\pi}{N+1} j + \psi)}{\sin \psi}) \tag{17.16}$$

(ii)

For this case we find

$$(\bar{k}-\pi)(N+1)+\psi = \pi - \psi + 2l\pi \tag{17.17}$$

This give us the following formula for the solution for this case

$$s_j = s^1(1+(-1)^j \frac{\sin \bar{k}(j-\frac{N+1}{2})}{\sin \bar{k}\frac{N+1}{2}}) \tag{17.18}$$

Where we have used a formula for the sin of the sum of two arguments and the fact that N is even

N odd

We can also for N odd distinguise between two different cases.

(i)

For this case we find

$$(\bar{k}-\pi)(N+1)+\psi \;\; = \;\; \psi + 2\pi l \tag{17.19}$$

So ψ is any real number and

$$\bar{k} = \frac{2l\pi}{N+1} \tag{17.20}$$

Where l is any integer. So these solutions have the same positions in detuning as the even supermodes when $R = 0$ The modes can be written as

$$s_j = s^1(1 - (-1)^j \frac{\sin(\frac{2l\pi}{N+1}j + \psi)}{\sin\psi}) \tag{17.21}$$

Where l is any integer and where we have used the fact that N is odd to write the integer multiplying π as a general even number.

(ii)

For this case we find

$$(\bar{k} - \pi)(N+1) + \psi = \pi - \psi \tag{17.22}$$

This give us the following formula for the solution for this case

$$s_j = s^1(1 - (-1)^j \frac{\cos\bar{k}(j - \frac{N+1}{2})}{\cos\bar{k}\frac{N+1}{2}}) \tag{17.23}$$

Where we have used a formula for the sin of the sum of two arguments and the fact that N is odd.

Case 1c

This case is defined by $0 < \Delta < 2$. From appendix J equation (15.14) we have that the general solution is

$$s_j = s^1 + x\sin(\bar{k}j + \psi) \tag{17.24}$$

The boundary conditions $s_0 = s_{N+1} = 0$ now gives

$$s^1 + x \sin \psi = 0 \tag{17.25}$$

$$s^1 + x \sin (\bar{k}(N+1) + \psi) = 0 \tag{17.26}$$

So $x = -\frac{s^1}{\sin \psi}$ and

$$\sin (\bar{k}(N+1) + \psi) = \sin \psi \tag{17.27}$$

So we have two different types solutions.

(i)

For this case we find

$$\bar{k}(N+1) + \psi = \psi + 2l\pi \tag{17.28}$$

So ψ can be any real number and

$$\bar{k} = \frac{2l\pi}{N+1} \tag{17.29}$$

We observe that these supermodes are in the same positions as the even supermodes from the case $R = 0$. The solutions in this case can be written as

$$s_j = s^1(1 - \frac{\sin (\frac{2l\pi}{N+1} j + \psi)}{\sin \psi}) \tag{17.30}$$

(ii)

For this case we find

$$\bar{k}(N+1)+\psi \;=\; \pi-\psi+2l\pi \tag{17.31}$$

Solving for ψ and inserting into (17.19) we find that the solution for this case is

$$s_j \;=\; s^1(1-\frac{\cos\bar{k}(j-\frac{N+1}{2})}{\cos\bar{k}\frac{N+1}{2}}) \tag{17.32}$$

Case 1d

This case is defined by $2<\Delta$. The general solution for this case is (15.16)

$$s_j \;=\; s^1+A\sinh\hat{k}j+B\cosh\hat{k}j \tag{17.33}$$

Applying the boundary conditions we find immidiately

$$s^1+B \;=\; 0 \tag{17.34}$$

$$s^1+A\sinh\hat{k}(N+1)+B\cosh\hat{k}(N+1) \tag{17.35}$$

So we have

$$b \;=\; -s^1 \tag{17.36}$$

$$a \;=\; -s^1\frac{1-\cosh\hat{k}(N+1)}{\sinh\hat{k}(N+1)} \tag{17.37}$$

Some hyperbolic identities gives the solution for this case as

$$s_j \;=\; s^1(1-\frac{\cosh\hat{k}(j-\frac{N+1}{2})}{\cosh\hat{k}\frac{N+1}{2}}) \tag{17.38}$$

Case 2

This case is defined by $\Delta = 2$. The general solution was in appendix J found to be (15.15)

$$s_j = s^2 j^2 + Aj + B \tag{17.39}$$

The solution that satisfie the boundary conditions is found to be

$$s_j = s^2 j(j - (N + 1)) \tag{17.40}$$

Observe that even if we now have found all the solutions to the recursion relation for the amplitude in the case of uniform injection, not all of them give the amplitude of a phaselocked constant phase solution to the laser array equations. This is because it must also be possible to satisfie equation (8.6). This is possible if the amplitude profile never is zero. So all lasers in the array must be on for a solution to exist when we have uniform injection. Also note that some of the formulas derived in this appendix predict arbitrary large maximum amplitude when the detuning approaches certain values. This does not mean that we are predicting infinite output from the array. Since the pumping is essentially proportional to the intensity,the pumping goes to infinity if the intensity goes to infinity. Physically there are strong restrictions on the maximum possible value of the injection that the array can survive. So the presence of values of the detuning where the output intensity goes to infinity only means that these points can not be approached to closely unless you adjust the injection amplitude a so as to keep the output intensity reasonable small.

This conclude the computation of the solution to the uniformly driven array in the general case $R \neq 0$.

Chapter 18

APPENDIX M

In this appendix we will prove that the amplitude profiles found in appendix L vary continously as a function of $\triangle$. Clearly we only have to investigate the points $\triangle = -2, 0, 2$.

$$\triangle = -2$$

We will distinguise between the cases N even and N odd.

(i) N even

From equations (17.7) and (17.18) we have

$$s_j = s^1(1 + (-1)^j \frac{\sinh \hat{k}(j - \frac{N+1}{2})}{\sinh \hat{k}\frac{N+1}{2}}) \qquad \text{for } \triangle < -2 \tag{18.1}$$

$$s_j = s^1(1 + (-1)^j \frac{\sin \bar{k}(j - \frac{N+1}{2})}{\sin \bar{k}\frac{N+1}{2}}) \qquad \text{for } \triangle > -2 \tag{18.2}$$

From equations (15.17) and (15.18) we have $\bar{k}$ and $\hat{k}$ as a function of $\triangle$

$$\bar{k} \;=\; \arctan \frac{\sqrt{4 - \triangle^2}}{|\triangle|} \tag{18.3}$$

$$\hat{k} = \ln \frac{1}{2}(|\triangle| + \sqrt{\triangle^2 - 4}) \tag{18.4}$$

So when $\triangle$ goes to -2 from below, $\hat{k} \to 0$ and when $\triangle$ goes to -2 from above, $\bar{k} \to 0$. In this limit the the fractions in equations (18.3) and (18.4) become $\frac{0}{0}$. Using L'Hopitals once on each fraction we find that the limits are the same since derivatives of sin and sinh behave similarly. The common limit is

$$s_j = s^1((-1)^j \frac{2}{N+1} j + 1 - (-1)^j) \tag{18.5}$$

(ii) N odd

From equations (17.8) and (17.21) we have

$$s_j = s^1(1 - (-1)^j \frac{\cosh \hat{k}(j - \frac{N+1}{2})}{\cosh \hat{k}\frac{N+1}{2}}) \tag{18.6}$$

for $\triangle < -2$

$$s_j = s^1(1 - (-1)^j \frac{\cos \bar{k}(j - \frac{N+1}{2})}{\cos \bar{k}\frac{N+1}{2}}) \tag{18.7}$$

for $\triangle > -2$

In this case the limit of the fraction is, for both equation (18.6) and (18.7) ,1. So the limit from above and below are the same and both are equal to

$$s_j = s^1(1 - (-1)^j) \tag{18.8}$$

$$\triangle = 0$$

From equations (17.18),(17.21),(17.27) and some trigonometric identities we find that for any N even or odd

$$s_j = s^1(1 - \frac{\cos(\bar{k} - \pi)(j - \frac{N+1}{2})}{\cos(\bar{k} - \pi)\frac{N+1}{2}} \qquad (18.9)$$

for $\triangle < 0$

$$s_j = s^1(1 - \frac{\cos \bar{k}(j - \frac{N+1}{2})}{\cos \bar{k}\frac{N+1}{2}} \qquad (18.10)$$

for $\triangle > 0$

It is now trivial that the left and right limit are equal when they exist. Since the denominator in the limit is $\cos \frac{\pi}{2}\frac{N+1}{2}$, it is clear that the limit exist if $N \neq 4l + 1$ for some integer l. If this is satisfied the common limit is

$$s_j = s^1(1 - \frac{\cos \frac{\pi}{2}(j - \frac{N+1}{2})}{\cos \frac{\pi}{2}\frac{N+1}{2}}) \qquad (18.11)$$

$$\triangle = 2$$

From equations (18.10) and (17.33) we have

$$s_j = s^1(1 - \frac{\cos \bar{k}(j - \frac{N+1}{2})}{\cos \bar{k}\frac{N+1}{2}} \qquad (18.12)$$

for $\triangle < 2$

$$s_j = s^1(1 - \frac{\cosh \hat{k}(j - \frac{N+1}{2})}{\cosh \hat{k}\frac{N+1}{2}}) \qquad (18.13)$$

for $\triangle > 2$

From equations (15.17) and (15.18) we observe that $\bar{k} \to 0$ when $\triangle$ goes to 2 from below and $\hat{k} \to 0$ when $\triangle$ goes to 2 from above. So the fraction in equation (18.12) and (18.13) goes to 1 when $\triangle$ approach 2 from above or below. So the

second term in the product in equation (18.12) and (18.13) goes to zero. But at the same time the factor $s^1 = \frac{aR}{2-\Delta}$ goes to infinity. Using l'Hopitals rule on both equations we find that they do in fact approach the same limit and this limit is the solution found in appendix L for $\Delta = 2$.

This complete the investigation of continuity of the profile as a function of Δ.

References

[1] L.A.Lugiato, C. Oldeano, L.M Narducci, "Cooperative frequency locking and stationary spatial structures in lasers",J.Opt.Soc.Am. B, Vol.5,No.5 May 1988,p 879-888

[2] M.Sargent III, M.O.Scully,and W.E.Lamb Jr., "laser physics", Reading,MA:Addison-Wesley 1974

[3] W.E.Lamb Jr., "Theory of an optical maser",Phys.Rew.,Vol 134 ,pp A1429-A1450, June 1964

[4] Sami T. Hendow and Murray Sargent III, "Theory of single mode laser instabilities", j. opt. soc. am B/Vol.2, Jan 1985,pp 84-101

[5] Amnon Yariv,"Quantum electronics, third edition" Wiley, 1987

[6] A. P. Bogatov, P. G. E, and B. N. Sverdlov, "anomalous interaction of spectral modes in a semiconductor Laser", IEEE Journal of quantum electronics, vol. qe-11,No.7,July 1975

[7] A.C.Newell "The Dynamics and Analysis of Patterns" Complex Systems, Ed. D. Stein, Addison-Wesley Longman Publishing Group Ltd.,1989

[8] Lange C. & Newell A. C. ;Siam J.Appl. Math. 27,441-56,1974.

[9] "Analytical description of ultrashort optical pulse propagation in a resonant medium" G. L. Lamb, Jr. Reviews of modern physics, Vol 43, No. 2, april 1971

[10] "Self induced transparancy" S. L. McCall, E. L. Hahn, Physical review, Vol.183, no.2, july 1969

[11] "Propagation of ultrashort optical pulses" G. L. Lamb Jr, Physics letter, August 1967

[12] "Pulse-area-pulse-energy description of a travelling-wave laser amplifier" S. L. McCall, E. L. Hahn, Physical Review A, Vol.2, No.3 september 1970.

[13] "Optical vorticies."P.Coullet, L. Gil, F. Rocca., Optics comm, Nov. 1989

[14] This is a very robust package of ode solvers written for stiff or non stiff odes. Authors: D. K. Kahaner, National bureau of standards, C. D. Sutherlands, Los Alamos National Laboratory

[15] MACLIB is a set of high level routines for discretization, grid generation etc. Authors: James M. Hyman, Bernard Larrouturou, group T-7, LASL.

[16] For a review see D. Botez and D.E.Ackley, IEEE Circuits and Devices mag. 2, 8 (1986).

[17] R. Elliott, R.K. Defreez, T.L. Paoli, R.D. Burnham and W. Streifer, IEEE J. Quantum Electron., QE-21,598 (1985).

[18] S.S. Wang and H.G. Winful, Appl Phys. Lett. **52**,1774 (1988)

[19] H.G.Winful and S.S. Wang, Appl. Phys. Lett. **53**,1894 (1988)

[20] E.Kapon, J. Katz and D. Botez, Appl. Phys. Lett. 44,293 (1984)

[21] E. J. Doedel, AUTO User Manual, Version September 1984.

[22] R. DeFreez (private communication)

[23] N. Yu, R. K. DeFreez, D. J. Bossert, R. A. Elliott, H. G. Winful and D. F. Welch, "Observation of sustained self-pulsation in CW operated flared Y-coupled laser arrays," Electron. Lett. **24**, 1203–1204 (September 15, 1988).

[24] R. K. DeFreez, D. J. Bossert, N. Yu, K. Hartnett, R. A. Elliott, and H. G. Winful, "Spectral and picosecond temporal properties of flared guide Y-coupled phase-locked laser arrays," *Appl. Phys. Lett.* **53**, 2380–2382 (December 12, 1988).

[25] R. K. DeFreez, Private communication.

[26] H. Adachihara and J.V. Moloney, (unpublished).

[27] C. H. Henry "Theory of the linewidth of semiconductor lasers." IEEE Journal of quantum electronics, vol. QE-18, No. 2, February 1982

[28] "Quantum electronics,third edition". Amnon Yariv,page 232 -260 (Wiley)

[29] "Advances in Diode Laser Pumps",W.Steifer, D.R. Scifres, G.L. Harnagle ,D.F. Welch,J. Berger,M. Sakamoto, IEEE JQE Vol. 24 ,No. 6, June 1988.

[30] "Handbook of mathematical functions" M. Abramowitz, A. Stegun.(Ed),Dover,1970

[31] "Perturbation Methods" Ali Nayfeh, Wiley interscience, 1972